UNIVERSIDAD COMPLUTENSE DE MADRID
FACULTAD DE CIENCIAS FÍSICAS

TESIS DOCTORAL

The role of vegetation in regional climate simulations

El papel de la vegetación en simulaciones climáticas regionales

MEMORIA PARA OPTAR AL GRADO DE DOCTOR

PRESENTADA POR

Jose Manuel Jiménez Gutiérrez

Directores

Juan Pedro Montávez Gómez
Francisco Valero Rodríguez

Madrid

UNIVERSIDAD COMPLUTENSE DE MADRID
FACULTAD DE CIENCIAS FÍSICAS

TESIS DOCTORAL

The role of vegetation in regional climate simulations

El papel de la vegetación en simulaciones climáticas regionales

MEMORIA PARA OPTAR AL GRADO DE DOCTOR

PRESENTADA POR

Jose Manuel Jiménez Gutiérrez

DIRECTORES

Juan Pedro Montávez Gómez

Francisco Valero Rodríguez

Madrid, 2022

The role of vegetation in regional climate simulations

El papel de la vegetación en simulaciones climáticas regionales

Memoria que presenta
Jose Manuel Jiménez Gutiérrez
para optar al grado de
Doctor en Ciencias Físicas

Directores:
Dr. Juan Pedro Montávez Gómez
Dr. Francisco Valero Rodríguez

Departamento de Física de la Tierra y Astrofísica
Facultad de Ciencias Físicas
Universidad Complutense de Madrid

A la memoria de Maria Luisa de Antonio y de Lola
En recuerdo de Manuel Vitutia Ciurana

Agradecimientos

Parecía que nunca iba a llegar este momento después de tanto tiempo pero al fin llegó. Han sido muchos años por los que ha pasado este trabajo desde que me matriculé en el Doctorado de Físicas en el año 2005. Y muchas las personas que me han ayudado y apoyado en estos 16 años. He pensado en dejarlo innumerables veces pero al final ha podido ser sobre todo gracias a mucha gente que me ha rodeado en este tiempo.

En primer lugar quisiera dar las gracias a Juan Pedro Montávez y Francisco Valero. A Juanpe, por todo lo que me ha ayudado en este trabajo desde el principio a pesar de la dificultad añadida de no estar en su grupo de trabajo en Murcia, haberme dedicado tanto tiempo, haberme enseñado tanto y abrirme el camino en mi carrera profesional. Te estoy profundamente agradecido Juanpe. A Paco Valero por haberme animado siempre a acabar este trabajo con el cariño que siempre me ha mostrado, recibirme siempre con los brazos abiertos y su sentido del humor y espabilarme tantas veces como ha hecho con un "Vamos Jose!!". Gracias Paco por haberme iniciado profesionalmente en un momento en el que estaba bastante perdido.

Los inicios de mi trabajo en el Departamento de Astrofísicas y Ciencias de la Atmósfera iban cargados de mucho temor e inseguridad por no saber si iba a encajar con mi formación de base. Pero el apoyo que recibí fue increible y me encontré con un grupo de personas a las que debo mucho, a las que estoy muy agradecido y guardo un especial cariño . Quisiera dar las gracias a Roland Aznar con quien hice mis primeros trabajos, por haberme ayudado con enorme paciencia en los tiempos iniciales en los que estuve en el Departamento. A Pedro Jiménez, por haberme enseñado tantas cosas en el tiempo que

estuvimos trabajando juntos a pesar de ciertas dificultades que existieron en algunos momentos. A Elena García-Bustamante por estar siempre dispuesta y sonriente a echarme una mano. Gracias a ti Elena, en una carambola vital un poco extraña pude entregar el antiguo DEA in extremis...A Fidel González por ser siempre tan cercano conmigo y su disposición a ayudarme siempre. Muchas gracias Fidel. A Etor Lucio y a Javier Díaz por haberme ayudado en esta última etapa con temas más prácticos en los que andaba un poco perdido. A otros compañeros y compañeras como Marisa Montoya, Jorge Navarro, Manuel Prieto, Daniel Paredes...con los que me fui encontrado y de los que me he llevado algo bueno. De todas estas personas de las que hablado destaco su gran profesionalidad y entusiasmo en su trabajo, y para mi han sido y son grandes ejemplos a seguir.

Muy agradecido a Marisa Martín por haberme apoyado en los momentos finales. Hay personas que en algún momento se convierten en tu ángel de la guarda y así ha sido contigo.

Muchas gracias Encarna por haberme ayudado en la recta final.

Quisiera dar las gracias a Jordi Vilá-Guerau de Arellano por las ideas aportadas en trabajos iniciales y que me han ido acompañando estos años. Simplificar lo más posible para poder entender mejor lo que uno está estudiando es una máxima que siempre tengo presente.

Quiero agradecer a compañeros de la Universidad de Murcia como Sonia Jerez o Juanjo Navarro por haberme ayudado en algunos de los trabajos que he realizado.

Quisiera agradecer a mis compañeros de Meteológica el apoyo y el ánimo que me han dado siempre para poder terminar este trabajo.

A todo los amigos y amigas que siempre me han preguntado como iba y que se han interesado por mi a lo largo de muchos años. A Charly, Marta, Fátima, mis amigos de The Hightowers...

A David por haberme serenado en los momentos que me he visto más desbordado y ayudarme como siempre a estar en el presente.

Quiero agradecer a mi madre, mi padre y mi hermana por haberme animado siempre a terminar este trabajo y a mostrarme el valor del trabajo bien hecho.

Por último y no menos importante, agradecer a mi mujer y a mis hijas por haber sido el empuje definitivo y la luz para poder acabar esta Tesis. Gracias Morgana...

Mi agradecimiento a los departamentos de Física de la Universidad de Murcia y de Física de la Tierra y Astrofísica de la Universidad Complutense de Madrid y su Instituto de Matemática Interdisciplinar (IMI) por haber proporcionado el ámbito de investigación y medios materiales necesarios para la culminación de esta tesis doctoral.

Contents

Summary

The role of vegetation in regional climate simulations

Introduction

Land surface atmosphere interactions are of great relevance in climate and weather. The biophysical variables of the earth's surface play a determining role in the exchanges of heat, momentum and humidity with the atmosphere. In this way, the correct representation and understanding of how these variables perform in Land Surface Models (LSMs) is crucial for the modeling of atmospheric processes.

Vegetation variability in its spatial and vertical dimension as well as the state, health or type of vegetation is described in the numerical prediction models by parameters such as albedo, fraction of vegetation cover (FVC), leaf area index (LAI), stomatal resistance, conductivity or roots depth.

The variable FVC represents the horizontal density of live vegetation and is calculated through the Normalized Difference Vegetation Index (NDVI). FVC defines how total evaporation is partitioned between evaporation from the soil and transpiration from plants. In some LSMs it has a decreasing effect on thermal conductivity, thus reducing heat transfer to deeper layers of the soil. These physical processes determine in a decisive way surface variables such as air temperature or relative humidity. For this reason, the variability in precipitation, fires or anthropogenic changes in the vegetation cover

imply a temporal and spatial heterogeneity of the FVC that have a not negligible impact in numerical simulations.

Main goals of the study

This thesis assesses the contribution of the variable FVC in the Noah LSM coupled to a climate version of the MM5 model in the domain of the Iberian Peninsula. The main goals are the next:

- Study the impact level of using different methodologies of calculation of FVC and its importance in a regional climate model (RCM).
- Assess the sensitivity of the Noah LSM to variations in the FVC variable in heat and humidity fluxes and its influence in temperature variations.
- Analyze the implications and potential improvements in the predictability of the model in temperature at 2 meters (T2m) by using a database of FVC with high temporal and spatial resolution instead of the usual climatologies.

Results

The most relevant results of this thesis are the following:

1. Based on three calculation methodologies, WETZEL, GUTMAN and ZENG and using the GIMMS (Global Inventory Modeling and Mapping Studies) database of NDVI, three different databases of FVC were generated in the period 1982-2006. The differences between these databases and their subsequent effect on heat fluxes and temperatures were evaluated when incorporated to an annual simulation. The comparison of the simulations with different databases in which differences in FVC are around 30 % in FVC could reach bias of 1 °C in monthly means of T2m.
2. For assessing the sensitivity of Noah LSM to changes in FVC, a set of ideal experiments were carried out, setting values of 30 % and 90 % in vegetation cover over space and time in a simulation of a complete year. The results showed that the minimum T2m always decrease when FVC increases. Regarding the maximum T2m, the effect of increasing the vegetation depends on the availability of soil moisture. With hydric stress the maximum T2m can increase with higher FVC, while without hydric stress the maximum T2m decrease.
3. By means of the Copernicus FVC database, a simulation was performed for the period 2000-2017 using monthly data for each year (COP-YEAR) and another from monthly

data generated with a climatology elaborated for the years of the simulation (COP-CLIM). These simulations were compared with a control simulation using the default FVC data from the Noah LSM based on climatologies (MM5-DEF). Analyzing the T2m fields of these simulations with observations, differences in BIAS and MAE are observed between the Copernicus and MM5-DEF simulations. The differences are more noticeable for the minimums and in the month of April with lower errors for the Copernicus simulations. Comparing the Copernicus simulations between them, there are no great difference in error globally, although some differences can be found in extreme years of vegetation cover (excess or defect). The results obtained with sensitivity experiment modifying the parameters that control thermal conductivity showed a relevant effect in simulated temperatures.

Conclusions

Among the most relevant conclusions of this study can be found that:

- Differences of up to 30 % of FVC can be found both in the use of different FVC calculation methodologies and in the interannual variability between wet and dry years. These differences can suppose relevant deviations in monthly means of T2m in simulations with RCMs.
- The sensitivity of T2m to changes in FVC is different depending on the month of the year and time of the day. A greater response is found in the months with the highest available radiative energy. While in the case of the minimum T2m the different response in the daily cycle is fundamentally dominated by the thermal conductivity, the maximum is controlled by the stomatal resistance parameterization of the model.
- The use of more realistic FVC databases does not have to imply an improvement in the predictability in RCMs. Instead, they can be a relevant element when testing and understanding the different processes parameterized in LSMs.

Resumen

El papel de la vegetación en simulaciones climáticas regionales

Introducción

Los procesos de interacción superficie atmósfera son de gran relevancia en clima y meteorología. Las variables biofísicas de la superficie terrestre tienen un papel determinante en los intercambios de calor, momento y humedad con la atmósfera. De esta manera, la correcta representación y comprensión de como estas variables intervienen en los modelos de superficie terrestre (LSM, del inglés) es crucial para la modelización de los procesos atmosféricos.

La variabilidad en la vegetación en su dimensión espacial y vertical así como de estado, salud o tipo de vegetación queda descrita en los modelos de predicción numérica por parámetros como albedo, fracción de cubierta vegetal (FVC), índice de área foliar (LAI), resistencia estomática, conductividad o profundidad de raíces.

La variable FVC representa la densidad horizontal de vegetación viva y se calcula a partir del Normalized Difference Vegetation Index (NDVI). FVC define como la evaporación total se reparte entre la evaporación del suelo y la transpiración de las plantas. En algunos LSMs tiene un efecto reductor de la conductividad térmica disminuyendo de esta manera la transferencia de calor hacia capas más profundas del suelo. Estos procesos físicos condicionan de manera determinante variables de superficie como la temper-

atura del aire o la humedad relativa. Por esta causa, la variabilidad en la precipitación, incendios o cambios antropogénicos en la cubierta vegetal implican una heterogeneidad temporal y espacial de la FVC que tienen un impacto nada despreciable en simulaciones numéricas.

Objetivos del estudio

La Tesis presentada evalúa la contribución de la variable FVC en el modelo Noah LSM acoplado a una versión climática del modelo MM5 en el dominio de la Península Ibérica. Los principales objetivos son los siguientes:

- Estudiar qué nivel de impacto puede tener emplear diferentes metodologías de cálculo de FVC y su trascendencia en modelos climáticos regionales (RCMs).
- Evaluar la sensibilidad del Noah LSM a las variaciones de la variable FVC en los flujos de calor y humedad y su traducción en las variaciones de temperatura.
- Analizar las implicaciones y las potenciales mejoras en la predictabilidad del modelo en la temperatura a 2 metros (T2m) al emplear una base de datos de FVC de alta resolución temporal y espacial en lugar de las climatologías habituales.

Resultados

Los resultados más relevantes de esta tesis son los siguientes:

1. A partir de tres metodologías de cálculo, WETZEL, GUTMAN y ZENG y empleando la base de datos GIMMS (Global Inventory Modeling and Mapping Studies) de NDVI, se generaron tres bases de datos distintas de FVC en el periodo 1982-2006. Se evaluaron las diferencias entre estas bases de datos y su posterior efecto en los flujos de calor y temperaturas al trasladarlo a una simulación anual. En la comparación entre las simulaciones con las distintas bases de datos con diferencias de FVC de hasta un 30%, se podían alcanzar bias de 1 °C en medias mensuales de T2m.
2. Se realizaron una serie de experimentos ideales fijando el valor de la FVC a un 30 % y un 90% de cobertura vegetal en el espacio y en el tiempo en una simulación de un año completo. Los resultados mostraron que las T2m mínimas siempre disminuyen cuando la FVC aumenta. Respecto a las T2m máximas, el efecto de incrementar la vegetación depende de la humedad disponible del suelo. Con stress hídrico las T2m máximas pueden aumentar con mayor FVC, mientras que sin stress hídrico las T2m máximas disminuyen.

3. Empleando la bases de datos de FCV Copernicus se realizó una simulación para el periodo 2000-2017 empleando datos mensuales para cada año (COP-YEAR) y, otra, con datos mensuales generados a partir de una climatología elaborada para los años simulados (COP-CLIM). Estas simulaciones se compararon con otra de control en la que se emplearon los datos de FVC por defecto del Noah LSM basados en climatologías (GUT-CLIM). El análisis de las simulaciones muestran diferencias tanto en la media como en la varianza de las series y un efecto en las tendencias de temperatura en el periodo simulado. Analizando los campos de T2m de estas simulaciones con observaciones se observan diferencias en BIAS y MAE entre las simulaciones Copernicus y GUT-CLIM. Las diferencias son más apreciables para las mínimas y en el mes de abril, con menores errores para las simulaciones Copernicus. Comparando las simulaciones Copernicus entre sí, no hay grandes diferencias en error entre ellas de manera global, aunque si que las hay en años extremos por exceso o por defecto en la cobertura de vegetación. Los resultados de experimentos de sensibilidad realizados con los parámetros que controlan la conductividad termica mostraron un impacto considerable en las temperaturas simuladas.

Conclusiones

Entre las conclusiones más relevantes de este estudio se encuentran:

- Diferencias de hasta un 30% de FVC se pueden encontrar tanto en el empleo de diferentes metodologías de cálculo de FVC como en la variabilidad interanual entre años húmedos y secos. Estas diferencias pueden suponer desvíos relevantes en medias mensuales de T2m en simulaciones con RCMs.
- La sensibilidad de la T2m a los cambios en la FVC es diferente dependiendo de la época del año y la hora del día. Se encuentra una mayor respuesta en los meses con mayor energía radiativa disponible. Mientras que la diferente respuesta en el ciclo diario, se encuentra controlada fundamentalmente en el caso de la T2m mínimas por la conductividad térmica y en el caso de las máximas por la parametrización de resistencia estomática del modelo.
- El empleo de bases de datos de FVC más realistas no tiene que suponer una mejora en la predictabilidad en RCMs. En cambio, pueden ser un elemento relevante a la hora de testar y comprender los diferentes procesos parametrizados en los LSMs.

List of acronyms

AVHRR	Advanced Very High Resolution Radiometer
BATS	Biosphere Atmosphere Transfer Scheme
BP	Before Present
BVOC	Biogenic Volatile Organic Compounds
DGVM	Dynamic Global Vegetation Model
E	Evapotranspiration
ECMWF	European Centre for Medium Range Weather Forecasts
FAO	Food and Agriculture Organization
FVC	Fraction Vegetation Cover
G	Ground heat flux
H	Sensible heat flux
IFS	Integrated Forecast System
IP	Iberian Peninsula
IPCC	Intergovernmental Panel on Climate Change
LAI	Leaf Area Index
LUCC	Land use/land cover change
LE	Latent heat flux
LSM	Land Surface Model
MM(5)	Mesoscale Model (5)
NCEP	National Centers for Environmental Prediction
NCAR	National Center for Atmospheric Research
NDVI	Normalized Difference Vegetation Index
NIR	Near-Infrared
NWPM	Numerical Weather Prediction Models
PBL	Planetary Boundary Layer
RCM	Regional Climate Model
Sib	Simple Biosphere Model
SM	Soil Moisture
T2m	2 meters air temperature
VIS	Red visible
WRF	Weather Research and Forecasting (model)

1

Introduction

There is a Spanish popular legend, attributed to the Greek Estrabon in his Geographica (first century B.C.) that says the following: "the Iberian Peninsula is so leafy that an squirrel could cross from south to north, jumping from tree to tree without touching the ground". This legend is false, because Estrabon never wrote it, and probably is extrapolated from some affirmations made in a documentary of a famous spanish naturalist called Felix Rodríguez de la Fuente. Indeed, the reality described by Pliny the Elder in Naturalis Historia in the first century A.C. was very different. He described the Iberian Peninsula (IP) as follows: “otherwise, the mountains of Hispanias, arid and barren and in which nothing else grows, have no choice but to be fertile in this good kind (of gold)". This kind of confussions about the supposed status of the vegetation two millennia ago, are in part sustained about the popular belief that in epochs previous to industrialization the earth surface was practically covered by vegetation. As was described by Pliny the Elder the reality was other in the case of the IP because in that times there were also natural barren an arid landscapes like nowadays. And besides of that, there were also large areas deforestated by human contribution, due to the massive logging carried out by Romans in the Mediterranean Basin (Hughes, 2011). So we find that a fully covered earth by vegetation is something difficult to find due to the natural variability of landscapes and anthropogenic changes in vegetation.

Nowadays vegetal landscape, is the result of a serie of events of various kinds, from geologic manifestations (plate movements, orogenies, etc...) to phenomena related with climate changes, that have implied important precipitation and temperature oscillations (marine transgressions and regressions). And of course, this landscape have been modeled by the effects of human activities like deforestation or agropastoral practices (Costa Tenorio et al., 1998). Sagan et al. (1979) made a interesting review of human

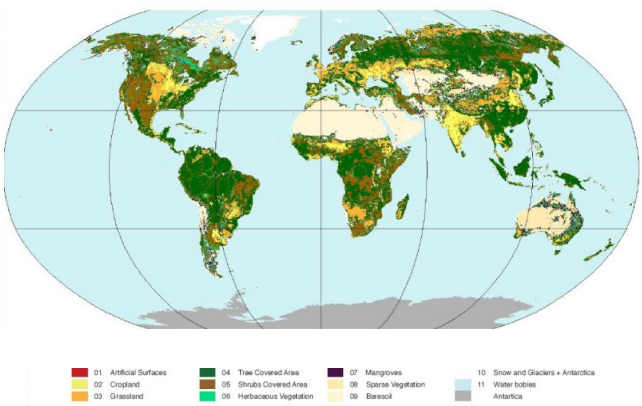

Fig. 1.1: Distribution of dominant land cover types. GLC-SHARE land cover database. Source: FAO

Land Cover types	Label
Artificial Surfaces	01
Cropland	02
Grassland	03
Tree Covered Areas	04
Shrubs Covered Areas	05
Herbaceous vegetation, aquatic or regularly flooded	06
Mangroves	07
Sparse vegetation	08
Baresoil	09
Snow and glaciers	10
Water bodies	11

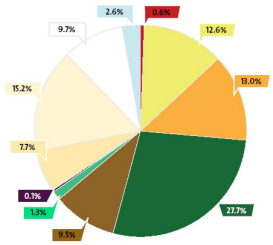

Fig. 1.2: Distribution of dominant land cover types. GLC-SHARE land cover database. Source: FAO

impact in earth surface from the epochs of huntering and gathering to technologist by way of agricultural with examples of enviromental changes and its timing. This kind of changes in vegetation due to natural or anthropogenic causes, are long term modifications that can last from years to millenials. But we find another modifications more

reduced in time scale as a response to seasonally varying weather patterns that are related with plants phisiology. This changes are related by the term phenology, that is defined as the timing of seasonal developmental stages in plant life cycles including bud burst, canopy growth, flowering, and senescence (Kimball, 2014). At last, forest fires can change large areas of vegetation cover in the scale of weeks-days although it can be a long term process of change too. About 65,000 fires take place every year in the European region, burning, on average, around half a million ha of forest areas and in the 95 % of the cases are due to human causes (Schmuck et al., 2011; San-Miguel-Ayanz et al., 2013).

In Figures 1.1 and 1.2 are depicted the distribution of dominant land covers of the GLC-SHARE database from Food and Agriculture Organization (FAO). There is a 28 % of the emerged earth covered by non vegetated surfaces (bare soil, snow and glaciers, water bodies and artificial surfaces) and the rest is covered by natural vegetation or croplands. These terrestrial biomes have a fundamental role in earth energy balance impacting weather and climate. Moreover, vegetation is a large yet variable sink and storage of CO_2 (McGuire et al., 2001) and in the process of photosynthesis is responsible for building up atmospheric oxygen to the level we enjoy today. Besides, vegetation is crucial in water cycle, controlling soil erosion, protecting the soil surface from raindrop splashing, increasing soil organic matter, soil aggregate stability, modifying soil chemistry, water holding capacity, hydraulic conductivity, retarding and reducing surface water runoff. As we can see vegetation cover has a vital importance in earth system and in our lifes.

In this framework, the work presented here will address the role of vegetation in weather and climate assessing its influence through the use of meteorological modeling. This introductory chapter will cover the main processes involved in land surface interactions with atmosphere with the aim of understanding the physical processes in which vegetation cover can be relevant. Then, will be reviewed how vegetation is considered in land surface models and which parameters are usually parameterized. At last, it will be treated how vegetation cover is relevant in the context of climate change.

1.1 Land surface interactions with atmosphere

1.1.1 Overview

Land surface interactions are mainly controlled by two processes that are basic for life on earth, **land water balance** and **land energy balance**. These main processes involving many others detailed processes are not separated and are coupled through evaporation. In the schematic representation of Seneviratne et al. (2010) we can see an overview of this two processes.

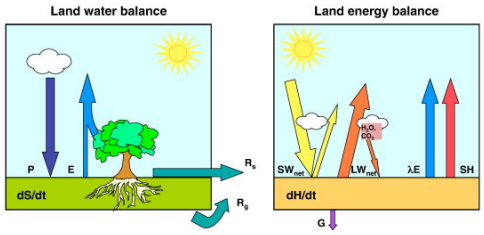

Fig. 1.3: Schematic of land water balance (left) and land energy balance (right) for a given surface layer. dS/dt refers to the change in water within the layer (soil moisture, surface water, snow). dH/dt represents the changes in energy for the same layer. See text for more details. Source: Seneviratne et al. (2010).

The **land water balance** for a surface layer including vegetation (Figure 1.3 left) without considering lateral exchange between adjacent soil volumes can be formulated as:

$$\frac{dS}{dt} = P - E - R_s - R_g \tag{1.1}$$

being dS/dt the change of water content within the given layer, P is precipitation, E is evapotranspiration, R_s is surface runoff and R_g is drainage. The evapotranspiration term E include bare soil evaporation, plants tranpiration, evaporation from the interception storage, snow, sublimation, and evaporation from surface water.

Utilizing energy provided by the energy balance, water is evaporated from open water surfaces and the soil, and is transpired by vegetation, being E the composite loss of water to the air from all sources. The water vapour is carried up into the atmosphere and eventually is cooled to its dewpoint and condenses as cloud droplets or ice crystals, that can grow in size and fall to surface as precipitation P (Oke, 1987). Then, P infiltrates into the ground and percolates downward, increasing soil moisture. The flow of R_s and R_g into rivers, lakes and ocean complete the cycle.

The **land energy balance** for the same surface soil layer (Figure 1.3 right) can be formulated as:

$$\frac{dH}{dt} = R_n - LE - H - G \tag{1.2}$$

and R_n is expressed as:

$$R_n = SW_{\downarrow} - SW_{\uparrow} + LW_{\downarrow} - LW_{\uparrow} \tag{1.3}$$

where dH/dt is the change of energy withing the considered surface soil layer (including vegetation), assumed to include all water storage components considered in 1.1. The net radiation (R_n) is separated into parts representing the incoming shortwave radiation ($SW_\downarrow$) from the sun and its reflected part ($SW_\uparrow$), longwave downwelling radiation ($LW_\downarrow$) and longwave upwelling radiation ($LW_\uparrow$). Finally, H is sensible heat flux, LE is latent heat flux and G is ground heat flux to deeper layers. For an infinitesimally small layer, dH/dt tends to zero and G is the ground heat flux at the surface.

This surface energy budget is initiated by the energy provided by sun radiation reaching the Earth's surface. The amount of solar energy absorbed by the surface ($SW_\downarrow$) is reduced from the top of atmosphere value due to absorption and reflection by clouds, scattering from air and reflection by surface albedo ($SW_\uparrow$). Energy from atmosphere that reaches the surface ($LW_\downarrow$), is due to emmision from clouds and gases from the atmosphere, and increases with increasing temperature, and increased concentrations of liquid water and greenhouse gases (H_2O and CO_2 mainly). The energy provided by this two radiation sources can be stored in the ground (G) or transfered to the atmosphere via sensible heat flux (H), latent heat flux (LE) or longwave radiation ($LW_\uparrow$). The partiotining of this energy into the storage (ground), sensible and latent heat components plays a significant role in determining the conditions of the atmospheric boundary layer affecting temperature, humidity and wind profile near the ground surface.

1.1.2 Surface terms in land water and energy balance

1.1.2.1 Sensible heat flux and latent heat flux

The partitioning of H and LE has a huge influence on the near surface variables, the depth and structure of the boundary layer, and the potential for precipitation (Stensrud, 2007).

Attending to Figure 1.4, can be seen how LE and H are significantly different considering distinct land types. For example, desert type has very low (high) LE (H) compared with crops type or forest type. But comparing locations with the same land type, the partition of energy can be quite different. Soil type, vegetation type and greenness and soil moisture determine how much energy is partitioned into H (warming air) and LE (moistening air).

H is defined as the rate of heat transfer per unit area from the ground to the atmosphere and can be expressed as:

$$H = \frac{\rho c_p (T_g - T_{air})}{r_H} \tag{1.4}$$

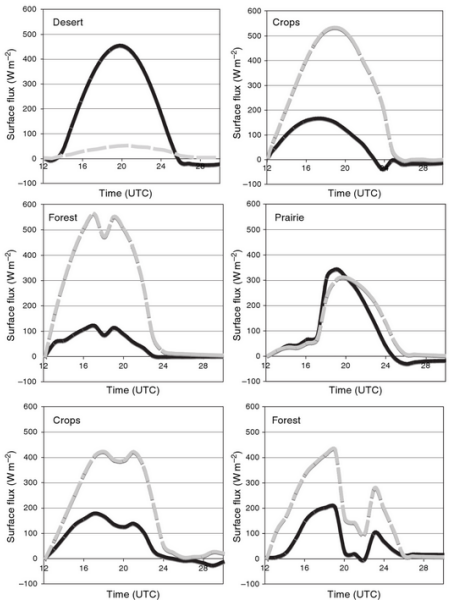

Fig. 1.4: Numerical model predictions of sensible (black) and latent (gray) heat flux for different land types over North America. Source: Stensrud (2007).

where ρ is air density, c_p is the specific heat of air, T_g is ground temperature, T_{air} is air temperature and r_H is defined as the resistance to heat flux.

LE is the rate of moisture transfer per unit area from the ground surface to atmosphere and can be expressed as:

$$LE = \frac{\rho L_v (q_{z_a} - q_{z_b})}{r_{V_{(a,b)}}} \tag{1.5}$$

where L_v is the latent heat of vaporization, r_V is the total resistance to latent heat flux and z_a and z_b refer to specific height where flux is calculated.

Both H and LE, are affected by the surface temperature and the air temperature, wind speed, wind shear and stability of the lower levels of the atmosphere. Vegetation influence H, owing to the height, coverage and structure of the vegetation affecting the ground and vegetation canopy temperatures, and the low-level wind shear. In the case of LE, vegetation plays a more dominant role, providing that it is able to transfer moisture from deep soil layers to the atmosphere. Soil type is important too, since water retention and infiltration differs between various soil types. And at last, soil moisture content is crucial in LE.

1.1.2.2 Ground heat flux

Ground heat flux is the rate of heat transfer from the ground surface into the deeper soil levels. As in the case of LE and H, it is influenced by surface temperature, soil type, soil moisture and vegetation. The upper 25 cm undergoes the largest diurnals changes in temperature, while in deeper layers changes occurs more slowly.

There is an approach implemented in multi-level soil models, that provides an equation for the ground surface and several specific soil levels below surface. This equation considers that the amount of heat transferred is proportional to the vertical temperature gradient (conduction):

$$G = -k_g \frac{\partial T}{\partial z} \tag{1.6}$$

where k_g is the thermal molecular conductivity and z increases in the downward direction. Considering no other sources and sinks of heat, and that ground heat flux $G = G_{z=0}$ at the ground surface(z=0), the second law of thermodynamics yields:

$$\frac{\partial T}{\partial t} = -\frac{1}{c_g} \frac{\partial G_{z=0}}{\partial z} \tag{1.7}$$

where c_g is the soil heat capacity and is equal to the soil density multiplied by the soil specific heat ($c_g = \rho_{soil}.c_{soil}$). Both, soil heat capacity and thermal conductivity are dependent upon the soil volumetric content and are depth varying.

1.1.2.3 Upwelling shortwave radiation

The upwelling shortwave radiation is controlled by albedo (0-1), that is defined as the fraction of the incoming solar radiation that is reflected upward from the Earth's surface. Surface albedo can change in bare soils by soil type and in vegetated surfaces can vary in function of type and coverage. Snow cover has a dramatically impact in albedo since new snow has an albedo near to 1 (practically all solar radiation is reflected). And not only that, but also the effect of human activities in land surface has a large impact in changing albedo, with activities like urbanization, deforestation, grazing or irrigation.

1.1.2.4 Upwelling longwave radiation

Upwelling longwave radiation can be expressed as:

$$LW_{\uparrow} = \varepsilon_g \sigma T_g^4 \tag{1.8}$$

where ε_g is the ground emissivity, σ is the Stefan-Boltzmann constant and T_g is the temperature at the ground surface. Surface emissivity is defined as the power by a body at temperature T to the power emitted by a black body at temperature T. The emissivity is defined as the ratio of the energy radiated from the surface to the energy radiated from an ideal emitter (black body emission / black body radiation) under the same conditions. It is a unitless quantity and ranges between approximately 0.6 and 1.0, but surfaces with emissivities less than 0.85 are typically restricted to deserts and semi-arid areas. Vegetation, water and ice have high emissivities above 0.95 in the thermal infrared wavelength range. In Figure 1.5 is depicted a global map from the ASTER Global Emissivity Database, where it can be observed the spatial variability of this variable.

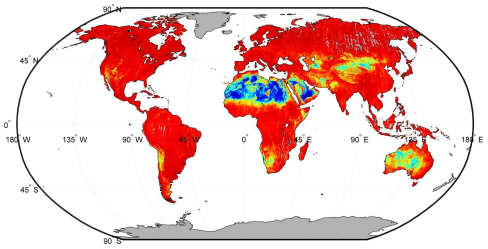

Fig. 1.5: Map of emmisivity calculated from ASTER Global Emissivity Database. Red colour indicates high emissivity values and blue colour low emissivity values. Source: NASA/GSFC/METI/ERSDAC/JAROS and U.S./Japan ASTER (www.asterweb.jpl.nasa.gov).

1.1.3 Land Surface Models (LSM)

Land surface interactions are considered from local scale to global scale in NWPM though Land Surface Models (LSMs). LSMs provide the physical lower boundary conditions in atmospheric models. The basic task of any LSM is to accurately simulate the partitioning of net radiation at the land surface into fluxes (H, LE and G) with the relevant information on land surface and climate data (Overgaard et al., 2006).

1.1.3.1 Evolution of Land Surface Models

LSMs have evolved in the last 50 years with models that have been adding increasing level of complexity that has involved multiple scientific disciplines. As a result, LSMs have expanded from their initial simple biophysical configurations, to include representations of soil moisture dynamics, stomatal functioning, land surface heterogeneity, surface hydrological processes, plant and soil carbon cycling, dynamic vegetation distributions, fire, urban environments, land cover and management, nitrogen cycling and crops. In Figure 1.6 is depicted the temporal evolution of LSMs and its increasing level of complexity with time.

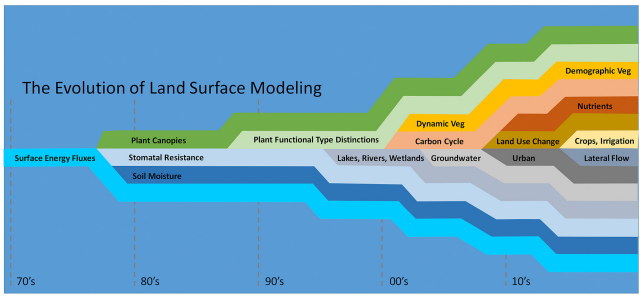

Fig. 1.6: A schematic depiction of the evolution of land surface model process representation through time, representing the approximate timing of emergence of different model components as commonly employed features of Earth system models. Source: Fisher and Koven (2020). Licensed under Creative Commons CC.

As a summary the next development chronology can be considered in LSM:

- **First-generation LSMs:** The first LSM was implemented by Manabe (1969) into a climate model using the Penman approach (Penman, 1948), assuming that the land surface evaporated water at the same rate as a wet surface (Overgaard et al., 2006). This parameterization has been considered as the "bucket" model, and used a simple energy balance equation, ignoring heat conduction into the soil as this model did not attempt to represent the seasonal or diurnal cycle (Pitman, 2003). This model implemented a globally constant soil depth and water holding capacity, where evaporation was limited by soil water content below a threshold. When soil moisture exceeded a prescribed limit, further precipitation generated runoff. The Manabe (1969) LSM and other simpler schemes considered in this group used simple bulk aerodynamic transfer formulations and tended to use uniform and prescribed surface parameters (albedo, z_0, water-holding capacity). Furthermore, vegetation was treated implicitly

and did not change with time and is common the inclusion of a single layer for soil moisture.

- **Second-generation LSMs:** This second generation models usually represent the vegetation-soil system such that the surface interacts with the atmosphere rather than being passive as occurred in the first generation LSMs (Sellers et al., 1997). The main milestone in this classification can be considered the work of Deardorff (1978) when he introduced a method for simulating soil temperature and moisture in two layers and vegetation as a single bulk layer. These second-generation models vary in detail, but they have many components in common: multiple soil layers, differentiation between soil and vegetation at the surface (albedo may vary spatially across a grid square), explicitly representation of the impact of vegetation on momentum transfer, explicit biophysical control on evaporation, model interception by the canopy and soil moisture parameterization mostly based in the set of diffusion equations based on Darcy's law (Pitman, 2003). Two of the most known second generation models are the Biosphere Atmosphere Transfer Scheme (BATS) (Dickinson, 1993) and the Sib model (Sellers et al., 1986).
- **Third-generation LSMs:** This LSMs include an explicit canopy conductance in order to improve the simulation of evapotranspiration and to address the issue of carbon uptake by plants. This models are able to respond physiologically as increasing CO_2 influences the canopy conductance and it can respond structurally by growing different leaves or taller trees (Pitman, 2003). In this way, LSMs can reproduce the response of the biosphere to increasing CO_2 a crucial aspect in climate change simulations.
- **Fourth-generation LSMs:** A further step in LSMs is integrating how the terrestrial biosphere respond to the atmosphere on time scales of months to years though the inclusion of ecological models. This models known as Dynamic Global Vegetation Models (DGVMs) incorporate a mechanism for changing the vegetation distribution with climate change. Another aspects considered are land use changes due to human activities with past and future estimated land use changes incorporated to climate models. Other processes considered are soil organic carbon, CH_4, N_2O, phosphorus and Biogenic Volatile Organic Compounds (BVOCs) cycles (Sato et al., 2015). At this moment modern LSMs encompasses a huge set of overlapping and interconnected disciplines relevant to this problem, like physics, biochemistry, physiology, ecology, hydrology, geography, statistics, mathematics, and high performance computing as has been reviewed by Fisher and Koven (2020).

1.2 Vegetation and land surface processes

Parameterization of vegetation in numerical weather prediction models (NWPM) is a challenging issue due to the complex mechanisms that surrounds the interactions between vegetation and atmosphere. Next is detailed how vegetation is described in NWPM and the most commom physical processes where it has a dominant role.

1.2.1 Characterization of vegetation in NWPM

There are three parameters widely used in NWPM that describes the state and the health of the vegetation: Leaf Area Index (LAI), Fraction Vegetation Cover (FVC) and vegetation type (Stensrud, 2007). These are defined as follows:

- **Fraction Vegetation Cover** is defined as the fraction of horizontal area associated with the photosynthetically active green vegetation that occupies a model grid cell (Gallo et al., 2001).
- **Leaf Area Index** is a measure of the vegetation biomass and is defined as the sum of the one-sided area of green leaves above a specified area of ground surface and plays an important role in determine the amount of transpiration by plants.
- **Vegetation type** specifies the dominant vegetation within a model grid cell.

There are ground based methods for obtaining this parameters but it would be impossible to use this routinely. In this way, collected data obtained from remote sensing are used for giving this information. One of the most common parameters used from remote sensing in this framework, is the **Normalized Difference Vegetation Index** (NDVI) that is expressed as:

$$NDVI = \frac{NIR - VIS}{NIR + VIS} \tag{1.9}$$

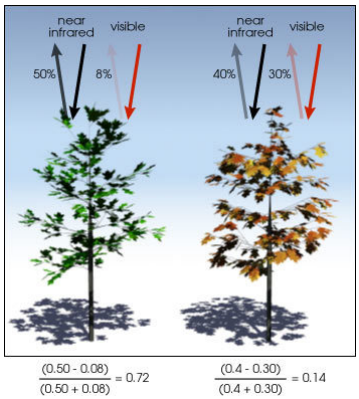

Fig. 1.7: NDVI is calculated from the visible and near-infrared light reflected by vegetation. Healthy vegetation (left) absorbs most of the visible light that hits it, and reflects a large portion of near-infrared light. Unhealthy or sparse vegetation (right) reflects more visible light and less near-infrared light. Illustration by Robert Simmon. Source: NASA Earth Observatory (https://earthobservatory.nasa.gov).

where NIR and VIS are the amounts of near-infrared and red visible, respectively, reflected by the vegetation and captured by the satellite sensor (Pettorelli et al., 2005). As is depicted in Figure 1.7, this index is based on the fact that bare soils or unhealthy vegetation are fairly constant in NIR and red visible and healthy vegetation absorbs most of the visible and reflect a great part of the NIR. This index is highly correlated with the photosynthetically active biomass, chlorophyll abundance and energy absorption (Myneni et al., 1995).

There are several datasets of NDVI, since these are generated from different satellite sensors and methods of postprocessing. Among these satellite sensors are remarkable the Advanced Very High Resolution Radiometer (AVHRR), the NASA's Moderate Resolution Imaging Spectrometers (MODIS), SPOT, LANDSAT, PROBA-V or Himawari. From this sources, different methods of correction for clouds, aerosols or satellite artifacts can be developed for obtaining the final NDVI datasets. This can lead to products with noteworthy differences between them and therefore influence the final calculation of products that describe vegetation, like FVC or LAI. This matter has been treated in Chapter 3, in Sections 3.2.1 and 3.3.

1.2.1.1 Fraction vegetation cover

FVC acts as the weighting factor between bare soil and canopy transpiration. In Figure 1.8 can be seen an example of calculation of FVC applying a color detection algorithm, and can be used as an illustration of how vegetation is represented through this variable in a model grid cell of a NWPM. But as commented previously, FVC is normally calculated from NDVI data since there is a strong relationship between this variables. The problem arises with the calculation methods, since there is a great variety of them found in the use of this variable in NWPM simulations. This has been adressed in Chapter 3, in Sections 3.2.2, 3.3.1 and 3.3.2 where differents methods of calculation of FVC are described and compared.

Another fact of relevance is the temporal resolution used for this variable. As commented in the introductory paragraph, changes in vegetation are affected by different temporal scales that using climatologies can mask. For example, changes related with phenology or the response of vegetation to interannual regimes of temperature and precipitation, can lead to great differences in FVC from year to year. This issue has been treated in Chapter 3, in Section 3.3.3 and more broadly in Chapter 5.

Spatial resolution is another aspect that matters in using FVC in NWPM. For example, NDVI from the Global Vegetation Index (GVI) with 16 km resolution from AVHRR sensor was employed by Gutman and Ignatov (1998) to derive the FVC dataset that is still used in the Weather and Research Forecasting (WRF) model. Nowadays, NDVI products can have a spatial resolution greater than 1 km, that can lead to detailed FVC datasets with greater spatial variability and with potential to improve NWPM simulations. In Chapter 5, is showed an example of using the Copernicus FVC dataset with a original resolution of 1 km instead of the FVC dataset commented previously used in WRF and MM5 models. In Section 5.1 are reviewed examples of using detailed FVC datasets.

1.2.1.2 Leaf Area Index

In Figure 1.9a is depicted a visual representation of LAI for different vegetation types. For example, semi arid shrublands have a LAI index of 0.8 compared to three-tiered forest with a LAI of 5. More leaves or more vertical density (larger LAI values) imply a greater amount of transpiration. One of the methods for calculation of LAI can be hemispherical photographs from ground (1.9b), where the ratio of the area of canopy to sky can gives an approximated value. LAI used in NWPM simulations is usually calculated from NDVI although NDVI has limited sense to LAI values greater than 3-4. As can be seen in a curve typically found when plotting values of NDVI versus LAI (Figure 1.10), this curve slowly asymptotes to the maximum NDVI value as LAI increses. So this is

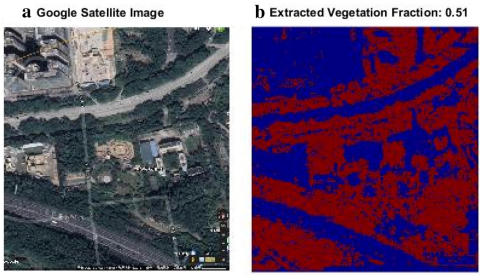

Fig. 1.8: a) Google image of an urban area in Shenzen (China) b) Vegetation fraction extracted by applying a color detection algorithm to an RGB version of the image. Source: Wong et al. (2019). Licensed under Creative Commons CC.

a reasonable relationship for midlatitude deciduous forests and grasslands, but is not accurated for coniferous forests or tropical regions. As was mentioned for FVC, temporal resolution and spatial resolution also matters in the calculation of LAI from NDVI data. FVC and LAI are not entirely independent parameters, depending on how LAI is defined. In this way, a quadratic relationship between NDVI and FVC is more suitable when LAI is less than 3 (Carlson and Rypley, 1997; Montandon and Small, 2008)

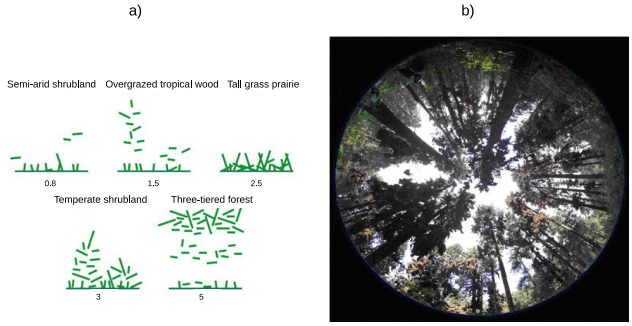

Fig. 1.9: a) Examples of LAI for several vegetation types. Source: Thomas C. Hart b) Example of hemispherical photograph of forest canopy. The ratio of the area of canopy to sky is used to approximate LAI. Source: S.B. Weiss.

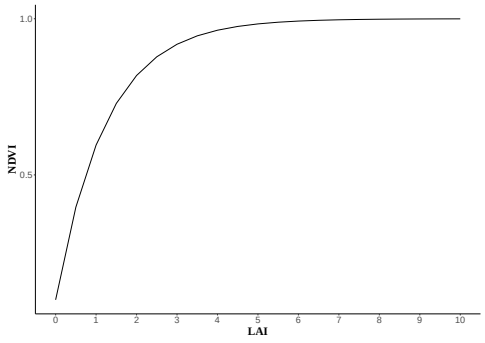

Fig. 1.10: Example of curve plotting values of NDVI and LAI. Saturation is reached when LAI is greater than values of 3-4, and values of NDVI are constant while LAI increase. Source: Stensrud (2007).

1.2.1.3 Vegetation type

From NDVI data, a large number of vegetation categories (255 in Eurasia, 961 globaly) can be clustered using unsupervised classification and an extensive post-classification stratification using remote sensing data (Loveland et al., 2000). But it would be very difficult to implement this in a NWPM and would have a great uncertainty of improvement in model results (Stensrud, 2007). In this manner, in NWPM are used normally less than 30 categories. An example of land use classification for Europe can be seen in Figure 1.11 where 13 land cover classes have been chosen. In most of the NWPM, vegetation classes are used to parameterize other physical parameters as roughness length, emmisivity or albedo with look-up tables, so its definition can have a large impact in land-atmosphere interactions.

1.2.2 Physical processes implied in vegetation-atmosphere interactions

1.2.2.1 Evapotranspiration control by plants

Plants use photosynthetically active radiation to combine water and CO_2 into sugars and other organic compounds. In this process of photosynthesis, is allowed the transfer of CO_2 from the atmosphere to plant's cells and then water loss occurs. Plants regulate the amount of CO_2 exchanged and water loss, by means of valve-like structures on the leaf surface called stomates. With this structures plants try to maximize the ratio

Fig. 1.11: Land cover map of Europe for the year 2017 with 13 land cover classes. Source: Malinowski et al. (2020).

between CO_2 exchanged and water loss and in order to capture the CO_2 needed for photosynthesis without losing too much water.

Hereafter, are enumerated some of the process that are relevant in plants evapotranspiration:

- Conservation of moisture when necessary by plants closing their stomates.
- Interception of precipitation and moisture on leaf surfaces.
- Effect of increasing atmospheric CO_2 due to burning fossils in some plants, acts decreasing evapotranspiration and increasing temperatures.

An example of how this can be parameterized in LSMs can be found for the Noah LSM in Section 2.2.3.3.

1.2.2.2 Momentum transfer

Vegetation canopies are a rough surface with large values of roughness length (z_0). These higher values of z_0 result in lower values of resistance parameters r_H and r_V and hence higher values of H and LE are found in vegetated surfaces (equations 1.4 and 1.5). In NWPM usually z_0 is provided as function of land cover type by means of look-up tables as was commented in Section 1.2.1.3.

Seasonal changes in vegetation can have a large impact in modify z_0 and therefore altering surface fluxes. Furthermore, vegetation have a great spatial variation creating a patchy landscape that can alter low level winds. For this reason is relevant a detailed

definition of this variable although the prescription with look-up tables can be inadequate for dealing the temporal variations that can occur in vegetation.

1.2.2.3 Soil moisture availability

Evaporation from bare soils occurs only in a shallow depth of soil. With very dry situations soil sealing and crusting can occurs acting as a barrier to further upward moisture transport through soil. But vegetated surfaces have the ability to drain deeper moisture sources, since rooting zone can extend over a deeper layer. In this way, rooting depth determines the active soil zone that has potential to return water back into the atmosphere via plant transpiration profoundly affecting land surface fluxes and carbon cycle (Yang et al., 2016b). In Figure 1.12 is depicted global spatial variability of rooting depth where deeper roots (typically greater than 1.5 m) are generally observed in tropical and subtropical regions and shallower hydrologically active soil layers (less than 0.5 m) occur in arid or cold regions.

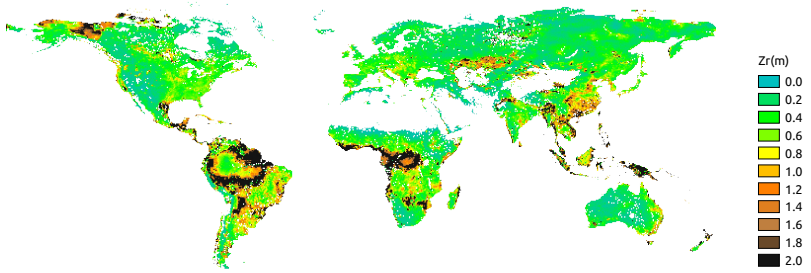

Fig. 1.12: Global spatial pattern of effective plant rooting depth (Zr). Source: Yang et al. (2016a).

This capacity of plants of extracting soil moisture from deep layers of the soil illustrates the importance of the amount, the type and the variability of vegetation in the control of LE fluxes.

1.2.2.4 Radiation and surface albedo

Vegetation type and amount influence the radiation that reach the surface and have an important effect in determine the surface albedo as it was described in Section 1.1. Physical schemes that considers a single temperature for the soil-vegetation surface don't need to take into account modifications in the radiation due to vegetation inluence. In this cases surface albedo can be parameterized with look-up tables depending of vegetation type or a gridded albedo can be considered using climatological or synchronous values.

More complex vegetation schemes, that include a separate temperature equations for the ground (mixture of ground cover and vegetation canopy) and the vegetation canopy, require some modifications to incorporate the multiple reflections of light by the leaves and the ground surface (Stensrud, 2007). As it was commented in the explanation of the NDVI index, leaves are highly absorbent in the visible wavelength interval between 400 and 720 nm, where absorption of radiation by chlorophyll in the leaves generally occurs (also called direct photosynthetically active radiation, PAR), and moderately reflective in the NIR. In this way, the approach of Sellers et al. (1986) in the Simple Biosphere Model (Sib) takes into acount modifications to the radiation calculations to produce values for PAR, diffuse PAR, NIR, diffuse NIR and diffuse infrared radiation. The albedo is allowed to vary during the daytime, requiring information on leaf angle, and leaf trasnmissions and reflection of radiation.

A sample of how surface albedo is modified by vegetation is showed in Figure 1.13 where globes cover most of Asia, eastern Europe and the Middle East, for each of the four seasons in the years 2003 and 2004. The globes in the image show a particular kind of albedo, formally known as Directional Hemispherical Reflectance (DHR), in which all scattering effects from the atmosphere are removed. A heavily vegetated surface area will therefore have a small DHR-PAR value (blue on the color scale) while non-vegetated areas where absorption is small in the PAR region will tend to have high values of DHR-PAR (green to red on the color scale). In this globes can be depicted the annual and interannual variations in albedo that can have a non negligible impact in NWPM.

The first example of how changes in vegetation can affect surface albedo and its impact in climate is founded in the 1970s in Charney (1975) who proposed a mechanism to link the Sahelian droughts to increase in albedo. This hypothesis relies only on the radiation balance (Patil et al., 2014) but later works emphasize that vegetation cover can change the absorption of solar energy by the surface as well as its redistribution to the atmosphere in the form of heat fluxes (Charney et al., 1977; Eltahir, 1998; Reale and Dirmeyer, 2000).

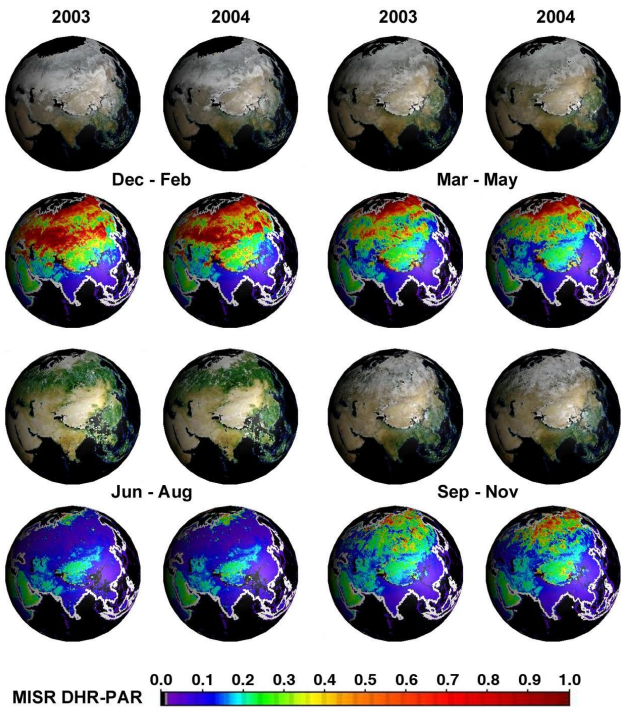

Fig. 1.13: Seasonal DHR-PAR (albedo) for years 2003 and 2004 obtained from NASA's Multi-angle Imaging SpectroRadiometer(MISR). Source: NASA/GSFC/LaRC/JPL/MISR Team (https://www.jpl.nasa.gov).

1.2.2.5 Vegetation change on soil properties

Vegetation can have a shadowing effect in soil due to the presence of roots and abundance of organic matter in the topsoil (Yang et al., 2005). This can affect heat transport through soil due to reduced thermal conductivity and hence reduced G (see equation 1.6). This reduction in G can be important since it implies greater enegy available for LE (Choudhury et al., 1987; Yang et al., 1999). Other changes in soil properties can include high porosity or high soil water potential that can enhance LE (Yang et al., 2005).

Different parameterizations can be found for dealing with soil and vegetation effect. One can be found in the European Centre for Medium Weather Forecast (ECMWF) model land surface scheme where soil heat flux is computed as the product of an empirical coefficient and the temperature difference between the surface and the (center of the)

upper soil layer (Viterbo and Beljaars, 1995). Another example is the approximation of Peters-Lidard et al. (1997) in which in the presence of a vegetation layer soil heat flux is reduced lowering heat thermal conductivity. This approximation will be covered in more detail in Section 2.2.3.

1.3 The role of human induced vegetation changes in the context of climate change

Variations in vegetation or land use type can induce significant changes in climate. In the early study of Sagan et al. (1979), was made an estimation of the probable anthropogenic global albedo change over the past millenia and suggested that humans have made substantial contributions to global climate changes during the past several millennia, and perhaps over the past million years. Chase et al. (2001) found that the historical total of human landcover changes have had a comparable effect on climate to that of historical increases in CO_2 and aerosols. In the Mediterranean area, Reale and Dirmeyer (2000) and Reale and Shukla (2000) performed an experiment to quantify the sensitivity of regional climate to changes in vegetation around the Mediterranean basin, corresponding to vegetation change during the Roman Classical Period (2000 years BP). Their results suggested that this large deforestation contributed to the dryness of the current climate through changes in surface albedo that has altered the atmospheric circulation over northern Africa and the Mediterranean.

Another effect of vegetation in the context of climate change is related with the ability of vegetation to effectively utilize increased carbon dioxide to increase global biomass. One of the effects is that this may result in reduced carbon dioxide warming from what otherwise would occur. Other effect indicated by Henderson-Sellers et al. (1995) is that such changes can lead to decreased evapotranspiration and increased temperatures in boreal and tropical forest, because plants open their stomata less and are therefore more water efficient.

An important conclusion raised by Cotton and Pielke Sr (2007) analyzing regional and global studies related with land use/land cover change (LUCC), is that the spatial patterning of this changes result in changes over time in regional tropospheric diabatic heating patterns. These changes in the patterns on the regional scale result in alterations in global circulation patterns that can have more of an influence than the more spatially homogeneous climate forcing of the radiative effect of increasing CO_2. An example of studying the characteristics of LUCC on Earth's surface energy balance can be found in Duveiller et al. (2018), and their results illustrate that biophysical effects of vegetation cover change vary considerably in geographic and climate space. Their assessment shows that in ecosystems where vegetation growth is limited by water availability the

climate impacts of a vegetation cover transition are dominated by changes in evapotranspiration, whereas in ecosystems where vegetation growth is limited by energy, such as boreal shrublands, the perturbation of the surface temperature is dominated by changes in the radiative and aerodynamic properties of those ecosystems. Comparing the effect of greenhouse change and LUCC and their impact on 20th century anthropogenic climate, a recent study of Yan et al. (2020b) restate the conclusions of Cotton and Pielke Sr (2007). In this work, one of the results is that the biogeophysical effect of historical LUCC can offset the warming induced by increased greenhouse gases, but the overall impacts of LUCC and greenhouse gases changes tend to be linear in their combination. They propose that more attention should be paid to the interactions between external forcings and internal variabilities, especially over the regions where nonlinearity is strong.

Another relevant fact considered by Cotton and Pielke Sr (2007) is that changes in vegetation in the perspective of global warming potential have been considered during a long time due to changes in surface albedo since this variable can be quantified in terms of radiative forcing. But vegetation changes are related not only with albedo but with LAI or FVC, that can affect partitioning of available energy into LE and H with a direct impact on near-surface air temperature and influence as a climate forcing. As has been commented previously, this regional land use changes induce a spatial redistribution of land surface H and LE patterns that results in a global climate change although global averaged values are unchanged. The work of Bright et al. (2017) compared the relevance of this non-radiative mechanisms respect to changes in surface albedo in the local direct temperature response by commom land cover and land management change perturbations. They found that non-radiative mechanism dominated in eight of nine of this commom perturbations.

In several articles (Pielke Sr, 2002; Pielke, 2005; Pielke Sr et al., 2011; Mahmood et al., 2016), Roger A. Pielke and collaborators have adressed that land use and land cover changes have not been adequately considered in the Intergovernmental Panel on Climate Change (IPCC). Although the effects on the impact on the atmospheric concentrations of CO_2 and CH_4 and on the global surface albedo have been included, the role of land use and land cover change and variability in altering climate variables has been mostly overlooked. In 2019, the IPCC special report of Climate Change and Land (Shukla et al., 2019) have considered this gap, and assesses climate forcing of land change at local, regional and global scales.

1.4 Study area

The study area in which the regional climate simulations are performed is the Iberian Peninsula (IP). IP is an interesting case study due to its varied orography, its position

affected by the Mediterranean and Atlantic Sea and its latitude in a transition between temperate and subtropical latitudes.

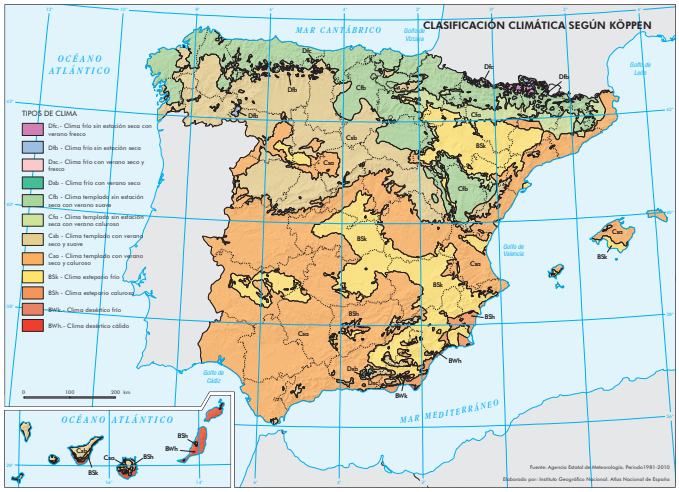

Fig. 1.14: Köppen climate classification from the Instituto Geográfico Nacional. Atlas Nacional de España (ANE) CC BY 4.0. Source: www.ign.es/resources/ane/participantes.pdf

The surface that range the IP has the enough width to act like a little continent, in which the interior lands can be partially out of sea influence. In this way, two areas with a remarkable effect in temperature are differentiated, a peripheral halo open to the Mediterranean and Atlantic influence, and a inner lands core with a clear continental tendency. Another relevant fact is the precipitation pattern, that mainly divides the IP in an humid and dry subregion. The humid subregion is defined mainly in the more septentrional areas, forming a large arc of convexity to the Nortwest ranging from Eastern Pyrenees to Southern Portugal, with an annual precipitation superior to 600 mm and reaching some interior mountain ranges with high relief. The dry region with a precipitation between 600 and 300 mm spans the rest two thirds of the IP, and this precipitation usually does not occurs in summer causing a relevant hydric stress. This dry region can be subdivided in a semiarid area with a precipitation less than 250 mm, that range some parts of the Ebro Valley and a great sector in the south east angle of the IP (Vilá Valentí, 1983). From this general climatic description, mediterranean climate is the dominant in the IP with mild and wet winters, warm and dry summers, and, autumn and springs variables in temperature and precipitation. Oceanic climate covers north-northwest of

the IP with high precipitations that are more reduced in summer and mild temperatures throughout the year, showing a reduced annual temperature range. The Köppen climate classification from the Instituto Geográfico Nacional is depicted in Figure 1.14 where are depicted the location of Mediterranean (Csa and Csb types), Oceanic (Cfb), Arid (Bw) and Semiarid (Bs) climates.

This climatic conditions and mainly the hydric regime define vegetation and soil conditions. In the humid IP dominate deciduous forests with deep soils, tending to pines and heather shrubs in siliceous soils. While in the dry IP, dominate shallow soils with xerophytic perennial plants with broad and needle leaves adapted to hydric stress.

In Figure 1.15 is depicted Copernicus Land Use (Buchhorn et al., 2021) in the area of the Iberian Peninsula. Agricultural areas cover most of the great vallleys of the IP (Ebro, Tajo, Duero, Guadiana) and forest land types cover above all the humid subregion and areas of high relief. Deciduous forests are represented mostly in the north of the IP .

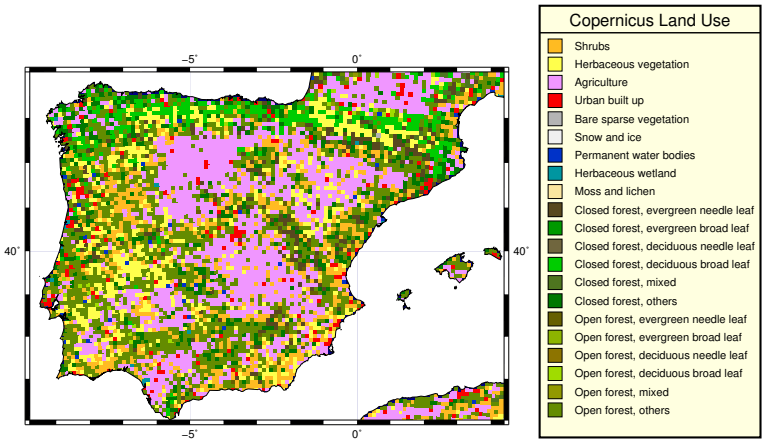

Fig. 1.15: Copernicus Land Use spanning the Iberian Peninsula.

1.5 Objectives of the Thesis

This Thesis assesses the contribution of the variable FVC in the Noah LSM coupled to a climate version of the MM5 model. FVC has a determinant role in the weighting of evaporation between bare soil and canopy transpiration. Reviewing subsection 1.2.2, the

main physical processes implied in Noah LSM in relation with FVC are evapotranspiration control by plants, soil moisture availability and vegetation change on soil properties. This physical processes can have a large impact in surface variables like air temperature or relative humidity due to the changes in the distribution of surface fluxes. In the framework of climate change, a proper consideration and knowledge of FVC is relevant since vegetation changes can be considered as a climate forcing at local, regional and global scales.

Regarding the aforementioned aspects, the main goals of this Thesis are the next:

- Assess the sensitivity of the Noah LSM to the variations in FVC.
- Analyze the implications and potential improvements in model performance of using a more realistic FVC dataset instead of the most common climatologies.

For reaching out this goals, first has been developed the task of studying the degree of impact of calculate FVC from NDVI data using different methodologies (Chapter 3). Three different methods of calculation have been compared and tested with the MM5 model, addressing its final impact in simulated fields of 2 meters air temperature (T2m) in a one year simulation. In Chapter 4, has been evaluated the effect of modifying FVC in surface fluxes and its final effect in maximum and minimum temperatures. This has been accomplished by means of two ideal simulations running during a year with fixed values of FVC of 30 % and 90 %, with the aim of simplify the obtained results. This has allowed a better understanding of the impact of soil moisture in canopy resistance and its final contribution to the allocation of energy between LE and H. Finally, in Chapter 5, a set of simulations spanning from year 2000 to 2017 have been conducted in order to assess the difference between use a climatological dataset of FVC with coarse resolution and the synchronous FVC dataset of Copernicus. For evaluating this differences, simulated surface fields of T2m have been compared with surface observatories and gridded datasets. Besides, simulated trends along the 18 years considered have been calculated and intercompared for a better understanding of how long term variations of FVC can affect simulated trends of T2m in a RCM.

This Thesis is structured in the following manner: Chapter 2 describes MM5 and Noah LSM models and the model configurations used in the simulations. Chapter 3 compares three different FVC calculation methodologies from NDVI data and its impact in a RCM. Chapter 4 address the main physical processes that affects the T2m response to changes in FVC. Chapter 5 shows the results of 2000-2017 regional climate simulations comparing a climatological FVC dataset with the varying temporal FVC Copernicus dataset. Chapter 6 presents the main conclusions of this Thesis.

2

Model description and configuration

This chapter describes the Noah LSM and the modeling setup used with the MM5 model (Grell et al., 1994) for Chapters 3, 4, 5 and 6. Although there are differences in the simulated period of this chapters the model setup is the same. The initial and boundary conditions for driving the simulations and the databases and look up tables used are also described in this chapter.

2.1 MM5 Model description

MM5 is the fifth generation of the NCAR/Penn State Mesoscale Model (Grell et al., 1994). The main characteristics of this model include (i) multiple-nest capability, (ii) nonhydrostatic dynamics, and (iii) a four-dimensional data assimilation (Newtonian nudging) capability, (iv) increased number of physics options, and (v) portability to a wider range of computer platforms, including OpenMP and MPI system.

Terrestrial and isobaric meteorological data are horizontally interpolated (programs TERRAIN and REGRID) from a latitude-longitude grid to a mesoscale, rectangular domain on either a Mercator, Lambert Conformal, or Polar Stereographic projection. Program INTERPF then performs the vertical interpolation from pressure levels to the σ coordinates of the MM5 model. After preparing the data, simulations can be performed with the module MM5.

2.1.1 Model horizontal and vertical grid

The modeling system usually gets and analyzes its data on pressure surfaces, but these have to be interpolated to the model's **vertical coordinate** before being input to the model. The vertical coordinate is terrain following (Figure 2.1) meaning that the lower grid levels follow the terrain while the upper surface is flat. Intermediate levels progressively flatten as the pressure decreases toward the chosen top pressure. A dimensionless quantity σ is used to define the model levels:

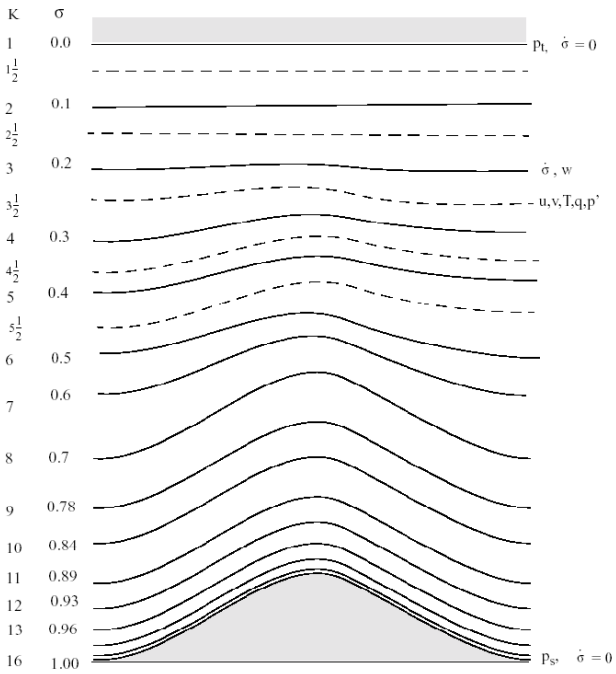

Fig. 2.1: Schematic representation of the vertical structure of the model. Example for 15 vertical layers. Dashed lines denote half-sigma levels and solid lines denote full-sigma levels. Source: Grell et al. (1994).

$$\sigma = \frac{(P_0 - P_t)}{(P_{S_0} - P_t)} \tag{2.1}$$

where P_0 is the reference-state pressure, P_t is a specified constant top pressure and P_{S_0} is the reference-state surface pressure. σ is zero at the model top and one at the model surface, and each model level is defined by a value of σ. The model vertical resolution is defined by a list of values between zero and one that do not necessarily have to be evenly spaced. Normally the resolution in the boundary layer is much finer than above.

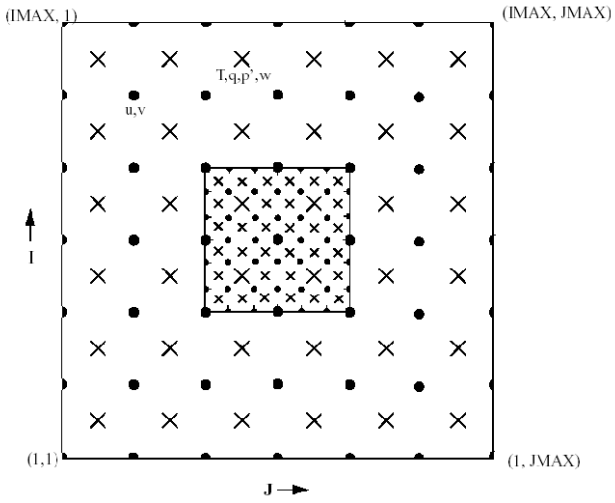

Fig. 2.2: Horizontal Arakawa B-grid staggering of the dot (u,v) and cross points (scalars). The smaller inner box is a representative mesh staggering for a 3:1 coarse-grid distance to fine-grid distance ratio. Source: Grell et al. (1994).

The **horizontal grid** has an Arakawa-Lamb B-staggering of the velocity variables with respect to the scalars. This is shown in Figure 2.2 where it can be seen that the scalars (T, q etc.) are defined at the center of the grid square, while the eastward (u) and northward (v) velocity components are collocated at the corners. The center points of the grid squares will be referred to as cross points, and the corner points are dot points. Hence horizontal velocity is defined at dot points, for example, and when data is input to the model the preprocessors do the necessary interpolations to assure consistency with the grid.

All the above variables are defined in the middle of each model vertical layer, referred to as half-levels and represented by the dashed lines in Figure 2.1. Vertical velocity is carried at the full levels (solid lines). In defining the σ levels it is the full levels that are listed, including levels at 0 and 1. The number of model layers is therefore always one

less than the number of full σ levels. Note also the I, J, and K index directions in the modeling system.

2.1.2 Nesting

MM5 contains a capability of multiple **nesting** with up to nine domains running at the same time and completely interacting. There are two possible options of nesting: two-way and one-way. "Two-way interaction" means that the nest's input from the coarse mesh comes via its boundaries, while the feedback to the coarser mesh occurs over the nest interior. The nesting ratio bewteen domains is always 3:1 for two-way interaction. One-way nesting considers that the model is first run to create an output that is interpolated using any ratio (not restricted to 3:1), and a boundary file is also created once a one-way nested domain location is specified. Therefore one-way nesting differs from two-way nesting in having no feedback and coarser temporal resolution at the boundaries. A possible configuration of nesting is shown in Figure 2.3. It can be seen that multiple nests are allowed on a given level of nesting (e.g. domains 2 and 3), and they are also allowed to overlap. Domain 4 is at the third level, meaning that its grid size and time step are nine times less than for domain 1. Each sub-domain has a "Mother domain" in which it is completely embedded, so that for domains 2 and 3 the mother domain is 1, and for 4 it is 3.

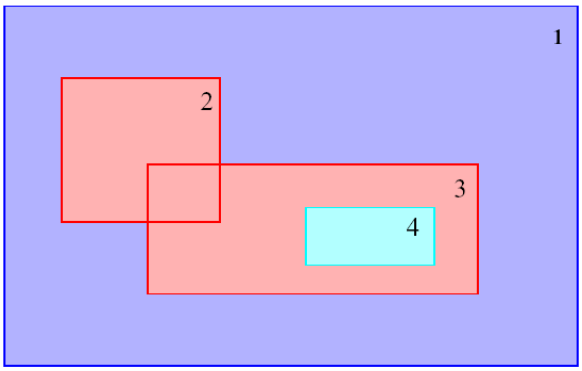

Fig. 2.3: Horizontal Arakawa B-grid staggering of the dot (u,v) and cross points (scalars). The smaller inner box is a representative mesh staggering for a 3:1 coarse-grid distance to fine-grid distance ratio. Source: Grell et al. (1994).

More details related with the basic equations of the model, derivation, coordinate transformation, spatial and temporal finite differencing can be found in (Grell et al., 1994).

2.2 Noah Land Surface Model

2.2.1 Brief history of Noah LSM development

The Noah land surface model (LSM) is one of the most robust and well established models of its kind for meteorological and climate modeling (Campbell et al., 2019). The origin of the Noah LSM is the Oregon State University LSM (OSU LSM) originally developed by Pan and Mahrt (1987). Chen et al. (1996) extended this model, including an explicit canopy resistance formulation used by Jacquemin and Noilhan (1990) and a surface runoff scheme of Schaake et al. (1996). The Noah LSM is the result of long-term, overlapping and continued development in land surface modeling initiated by the four agencies that comprise its name: National Center for Atmospheric Research (NCAR), Oregon State University, the U.S. Air Force, and National Centers for Environmental Prediction's (NCEP's) Office of Hydrology (Campbell et al., 2019). This model has a long history of development for more than three decades (Mahrt and Ek, 1984; Mahrt and Pan, 1984; Chen et al., 1996; Ek et al., 2003; Niu et al., 2011) and has been widely studied in the MM5 and WRF community. Noah LSM has been used by the National Centers for Environmental Prediction (NCEP) formerly in the Eta model (Ek et al., 2003) and currently in the Global Forecast System (GFS) and North American Mesoscale (NAM).

The Noah LSM version used in these simulations is 2.7.1 (Ek et al., 2003), currently used in GFS. The treatment of FVC remains the same in subsequent versions of Noah LSM, except for the calculation of z_0 and emmisivity that are FVC dependent in version 3.2 (Best et al., 2015).

The evolution of Noah LSM incorporating characteristics of third generation models (see Section 1.1.3.1) is the Noah with multiparameterization options model (Noah-MP) (Niu et al., 2011). This LSM considers the next augmentations respect the Noah-LSM: 1) a vegetation canopy layer to compute the canopy and the ground surface temperatures separately, 2) a modified two-stream radiation transfer scheme considering canopy gaps to compute fractions of sunlit and shaded leaves and their absorbed solar radiation, 3) a Ball-Berry type stomatal resistance scheme that relates stomatal resistance to photosynthesis of sunlit and shaded leaves, 4) and a short-term dynamic vegetation model. The design of the augmented Noah enables the choice of multiple, alternative options for each physical process.

2.2.2 Description of the model

Noah LSM is based on the coupling of the diurnally dependent Penman potential evaporation approach of Mahrt and Ek (1984), the multilayer soil model of Mahrt and Pan (1984), and the primitive canopy model of Pan and Mahrt (1987). It has been extended by Chen et al. (1996) to include the modestly complex canopy resistance approach of Noilhan and Planton (1989) and Jacquemin and Noilhan (1990). It has one canopy layer and the following prognostic variables: soil moisture (SM) and temperature in the soil layers, water stored on the canopy, and snow stored on the ground. For the soil model to capture the daily, weekly, and seasonal evolution of SM and also to mitigate the possible truncation error in discretization, four soil layers are used, and the thickness of each layer from the ground surface to the bottom are 0.1, 0.3, 0.6, and 1.0 m, respectively. The total soil depth is 2 m, with the root zone in the upper 1 m of soil. Thus, the lower 1-m soil layer acts like a reservoir with a gravity drainage at the bottom. An schematic representation of Noah LSM is depicted in Figure 2.4.

According to the classification given in Section 1.1.3.1, Noah LSM uses bulk aerodynamic transfer equations and calculates evaporation based on Penman approach that are commom in first generation models. On the other hand, a combined surface layer of vegetation and soil surface over which surface energy fluxes are computed and multiple soil layers, have characteristics of second generation models.

2.2.3 Physics model

2.2.3.1 Surface energy balance

Following equations 1.2, 1.3, 1.8, land surface energy balance in Noah LSM (Ek and Mahrt, 1991; Zheng et al., 2015) is written as:

$$S_{\downarrow} - S_{\uparrow} + \varepsilon_g (L_{\downarrow} - \sigma T_g^4) = G_0 + H + LE \tag{2.2}$$

where $S_{\downarrow}$ ($\mathrm{Wm^{-2}}$), $S_{\uparrow}$ ($\mathrm{Wm^{-2}}$), ε_g (unitless), $L_{\downarrow}$ ($\mathrm{Wm^{-2}}$), σ (taken as 5.67×10^{-8} $\mathrm{W\ m^{-2}\ K^{-4}}$) , T_g (K), G_0 ($\mathrm{Wm^{-2}}$), H ($\mathrm{Wm^{-2}}$) and LE ($\mathrm{Wm^{-2}}$) were previously defined in Section 1.1.

The sensible heat flux is described with bulk equations based on the Monin-Obukhov similarity theory (Chen et al., 1997) as:

$$H = \rho c_p C_h (\theta_g - \theta_{air}) \tag{2.3}$$

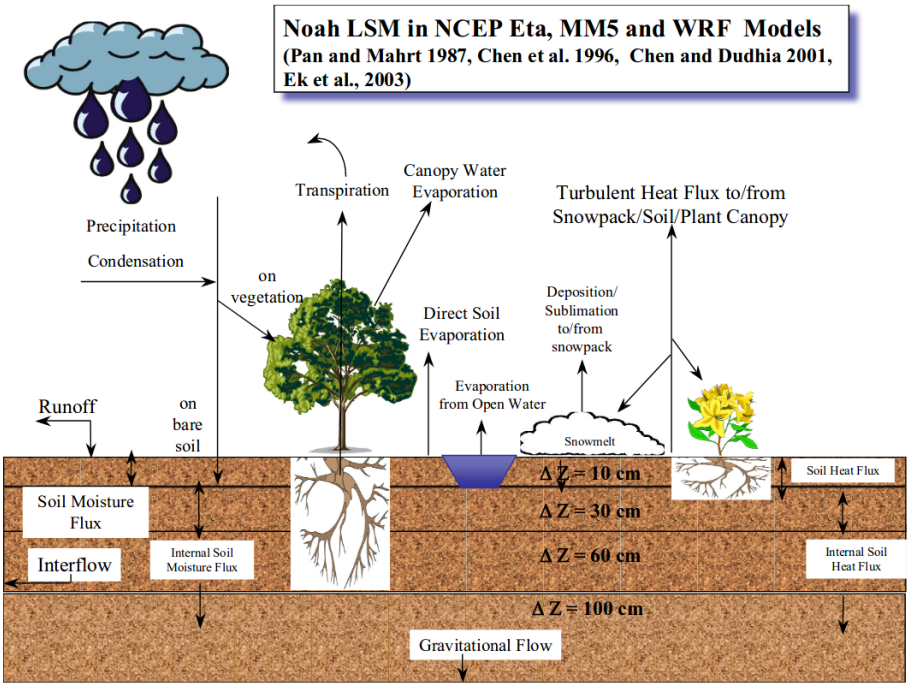

Fig. 2.4: Schematic representation of the Noah LSM with the processes involved on bare soil, vegetated soil, snow and open water. Representation of soil layers depicting soil misture flux, gravitational flow and soil heat flux. Source: Chen (2007).

where ρ (kg m^3), c_p (J kg^{-1} K^{-1}) were defined in 1.4. C_h is the surface exchange coefficient for heat transfer (unitless), θ_g is the potential temperature at surface (K) and θ_{air} is the potential air temperature (K).

The potential evapotranspiration LE_p is calculated diurnally from 1.5 using a Penman-based approach in this way (Chen et al., 1996; Mahrt and Ek, 1984):

$$LE_p = \frac{\Delta(R_n - G_0 + \rho L_v C_h u(q_s - q)}{1 + L_v} \tag{2.4}$$

where Δ is the slope of the relation between the saturated vapor pressure and the temperature (kPaK^{-1}), and q_s (q) is the saturated (actual) specific humidity (kgkg^{-1}). R_n is net radiation (Wm^{-2}) (see equation 1.3) and L_v (Jkg^{-1}) were defined previously in Section 1.1.

The ground surface heat flux, G_0, is calculated following Fourier's law using the temperature gradient between the surface and the midpoint of the first soil layer according to:

$$G_0 = K_t \frac{T_g - T_{s,1}}{\Delta z_1} \tag{2.5}$$

where K_t is the thermal heat conductivity of the surface layer (W m^{-1} K^{-1}), $T_{s,1}$ is the temperature of the first soil layer (K) and Δz_1 is the depth bewteen the surface and the midpoint of the first soil layer (m). G_0 is the upper boundary condition for the soil thermodynamic model.

The estimation of the ground surface temperature, is calculated following a linearization based on a first-order Taylor series expansion:

$$T_g^4 \approx T_{air}^4 \left[1 + 4\left(\frac{T_g - T_{air}}{T_{air}}\right)\right] \tag{2.6}$$

Substitution of eq. 2.6 into the surface energy balance equation (eq.2.2) yields the following expression for the ground surface temperature:

$$T_g = T_a + \frac{S_\downarrow - S_\uparrow + \varepsilon_g L_\downarrow - H - LE - G_0}{4\varepsilon_g \sigma T_{air}^3} - \frac{1}{4} T_{air} \tag{2.7}$$

2.2.3.2 Soil heat flow

Soil thermodynamics are treated by the usual diffusion prognostic equation for soil temperature (T):

$$C(\Theta)\frac{\partial T}{\partial t} = \frac{\partial}{\partial z}(K_t(\Theta)\frac{\partial T}{\partial z}) \tag{2.8}$$

where the volumetric heat capacity C (Jm^{-3}K^{-1}) and the thermal conductivity K_t are formulated as functions of volumetric soil water content Θ (fraction of unit soil volume occupied by water). C is linearly related to Θ, and K_t is a highly nonlinear function of Θ and increases by several orders of magnitude from dry to wet soil conditions (Ek and Mahrt, 1991). The layer-integrated form of Eq. 2.8 for the ith soil layer is:

$$\Delta z_i C_i \frac{\partial T_i}{\partial t} = (K_t \frac{\partial T}{\partial z})_{z_{i+1}} - (K_t \frac{\partial T}{\partial z})_{z_i} \tag{2.9}$$

The prediction of T_i is performed using the fully implicit Crank-Nicholson scheme. In the top layer the last term in 2.9 represents G_0, and is computed using the surface skin temperature T_g as was showed in Eq. 2.5.

K_t is a function of soil texture and increases by increasing SM content. The effect of increasing K_t is greater G and leads to a more damped diurnal signal in T2m.

In the presence of a vegetation layer, G is reduced because of lowered K_t through vegetation (Ek et al., 2003). In the Noah-LSM is used the explicit approach of Peters-Lidard et al. (1997) where the soil thermal conductivity under vegetation (K_v) is reduced from the "bare soil" value (K_t) by an exponential function of LAI. In the case of the Noah-LSM has adopted a similar formulation using the FVC where:

$$K_{veg} = K_t exp(-\beta_{veg} FVC) \tag{2.10}$$

where β_{veg} is an empirical coefficient equal to 2.0 following tests with the offline Noah LSM (see Figure2.5).

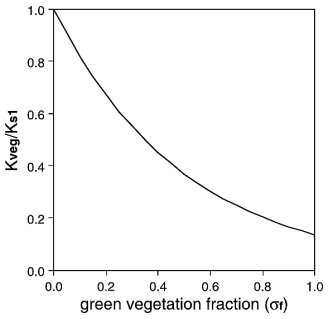

Fig. 2.5: Ratio of soil thermal conductivity under vegetation to bare soil soil thermal conductivity (K_{veg}/K_t) as a function FVC. Source: Ek et al. (2003). Copyright 2003 Wiley. Used with permission from Ek et al. (2003).

2.2.3.3 Soil hydrology

The prognostic equation for the volumetric SM content(Θ) is:

$$\frac{\partial \Theta}{\partial t} = \frac{\partial}{\partial z}(D\frac{\partial \Theta}{\partial z}) + \frac{\partial K}{\partial z} + F_\Theta \tag{2.11}$$

where both the soil water diffusivity D and hydraulic conductivity K are functions of Θ, and F_Θ represents sources and sinks (i.e., precipitation, evaporation, and runoff) for soil water. The above is the diffusive form of Richard's equation derived from Darcy's law under the assumption of a rigid, isotropic, homogeneous, and one-dimensional ver-

tical flow domain (Hanks and Ashcroft, 1986), and thereby the soil water diffusivity D is given by $D = K(\Theta)(\partial\Psi/\partial\Theta)$ where in Ψ is the soil water tension function. Cosby et al. (1984), resolved K and Ψ by $K(\Theta) = K_s(\Theta/\Theta_s)^{2b+3}$ and $\Psi(\Theta) = \Psi_s/(\Theta/\Theta_s)^b$, where b is a curve-fitting parameter. K_s, Ψ and b depends on soil type.

The hydraulic conductivity ,K, and, diffusivity, D, are highly nonlinearly dependent on the SM, changing several orders of magnitude, even for a small variation in SM, especially when the soil is very dry.

For the case of the MM5 model, with four soil layers, expanding F_Θ:

$$d_{z_1}\frac{\Theta_1}{\partial t} = -D(\frac{\partial\Theta}{\partial z})_{z_1} - K_{z_1} + P_d - R - E_{dir} - E_{t_1}, \tag{2.12}$$

$$d_{z_2}\frac{\Theta_2}{\partial t} = D(\frac{\partial\Theta}{\partial z})_{z_1} - D(\frac{\partial\Theta}{\partial z})_{z_2} + K_{z_1} - K_{z_2} - E_{t_2}, \tag{2.13}$$

$$d_{z_3}\frac{\Theta_3}{\partial t} = D(\frac{\partial\Theta}{\partial z})_{z_2} - D(\frac{\partial\Theta}{\partial z})_{z_3} + K_{z_2} - K_{z_3} - E_{t_3}, \tag{2.14}$$

and

$$d_{z_4}\frac{\Theta_4}{\partial t} = D(\frac{\partial\Theta}{\partial z})_{z_3} + K_{z_3} - K_{z_4}, \tag{2.15}$$

where d_{z_i} is the ith layer thickness, P_d the precipitation not intercepted by the canopy, and E_{t_i} the canopy transpiration taken by the canopy root in the ith layer within the root zone layers (three layers of root zone in the coupled MM5-LSM). At the bottom of the soil model, the hydraulic diffusivity is assumed to be zero, so that the soil water flux is due only to the "gravitational" percolation term K_{z_4}, also named subsurface runoff or drainage (Chen and Dudhia, 2001).

Surface runoff, R, is defined as the excess of precipitation not infiltrated into the soil ($R = P_d - I_{max}$), that depends on saturated hydraulic conductivity determined by specific soil texture of each type, I_{max} being the maximum infiltration.

The total evapotranspiration (E) from the soil canopy surface, used in the single surface energy balance, is divided in three components:

$$E = E_{dir} + E_c + E_t \tag{2.16}$$

where E_{dir} is the direct evaporation from the top shallow soil layer, E_c is the evaporation of precipitation intercepted by the canopy and E_t is the transpiration through canopy and roots. FVC is critical in partitioning E in this three components and below is detailed how this is parameterized in the MM5-Land Surface Model as is described in Chen and Dudhia (2001). The direct evaporation from the ground surface adopts a simple linear form (Mahfouf and Noilhan, 1991):

$$E_{dir} = (1 - FVC)\beta E_p \tag{2.17}$$

and

$$\beta = \Theta_1 - \Theta_w / \Theta_{ref} - \Theta_w \tag{2.18}$$

where E_p is the potential evaporation, Θ_{ref} is the field capacity and Θ_w is the wilting point. E_{dir} can reach the potential rate when the SM at the surface is rather moist. In another way, direct evaporation can only proceed at the rate by which the top soil layer can transfer water from below and is controlled by Θ_{ref} and Θ_w. These values refer to an upper reference value, where transpiration begins to decrease due to a deficit of water (Θ_{ref}) and the plant wilting factor, Θ_w, which is the value where transpiration stops (Ek and Mahrt, 1991; Mahrt and Pan, 1984).

The wet canopy evaporation is defined as

$$E_c = FVC\ E_p (\frac{W_c}{S})^{0.5} \tag{2.19}$$

where $\partial W_c / \partial t = FVC\ P - D - E_c$, W_c is the intercepted canopy water content, S is the maximum canopy capacity, P is the total precipitation reached on the vegetation, and D is the rain through fall from the canopy. If W_c exceeds S, then the excess precipitation or drip (D) reaches the ground.

The transpiration rate released by the canopy (E_t) is based on the potential evaporation (E_p) and is controlled by plant stress through time-dependent canopy resistance index (R_c) and intercepted canopy water content (W_c) :

$$E_t = FVC\ E_p\ B_c [1 - (\frac{W_c}{S})^{0.5}] \tag{2.20}$$

where B_c is a function of canopy resistance and $(W_c)/S_n)$ serve as a weighting coefficient to suppress E_t in favor of E_c as the canopy surface becomes increasingly wet (Chen et al., 1996).

B_c is defined as

$$B_c = \frac{1 + \frac{\Delta}{R_r}}{1 + R_c C_h} + \frac{\Delta}{R_r} \tag{2.21}$$

where C_h is the surface exchange coefficient for heat and moisture, Δ depends on the slope of the saturation specific humidity curve and R_r is a function of the surface air temperature. The canopy resistance, R_c, follows the formulation of Jacquemin and Noilhan (1990) and is a function of the solar radiation deficit (F_1) ,the vapor pressure deficit (F_2), the air temperature deficit (F_3) , the SM deficit (F_4), the minimum stomatal resistance (R_{cmin}) and the leaf area index (LAI):

$$R_c = \frac{R_{cmin}}{LAIF_1F_2F_3F_4}, \tag{2.22}$$

$$F_1 = \frac{R_{cmin}/R_{cmax} + f}{1 + f}, \text{(solar radiation deficit)} \tag{2.23}$$

where $f = 0.55\frac{R_g}{R_{gl}}\frac{2}{LAI}$,

$$F_2 = \frac{1}{1 + h_s[q_s(T_a) - q_a]}, \text{(vapor pressure deficit)} \tag{2.24}$$

$$F_3 = 1 - 0.0016(T_{ref} - T_a)^2, \text{(air temperature deficit)} \tag{2.25}$$

$$F_4 = \sum_{i=1}^{3} \frac{(\Theta_i - \Theta_w)dz_i}{(\Theta_{ref} - \Theta_w)(dz_1 - dz_2)}, \text{(soil moisture deficit)} \tag{2.26}$$

where $q_s(T_a)$ is the saturated water vapor mixing ratio at the temperature(T_a), R_{cmax} is the cuticular resistance of the leaves and set to 5000 $sm^{-}1$ and d_{Zi} is the depth of the specific soil layer. F_1, F_2, F_3 and F_4 are constrained between 0 and 1.

The canopy resistance provides an important link in the soil-vegetation-atmosphere continuum and describes the resistance of vapour flow through the transpiring canopy. The inclusion of canopy resistance avoid the overestimation of evaporation in wet periods. In this manner, the water retained in the deep soil can be drawn up from the root zone, releasing this water storage in follow-on dry periods. This point is critical in simulations of longer seasonal evolution of evaporation and in simulate properly its diurnal and seasonal cycle.

The most important factor in modulating the canopy resistance in semiarid regions like Mediterranean areas, is the SM deficit (F_4) (Matsui et al., 2005). A nonlinear SM stress function is implemented to take into account the sub-grid variability of SM, which content is rarely homogeneous in nature. In this way, the evaporation can be maintained beyond the wilting point and can be reduced when the averaged SM is near the field capacity.

It is important to notice that the drying cycle timescales of E_{dir} or E_c versus E_t are quite different. E_{dir} and E_c represent fast changing evaporation due to small water capacity and low resistance, while the higher resistance in E_t combined with the deep root zone, maintain relatively high evaporation for several weeks or more depending on the last significant rainfall (Chen et al., 1996).

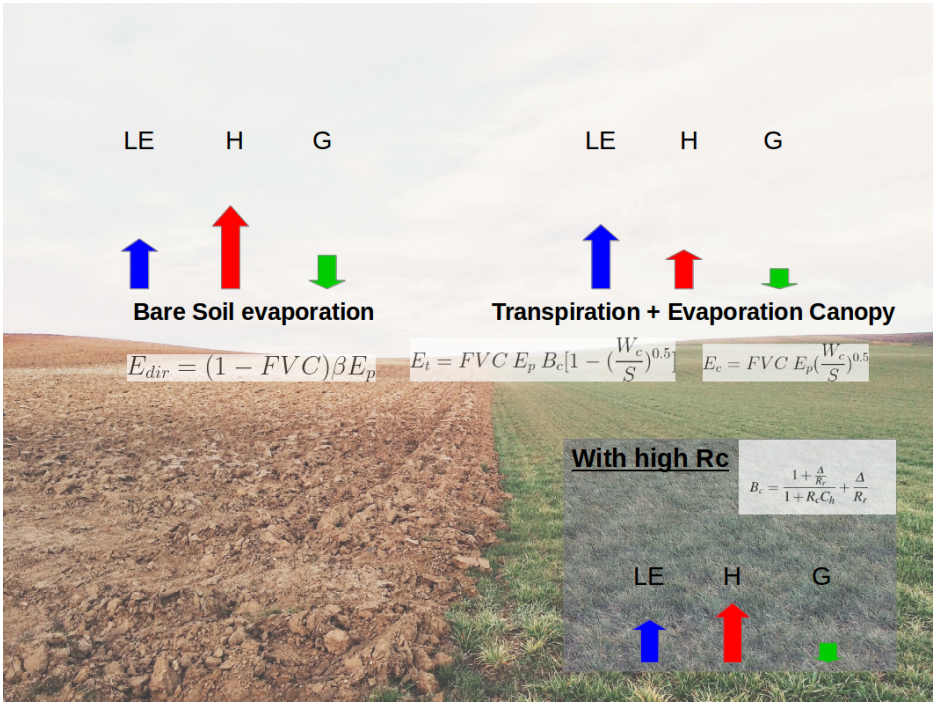

Fig. 2.6: Main land surface processes affected by FVC during daytime

2.2.4 Summary of Fraction Vegetation Cover (FVC) parameterization in Noah LSM

As a summary and with a didactive aim, in Figures 2.6 and 2.7 are depicted the main effects of FVC in Noah LSM. Following Figure 2.6, during the day the effect of increasing FVC should increase proportionately E_t and E_c. In contrast, E_{dir} should decrease simply because the bare soil fraction is reduced by the higher values of FVC. In this way, in presence of vegetation LE fluxes would be increased and following Eq. 2.2 counterbalanced by H and G. So as LE increases, less energy can be available for increasing near surface temperature (H) and for heating the soil layers (G). The available soil moisture in an important factor in canopy resistance calculation as was commented previously. Accordingly as the the soil moisture deficit is higher, E_t and E_c are reduced and an increase in FVC can lead to an inhibition of total evaporation bigger than if the surface is less vegetated since bare soil evaporation E_{dir} is not involved.

During night, as depicted in Figure 2.7, the main process in which FVC is implied is related with G. This variable is directly influenced by FVC because of the parameterization described in equation 2.10, that implies a shadowing effect of vegetation and a reduction in the soil thermal conductivity and consequently in lowered soil heat flux. This decrease in soil heat flux implies less energy released from deeper soil layers to surface, and thus lower T_g values. Owing to at night, dominant flux component is G (LE and H are less relevant) this effect can be more evident on nighttime T_g, and therefore in T2m. The effect of FVC in diminishing soil thermal conductivity can be relevant at daytime too, because, as G values are lowered H and LE become higher. This reduction of G during daytime provokes less transfer of energy to deeper soil layers.

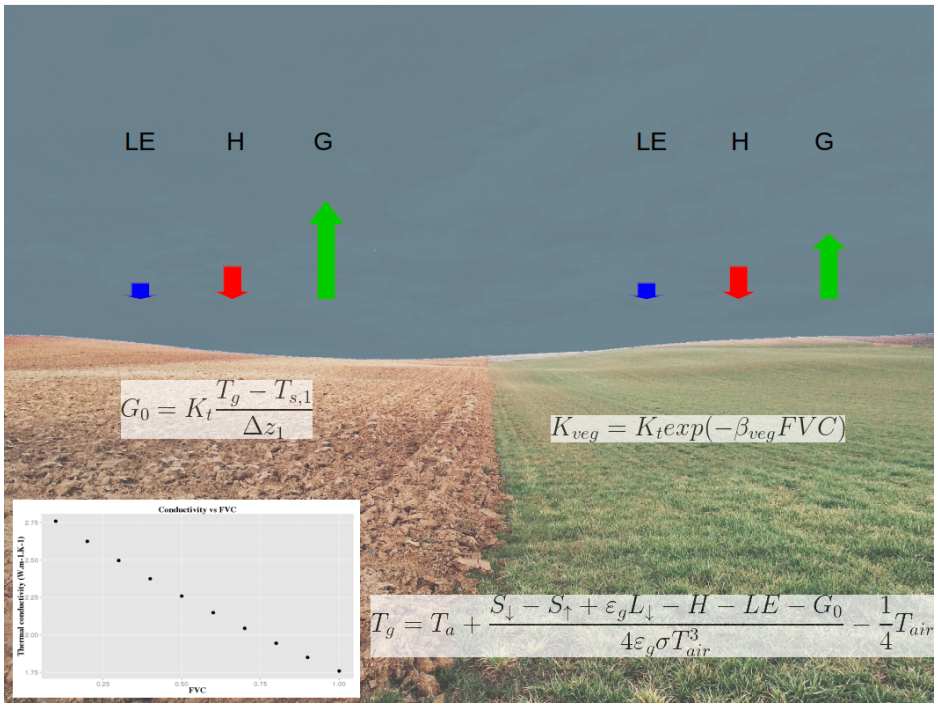

Fig. 2.7: Main land surface processes affected by FVC during nighttime

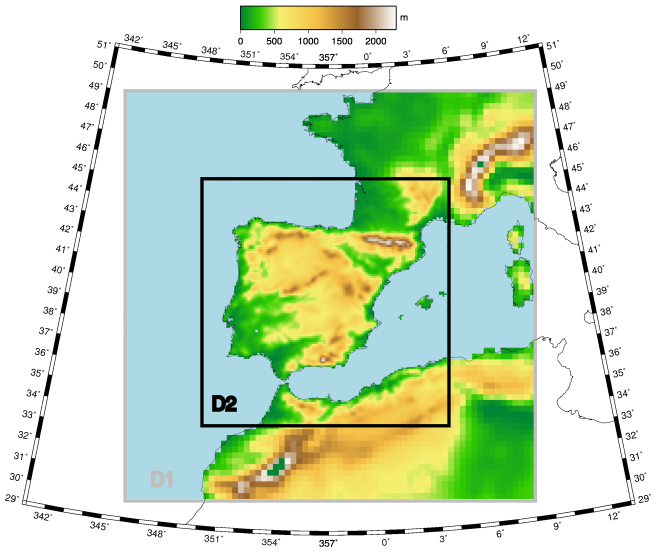

Fig. 2.8: RCM spatial domains. Mother domain, D1 (30 km), and inner domain, D2 (10 km). Topography of the spatial domains. Source: Jiménez-Gutiérrez et al. (2019).

2.3 Model configuration

2.3.1 Domain configuration

The **spatial configuration** consists of two-way nested domains with 30 and 10 km horizontal resolution respectively (Figure 2.8). The first domain has 80 X 80 grid points covering southwest Europe (Spain, France, North Italy, Alps) and part of North Africa. The second domain is centered in the Iberian Peninsula and has 136 X 136 grid points. In the simulations performed in this work Lambert Conformal projection has been chosen because is the most suitable for mid-latitudes regions as the Iberian Peninsula.

The **vertical grid** considers 24 sigma levels in the vertical up to 100mb which are: 1.00, 0.99, 0.98, 0.96, 0.93, 0.89, 0.85, 0.80, 0.75, 0.70, 0.65, 0.60, 0.55, 0.50, 0.45, 0.40, 0.35, 0.30, 0.25, 0.20, 0.15, 0.10, 0.05 and 0.00.

The **time step** for the numerical resolution of the basic equations (dt) is theoretically optimised if chosen to be (in seconds) three times the horizontal grid distance of each domain or subdomain (expressed in km). In this way, dt = 270 s is chosen for D1 and

dt = 90 s for D2. Sometimes time-step of D2 can led to some model instabilities and is neeeded to reduce it and restart the simulation until it works.

A **relaxation lateral boundary** (6 grid boxes) has been used in the configuration of the model, with a progressive decreasing of the boundary conditions towards the centre of the simulation domain (Davies, 1976). Hence, first five points from the borders of each domain, that are taken as the blending area and namely affected by the relaxation from an outer coarser resolution to a finner one, are neglected in all the analysis performed.

2.3.2 Regional climate simulation strategy

All the simulations performed independently of the whole simulated period, consist in **one-year simulations with a previous spin-up period of 4 months starting in september of the previous year** that is discarded every time. Regarding the initialization of the model, the most common methodologies in dynamical regional climate downscaling employs a continuous integration of the model with a single initialization. But it has been proved that reinitialization runs, prevents the regional model from deviating too much from the driving conditions during the course of long integrations (Lo et al., 2008). Although this can be easier achieved by using 3-D nudging, this technique restricts so much that the regional model develops its own variability and thus hinders the study of the contribution of regional circulations and local processes. Considering the spin-up period, the period that is integrated just so that the regional model reaches the dynamical equilibrium, soil variables, especially soil moisture, present the largest requirements. In this case, the approach of Christensen et al. (1997) letting four months at each reinitialization has been chosen. This simulation strategy has been considered succesfully in several regional climate model (RCM) simulations (Jerez et al., 2010; Gómez-Navarro et al., 2012b; Jerez et al., 2013; Lorente-Plazas et al., 2015; Fernández-Montes et al., 2017).

Physical Schemes	**Option**
Cumulus parameterization	Grell
Microphysics	Simple Ice
Radiation scheme	RRTM
PBL	MRF
Surface scheme	Noah LSM

Table 2.1: Physical parameterizations considered in all simulations

2.3.3 Physics options

Below are detailed the physical configuration chosen in all the simulations performed in this work. See table 2.1 for a summary of the physics options.

- **Cumulus parameterization: Grell**. Based on rate of destabilization or quasi-equilibrium, simple single-cloud scheme with updraft and downdraft fluxes and compensating motion determining heating/moistening profile. Useful for smaller grid sizes 10-30 km, tends to allow a balance between resolved scale rainfall and convective rainfall. Shear effects on precipitation efficiency are considered (Grell, 1993).
- **Microphysics: Simple Ice**. Adds ice phase processes to above without adding memory. No supercooled water and immediate melting of snow below freezing level (Dudhia, 1989).
- **Radiation scheme: Rapid Radiative Transfer Model (RRTM)**. Uses a correlated-k model to represent the effects of the detailed absorption spectrum taking into account water vapor, carbon dioxide and ozone. It is implemented in MM5 to also interact with the model cloud and precipitation fields (Mlawer et al., 1997).
- **Planetary Boundary Layer scheme: Medium-Range Forecast PBL scheme (MRF)**. Efficient scheme based on Troen-Mahrt representation of countergradient term and K profile in the well mixed PBL, as implemented in the NCEP MRF model. See Hong and Pan (1996) for details.
- **Surface scheme: Noah LSM**. Noah LSM is detailed in Section 2.2.

2.3.4 Initial and boundary conditions

2.3.4.1 ERA Interim reanalysis

ERA-Interim reanalysis (Dee et al., 2011) are used to provide atmospheric as well as soil moisture and soil temperature initial and boundary conditions. Boundary conditions are updated every six hours at 00, 06, 12 and 18 UTC. The ERA-Interim atmospheric model and reanalysis system uses cycle 31r2 of ECMWF's Integrated Forecast System (IFS), which was introduced operationally in September 2006, configured for the following spatial resolution: 60 levels in the vertical with the top level at 0.1 hPa, T255 spherical-harmonic representation for the basic dynamical fields and a reduced Gaussian grid with approximately uniform 79 km spacing for surface and other grid-point fields.

Vegetation Integer Identification	Vegetation Description	Albedo(%)		Moisture Avail. (%)		Emissivity (% at 9 μ m)		Roughness Length (cm)		Thermal Inertia (cal cm^{-2} k^{-1} s$^{-1/2}$)	
		Sum	Win	Sum	Win	Sum	Win	Sum	Win	Sum	Win
1	Urban	15	15	10	10	88	88	80	80	0.03	0.03
2	DryInd Crop. Past.	17	23	30	60	98.5	92	15	5	0.04	0.04
3	Irrg. Crop. Past.	18	23	50	50	98.5	92	15	5	0.04	0.04
4	Mix. Dry/Irrg.C.P.	18	23	25	50	98.5	92	15	5	0.04	0.04
5	Crop./Grs. Mosaic	18	23	25	40	99	92	14	5	0.04	0.04
6	Crop./Wood Mosc	16	20	35	60	98.5	93	20	20	0.04	0.04
7	Grassland	19	23	15	30	98.5	92	12	10	0.03	0.04
8	Shrubland	22	25	10	20	88	88	10	10	0.03	0.04
9	Mix Shrb./Grs.	20	24	15	25	90	90	11	10	0.03	0.04
10	Savanna	20	20	15	15	92	92	15	15	0.03	0.03
11	Decids. Broadlf.	16	17	30	60	93	93	50	50	0.04	0.05
12	Decids. Needlf.	14	15	30	60	94	93	50	50	0.04	0.05
13	Evergrn. Braodlf.	12	12	50	50	95	95	50	50	0.05	0.05
14	Evergrn. Needlf.	12	12	30	60	95	95	50	50	0.04	0.05
15	Mixed Forest	13	14	30	60	94	94	50	50	0.04	0.06
16	Water Bodies	8	8	100	100	98	98	.01	.01	0.06	0.06
17	Herb. Wetland	14	14	60	75	95	95	20	20	0.06	0.06
18	Wooded wetland	14	14	35	70	95	95	40	40	0.05	0.06
19	Bar. Sparse Veg.	25	25	2	5	85	85	10	10	0.02	0.02
20	Herb. Tundra	15	60	50	90	92	92	10	10	0.05	0.05
21	Wooden Tundra	15	50	50	90	93	93	30	30	0.05	0.05
22	Mixed Tundra	15	55	50	90	92	92	15	15	0.05	0.05
23	Bare Grnd. Tundra	25	70	2	95	85	95	10	5	0.02	0.05
24	Snow or Ice	55	70	95	95	95	95	5	5	0.05	0.05
25	No data										

Fig. 2.9: Description of 25-category (USGS) vegetation categories and physical parameters for N.H. summer (15 April - 15 October) and winter (15 October - 15 April). Source: Grell et al. (1994).

2.3.4.2 Topography and land use. Surface physical parameters

Topography data are derived from the GTOPO30 data from the USGS EROS Data Center (Gesch et al., 1999). Elevation data for the simulations carried out is depicted in Figure 2.8. Land use data are derived from the 30 sec data USGS version 2 land cover data with 25 categories described in table 2.9 and depicted for the study area in Figure 2.10. As was treated in Section 1.2.1.3 in the MM5 model (as in other many models) is used the consideration that each grid cell of the model has assigned a land use type and this defines some surface parameters. In this case, emissivity, and thermal inertia depends on land use type. Soil moisture is not prescribed with Noah LSM surface scheme since it has a dynamical approach as has been commented in 2.2.

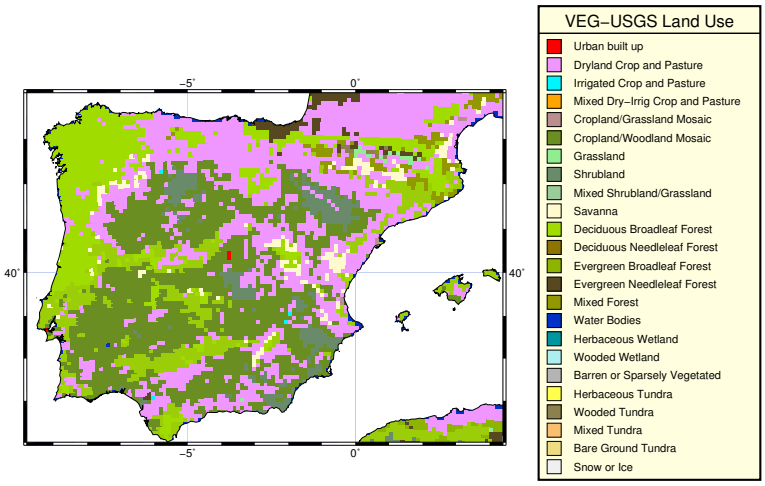

Fig. 2.10: USGS version land cover data of D2 domain grid points considered in RCM simulations of this work (resolution of 0.1 °X 0.1 °).

2.3.4.3 Soil types

Soil type is needed as input in Noah LSM and is derived from a 30 sec dataset from FAO with 17 categories. As was commented with land use type, each grid cell has a soil type and several soil parameters depends on it. A detailed list of the parameters for each soil type is depicted in table 2.11. Soil types for the study area are showed in Figure 2.12.

2.3.4.4 Vegetation fraction

Noah LSM in MM5 and WRF model uses a default FVC monthly climatological data. This commonly used database is described in Gutman and Ignatov (1998) which consist of a 5-year FVC climatology derived from AVHRR, for the period April-December of 1985,from 1986 to 1990 and the period January-March of 1991 with a spatial resolution of 0.15 °. More details in how this dataset is calculated can be found in 3.2.2 and more precisely in 3.2.2.2. In Figure 2.13, is showed the original FVC climatology used by Noah LSM in the study area for all months of the year.

In the next chapters, this FVC original database has been modified in three ways:

Soil Integer Identification	Soil Description	Max moisture content	Reference soil moisture	Wilting point soil moisture	Air dry moist content limits	Saturation soil potential	Saturation Soil conducti-vity (10^{-6})	B parameter	Saturation soil diffusivity (10^{-6})	Soil diffu./ condu. coef.
1	Sand	0.339	0.236	0.010	0.010	0.069	1.07	2.79	0.608	- 0.472
2	Loamy Sand	0.421	0.283	0.028	0.028	0.036	14.10	4.26	5.14	- 1.044
3	Sandy Loam	0.434	0.312	0.047	0.047	0.141	5.23	4.74	8.05	- 0.569
4	Silt Loam	0.476	0.360	0.084	0.084	0.759	2.81	5.33	23.9	0.162
5	Silt	0.476	0.360	0.084	0.084	0.759	2.81	5.33	23.9	0.162
6	Loam	0.439	0.329	0.066	0.066	0.355	3.38	5.25	14.3	- 0.327
7	Sandy Clay Loam	0.404	0.314	0.067	0.067	0.135	4.45	6.66	9.90	- 1.491
8	Silty Clay Loam	0.464	0.387	0.120	0.120	0.617	2.04	8.72	23.7	- 1.118
9	Clay Loam	0.465	0.382	0.103	0.103	0.263	2.45	8.17	11.3	- 1.297
10	Sandy Clay	0.406	0.338	0.100	0.100	0.098	7.22	10.73	18.7	- 3.209
11	Silty Clay	0.468	0.404	0.126	0.126	0.324	1.34	10.39	9.64	- 1.916
12	Clay	0.468	0.412	0.138	0.138	0.468	0.974	11.55	11.2	- 2.138
13	Organic Materials	0.439	0.329	0.066	0.066	0.355	3.38	5.25	14.3	- 0.327
14	Water	1.0	0.0	0.0	0.0	0.0	0.0	0.0	0.0	0.0
15	Bedrock	0.200	0.108	0.006	0.006	0.069	141.0	2.79	136.0	- 1.111
16	Other	0.421	0.283	0.028	0.028	0.036	14.10	4.26	5.14	- 1.044
17	No data									

Fig. 2.11: Description of 17-category Soil categories and physical parameters. Source: Grell et al. (1994).

- FVC calculation from NDVI GIMMS data with the nominated ZENG, WETZEL and GUTMAN methods (Chapter 3).
- FVC fixed to spatial constant values of 90 % and 30 % (Chapter 4).
- FVC obtained from Copernicus database (Chapter 5).

2.3.4.5 Deep soil temperature

Deep soil temperature needed in Noah LSM as lower boundary condition is calculated from a Global Annual Deep Soil Temperature Dataset from ECMWF analysis with 1 deg resolution. This temperature depends on the ECMWF model orography, so it is first adjusted to the 1000-mb level using the ECMWF annual analyzed surface pressure according to the standard atmosphere lapse rate. It is then adjusted to the MM5 orography following the same procedure so it reflects the MM5 high-resolution topography. More details can be found in Chen and Dudhia (2001).

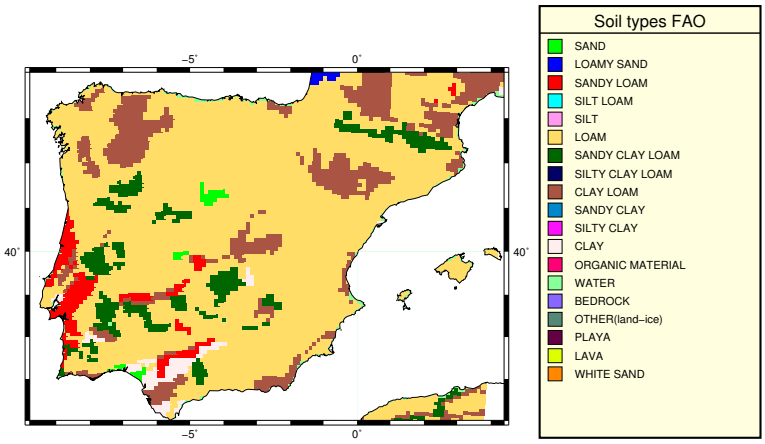

Fig. 2.12: Soil categories of D2 domain grid points considered in RCM simulations of this work (resolution of 0.1 °X 0.1 °).

2.3.4.6 Vegetation parameters

There are a set of vegetation parameters used in Noah LSM that depends on land use type. The parameters R_{cmin} and R_{gl} are used in equation 2.23 (see Section 2.2.3.3). R_{cmin} together with LAI is used in equation 2.22 in the calculation of R_c. And the parameter h_s is used in the calculation of vapor pressure deficit in 2.24. In table 2.2 are defined the values of this parameters for each vegetation type (Chen and Dudhia, 2001).

Regarding albedo, is a fundamental variable in the study of vegetation in RCM simulations as was commented in 1.2.2.4. Besides, of the prescription with a look-up table there is an option in the MM5 model of including monthly gridded values of albedo. This consideration has been out of the scope of this work and would have meant a more complete study. Anyway, Crawford et al. (2001) showed that the impact of changing albedo on surface heat fluxes is much smaller, an order of magnitude, than changing FVC, so the results showed in next sections explain the main impacts of changing vegetation in RCM simulations.

LAI in this approach of the Noah LSM is considered as a fixed value of 4. More details of the relation between LAI and FVC are given in Chapter 3 in Section 3.1.

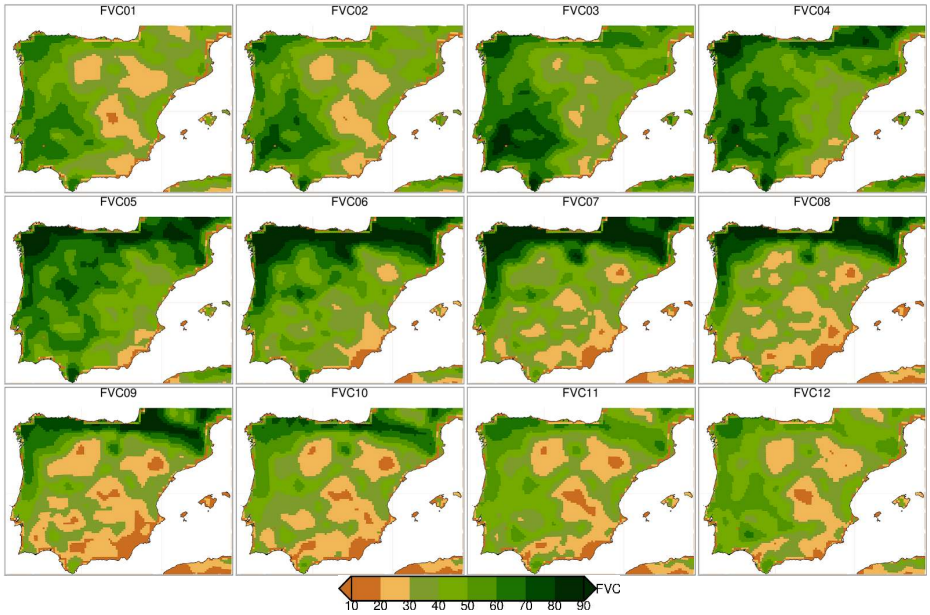

Fig. 2.13: FVC from January to December in the study area for D2 domain using Gutman and Ignatov (1998) original climatology. In the header of each plot is indicated the month of the year. Green colours are related with high values of FVC and brown colours with low values.

id	albedo	z_0 (m)	R_{cmin} ($sm^{-}1$)	R_{gl}	h_s	LAI	Vegetation description
1	.15	1.00	200.	999.	999.0	4.0	Urban and Built-Up Land
2	.19	.07	40.	100.	36.25	4.0	Dryland Cropland and Pasture
3	.15	.07	40.	100.	36.25	4.0	Irrigated Cropland and Pasture
4	.17	.07	40.	100.	36.25	4.0	Mixed Dryland/Irrigated Cropland and Pasture
5	.19	.07	40.	100.	36.25	4.0	Cropland/Grassland Mosaic
6	.19	.15	70.	65.	44.14	4.0	Cropland/Woodland Mosaic
7	.19	.08	40.	100.	36.35	4.0	Grassland
8	.25	.03	300.	100.	42.00	4.0	Shrubland
9	.23	.05	170.	100.	39.18	4.0	Mixed Shrubland/Grassland
10	.20	.86	70.	65.	54.53	4.0	Savanna
11	.12	.80	100.	30.	54.53	4.0	Deciduous Broadleaf Forest
12	.11	.85	150.	30.	47.35	4.0	Deciduous Needleleaf Forest
13	.11	2.65	150.	30.	41.69	4.0	Evergreen Broadleaf Forest
14	.10	1.09	125.	30.	47.35	4.0	Evergreen Needleleaf Forest
15	.12	.80	125.	30.	51.93	4.0	Mixed Forest
16	.19	.001	100.	30.	51.75	4.0	Water Bodies
17	.12	.04	40.	100.	60.00	4.0	Herbaceous Wetland
18	.12	.05	100.	30.	51.93	4.0	Wooded Wetland
19	.12	.01	999.	999.	999.0	4.0	Barren or Sparsely Vegetated
20	.16	.04	150.	100.	42.00	4.0	Herbaceous Tundra
21	.16	.06	150.	100.	42.00	4.0	Wooded Tundra
22	.16	.05	150.	100.	42.00	4.0	Mixed Tundra
23	.17	.03	200.	100.	42.00	4.0	Bare Ground Tundra
24	.70	.001	999.	999.	999.0	4.0	Snow or Ice

Table 2.2: Vegetation related parameters in the Noah LSM. This parameters are albedo, roughness length (z_0, minimum stomatatal resistance (R_{cmin}), visible solar flux (R_{gl}), parameter used in vapor pressure deficit (h_s) and LAI. Source: Grell et al. (1994).

3

Impacts of Green Vegetation Fraction derivation methods on Regional Climate Simulations*

This chapter is focused in present different sources of variability that can affect the calculation of FVC and how these can be translated in simulated fields of 2 meter air temperature (T2m) in a regional climate model (RCM). Firstly, the comparison of two different NDVI databases from which FVC is obtained is performed in order to point out that great differences can be found between different sources and can condition final calculation of FVC. Then, three different methods of calculation of fraction vegetation cover (FVC) are presented, assessing its differences and how these are translated to surface simulated fields of T2m. At last, the effect of using climatological values of FVC instead of synchronous data has been explored simulating a dry and a wet year.

3.1 Introduction

As reviewed in the introductory chapter in Section 1.1 land surface features play a very important role in modulating surface-atmosphere interactions. Surface components like soil moisture, albedo, emissivity, surface roughness, vegetation type and amount are

* The main contents of this chapter are included in:
- J. M. Jiménez-Gutiérrez, F. Valero, S. Jerez, and J. P. Montávez, 2019: Impacts of green vegetation fraction derivation methods on regional climate simulations. *Atmosphere*, 10(5), 281. (Jiménez-Gutiérrez et al., 2019)

fundamental since they control the energy partition at surface (Jerez et al., 2012). Therefore, the representation of all these variables in land surface models (LSMs) is crucial for modeling atmospheric processes.

Atmosphere and vegetation interact in different ways, controlling evapotranspiration, moisture availability, momentum transfer or partitioning radiation (see Section 1.2.2 for more details). Therefore, realistic characterization of vegetation through FVC, leaf area index (LAI) and vegetation class as detailed in Section 1.2.1, should lead to a better reproduction of atmosphere-surface processes.

Different methodologies have been reported for obtaining FVC and LAI through satellite NDVI data (Chang and Wetzel, 1991; Gutman and Ignatov, 1998; Zeng et al., 2000; Li and Zhang, 2016). According to Gutman and Ignatov (1998) both parameters should not be used simultaneously in the same parameterization. Therefore, it is necessary to prescribe one of the indices and derive the other. Gutman and Ignatov (1998) and Carlson et al. (1990) argued that is preferable to derive FVC and prescribe LAI, because the exponential dependence of LAI and NDVI saturates after a certain threshold, becoming LAI insensitive to changes in NDVI. Some other authors (Sellers et al., 1996; Zeng et al., 2000) recommend to derive LAI (fixing FVC), because they assume that spatial and seasonal variations of NDVI are related with variations of LAI and validation of FVC is problematical because of the requirement of information at the scale of individual plant elements. Anyway, Godfrey et al. (2002) argue that errors introduced by the dual specification of vegetation parameters from a single NDVI observation are likely smaller than uncertainties associated to initial conditions.

The role of vegetation parameters (FVC and LAI) is relevant for weather forecasting and climate change assessments (Hanamean Jr et al., 2003). Their impact on land surface processes has been studied in the Eta operational model (Ek et al., 2003; Kurkowski et al., 2003; Marshall et al., 2003) and the Weather Research and Forecasting model (WRF) (Hong et al., 2009; Limei et al., 2015; Cao et al., 2015; Xu et al., 2017; Zhang et al., 2017; Wen et al., 2013). The relevance of using realistic information of the vegetation state on RCM performance has been analyzed in several works. Meng et al. (2014) and Müller et al. (2014a) study the impact of vegetation in concrete cases of droughts in Australia and South America. Other works investigate the contribution of near real time values of vegetation fraction to simulated precipitation. For instance, vegetationâĂŞatmosphere feedback in monsoon systems (Matsui et al., 2005; Notaro et al., 2017), severe convection episodes (James et al., 2009), or improving model performance in oasis-desert systems (Zhang et al., 2014). Other interesting studies focus on vegetation effects on regional climate simulations in complex urban areas like Los Angeles (Vahmani and Hogue, 2014; Vahmani and Ban-Weiss, 2016).

However, the characterization of vegetation is subjected to several sources of uncertainty. On one hand, there are several NDVI database available for obtaining FVC data. They differ in aspects such as the methods for correcting errors, type of satellite, etc. The

differences among these NDVI databases reach, for example, similar values to the observed trends in the phenological phases (Stockli and Vidale, 2004). On the other hand, several methodologies can be used to obtain FVC or LAI from NDVI data (Gutman and Ignatov, 1998; Kurkowski et al., 2003; Miller et al., 2006; Stensrud, 2007). Crawford et al. (2001) points out that differences up to 25% in LAI and FVC can easily occur among the different methodologies, similar values to the FVC interannual variability.

In addition, most of the standard configurations of NWPM and RCM use climatological values of vegetation parameters. However, the vegetation has a strong interannual variability (Crawford et al., 2001; Meng et al., 2014; Xu et al., 2017) as was commented in Section 1.2.1.1 leading this to a non-suitable characterization of surface properties. A known limitation is that surface properties can vary at several time scales depending on climate conditions and other processes such as urbanization, forest fires or changes in crops (Myneni et al., 1997).

As an example of the impact of using different approaches with FVC datasets in a LSM, Miller et al. (2006) describe, using the Noah LSM, noteworthy differences in surface fluxes, comparing a 5-year climatology data from Advanced Very High Resolution Radiometer (AVHRR) and NASA's Moderate Resolution Imaging Spectrometers (MODIS) data from the year 2000. With differences of 25 % in FVC in monthly-averaged values for all pixels of dry land and cropland of the same 2-degree box, transpiration was modified in 30 Wm^{-2}, latent heat fluxes in 10 Wm^{-2}, and sensible heat fluxes in -20Wm^{-2}. Other works, where real-time satellite data have been used instead of climatological values, have found improvements in the forecasts of T2m in RCM simulations (Kurkowski et al., 2003; Refslund et al., 2014). While other studies, indicates that the model sensitivity is not reliable with improved vegetation parameters (Matsui et al., 2005; Godfrey et al., 2002; Hong et al., 2009), stressing the significance of minimizing errors in surface initial conditions (especially soil moisture) or canopy resistance parameterization.

The objective of this Chapter is to assess the impact on T2m simulated by a RCM, of the uncertainty associated to the use of different NDVI data, different methodologies for obtaining FVC, as well as the temporal variability of surface properties in regional climate simulations.

3.2 Methods and data

3.2.1 Normalized Difference Vegetation Index (NDVI) data

The Normalized Difference Vegetation Index (NDVI) defined in Section 1.2.1 is highly correlated with the photosynthetically active biomass, chlorophyll abundance and energy

absorption (Myneni et al., 1995) and has been widely used in studies involving land-biosphere interactions (Gutman and Ignatov, 1998; Crawford et al., 2001; Kurkowski et al., 2003; Zhou et al., 2003; Miller et al., 2006).

Among the NDVI datasets reviewed in Section 1.2.1, products from Advanced Very High Resolution Radiometer (AVHRR) sensor are an invaluable and irreplaceable archive of historical land surface information and the most used dataset for deriving NDVI due to its long record. Since 1984 several global land surface NDVI data have been derived from AVHRR, as can be the Global Vegetation Index (GVI) dataset (Tarpley et al., 1984; Gutman et al., 1995), the NASA Pathfinder 8-km dataset (James and Kalluri, 1994) and the GIMMS-NDVI(Pinzon, 2002; Tucker et al., 2005). Others datasets in turn, as the EFAI-NDVI (Stockli and Vidale, 2004), have been derived from the NASA Pathfinder 8-km data. These datasets are corrected taking into account artifacts from sensors, orbital drifting, atmospheric corrections and cloud screening.

Therefore, NDVI values can vary from a database to another in an remarkable way. The GIMMS-NDVI and EFAI-NDVI datasets were chosen to perform our analysis of comparison of NDVI data. The selection was done following criteria of NDVI data already processed, easily/free availability and temporal extension.

The EFAI-NDVI covers the period 1982-2001 and corrects the original AVHRR data to create a continuous dataset of 10-day temporal and 0.1° spatial resolutions with global coverage. The correction method implies a spatial interpolation of missing values and processing artifacts as well as a temporal interpolation of the NDVI series throughout a Fourier adjustment algorithm (Sellers et al., 1996; Stockli and Vidale, 2004).

The GIMMS-NDVI (Tucker et al., 2004) from AVHRR dataset covers from 1982 to 2006 with a spatial resolution of 8 km. This database has been corrected for calibration, view geometry, volcanic aerosols, and other effects non related to vegetation change. In particular, NOAA-9 descending node data from September 1994 to January 1995, volcanic stratospheric aerosol correction for 1982-1984 and 1991-1994, and improved NDVI using empirical mode decomposition/reconstruction to minimize effects of the orbital drift.

3.2.2 Deriving FVC from NDVI data

FVC calculation from NDVI data (Montandon and Small, 2008) can be based on linear models (Gutman and Ignatov, 1998) or quadratic models (Carlson and Rypley, 1997). These methods take as reference bare soil ($NDVI_0$) and dense green vegetation ($NDVI_\infty$). Such values can be prescribed or estimated from the actual NDVI data. For instance, Montandon and Small (2008) studied the impact of varying $NDVI_0$, showing how its underestimation yields a FVC overestimation.

In this study, three linear models, WETZEL, GUTMAN and ZENG have been selected as a basis to study the uncertainty in FVC calculation and its impacts on RCMs runs. These methods present different degrees of complexity, being the WETZEL/ZENG method the most simple/complex, while GUTMAN is of intermediate complexity. This latter has been extensively used in generating data for NWPMs.

The three methodologies have been applied to the GIMMS-NDVI data. Monthly FVC values have been calculated from 1982 to 2006 with a spatial resolution of 0.1 °.

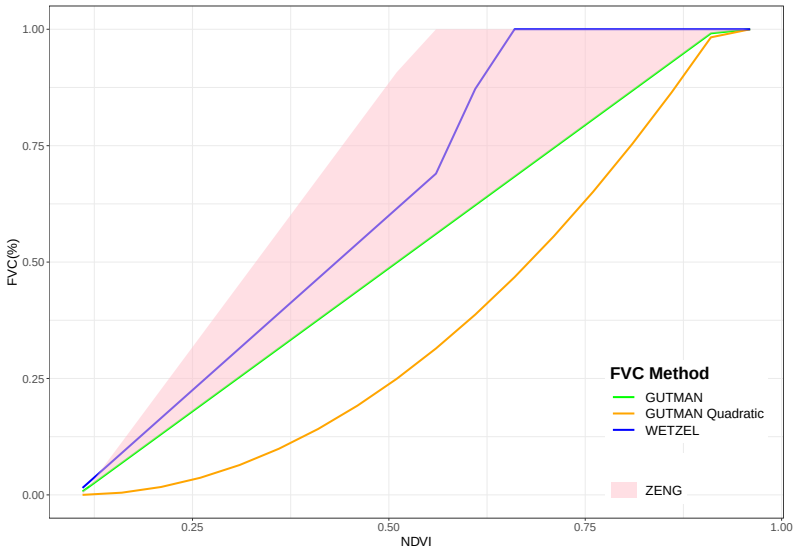

Fig. 3.1: Relationship between FVC and NDVI for the ZENG (red area), GUTMAN, WETZEL, and GUTMAN Quadratic methods. Source: Jiménez-Gutiérrez et al. (2019).

3.2.2.1 WETZEL method

In Chang and Wetzel (1991) a two-line-segment method is presented. The slope of the linear relationship between NDVI and FVC changes when NDVI exceeds 0.547. The relation is as follows:

$$FVC = \begin{cases} 1.5(NDVI - 0.1), NDVI \leq 0.547 \\ 3.2(NDVI) - 1.08, NDVI > 0.547 \end{cases} \quad (3.1)$$

being FVC constrained to be between 0 and 1.

The FVC data obtained by this method is used in the MM5 LSM model by Crawford et al. (2001) and in the ETA model by Kurkowski et al. (2003).

3.2.2.2 GUTMAN method

This method uses the following simple linear relationship between NDVI and FVC:

$$FVC = \frac{NDVI_{val} - NDVI_0}{NDVI_\infty - NDVI_0} \quad (3.2)$$

where $NDVI_0$ and $NDVI_\infty$ are the values for bare soil and dense green vegetation.

Gutman and Ignatov (1998) take $NDVI_0$=0.04 and $NDVI_\infty$=0.52, which correspond respectively to the minimum NDVI value of the desert cluster and the maximum NDVI value of the evergreen cluster in their study with GVI data. These values are in principle, region and season specific, since they depend on the soil and vegetation types and the vegetation chlorophyll content (Price, 1992). However, the authors take this assumption because there are many intermediate cases that make the evaluation difficult for other surface types. In this work, $NDVI_0$ and $NDVI_\infty$, have been set to 0.1 (2% percentile of bare soil) and 0.91 (98% Evergreen vegetation) using the GIMMS-NDVI database.

3.2.2.3 ZENG method

This method includes procedures that involve the analysis of NDVI data as a function of biome or land cover type. This approach has been used in several works (Zeng et al., 2000; Gallo et al., 2001; Miller et al., 2006; Hong et al., 2009). It follows the simple relationship between FVC and NDVI described by Gutman and Ignatov (1998) (Eq. 3.2). The values of $NDVI_\infty$ are calculated analyzing the frequency distribution of maximum NDVI for each land cover type.

This study uses the University of Maryland Department (UMD) global land cover classification (Hansen et al., 1998, 2000). This land cover database has been chosen because it was created using the same NDVI data as the GIMMS-NDVI database. Figure 3.5a (forest types) and 3.6a (shrubland, cropland and grassland) show the spatial distribution as well as the relative frequency distributions of NDVI.

According to Zeng et al. (2000) $NDVI_{\infty}$ is low sensitive to the exact percentile used for a given vegetation type. In this work the $NDVI_{\infty}$ is chosen getting the 98th percentile as adopted in other studies ((Sellers et al., 1996);(Gallo et al., 2001)). For $NDVI_0$, the 5th percentile of the no-vegetation category is taken for all vegetation types. North Africa has been included to have a more suitable value for bare soil. Regarding $NDVI_{val}$, Zeng et al. (2000) estimated FVC as independent of season, then $NDVI_{val}$ (eq. 3.2) is the annual maximum in a given pixel in order to minimize the effects of cloud contamination. However, in our case, $NDVI_{val}$ correspond with each of the 15-day values of the GIMMS-NDVI database in a given pixel, since we precisely want that FVC varies with time.

As a help for understanding differences between the methods, Figure 3.1 shows the relationships between FVC and NDVI for the three methods. The ZENG method (red area) provides wider range of values of FVC depending of land type frequency distribution of NDVI. The GUTMAN method (green line) agrees with the lower correspondence between NDVI and FVC of the ZENG method, explaining the lower values of FVC. On the other hand, the WETZEL method produce higher FVC values in areas where NDVI is larger than the rupture point (0.547), especially in the north of IP.

3.2.3 Regional climate model experiments

The description of the model configuration and the simulated domains is given in Section 2.3. The way for accomplish the objectives of this Chapter is with a two set of experiments. The first set investigates the effect of using different methodologies in constructing the FVC database used in the simulations. For this task, firstly a 5-year FVC climatology has been constructed for the same period of Gutman and Ignatov (1998) (april 1985-march 1991) with the ZENG, GUTMAN and WETZEL methods from the GIMMS-NDVI data. Then three runs for the year 1995 were performed using such FVC climatologies. The second set of simulations explores the role of introducing synchronous FVC data for a given year respect to the use of climatological values of this variable. For this case, two pairs of runs were carried out choosing the ZENG method for the years 1995 (a dry year) and 1996 (a wet year). Each pair consists of a simulation using the period of the 5-year FVC climatology (CLIM) described before and the other one using the FVC values for such year (YEAR). The ZENG method has been chosen, among the three options,because it presents and intermediate behaviour between WETZEL and GUTMAN (see Figure 3.4) as well as it has been evaluated in previous works (Zeng et al., 2000). In all simulations the FVC databases generated have a resolution of 0.1 ° X 0.1 °, instead of the original resolution of 0.15 ° X 0.15 ° used by Gutman and Ignatov (1998).

3.3 Results

NDVI database comparison

Figure 3.2 shows the NDVI for the two datasets in a dry year (1995) and a wet year (1996) for January and July over the IP. It is remarkable that they differ in magnitude but spatial variability is quite similar (spatial correlation over 0.97). The differences are higher when comparing years with different precipitation regime, where NDVI values differ up to 30% in the summer (not shown).

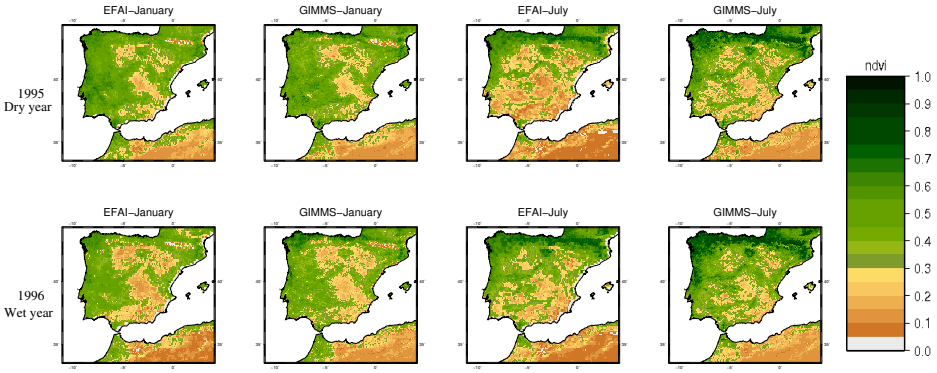

Fig. 3.2: EFAI-NDVI and GIMMS-NDVI for January and July for a wet year (1996) and a dry year (1995) in the IP. Source: Jiménez-Gutiérrez et al. (2019).

The 12 months run-mean series of the spatially averaged NDVI over the IP for the period 1982-1998 is shown in Figure 3.3a. Series show a quite different interannual variability for the whole period; the EFAI-NDVI has a greater variability and lower mean values than the GIMMS-NDVI. We attribute the disagreement (almost a periodical signal not attributable to natural variability) to the solar zenith angle correction implemented in the GIMSS-NDVI that avoids artificial trends derived from orbital drifting. At this point we conclude that the EFAI-NDVI should not be used for characterizing the vegetation properties in RCMs. Therefore, we will focus our study on the GIMMS-NDVI data. In addition, GIMMS-NDVI has a longer record, because of the compatibility with AVHRR data with MODIS and SPOT Vegetation satellite data, that have continuation till nowadays.

Usually FVC is implemented using climatological values in NWPMs and RCMs. We compare the spatially averaged NDVI over the IP, with monthly climatological values

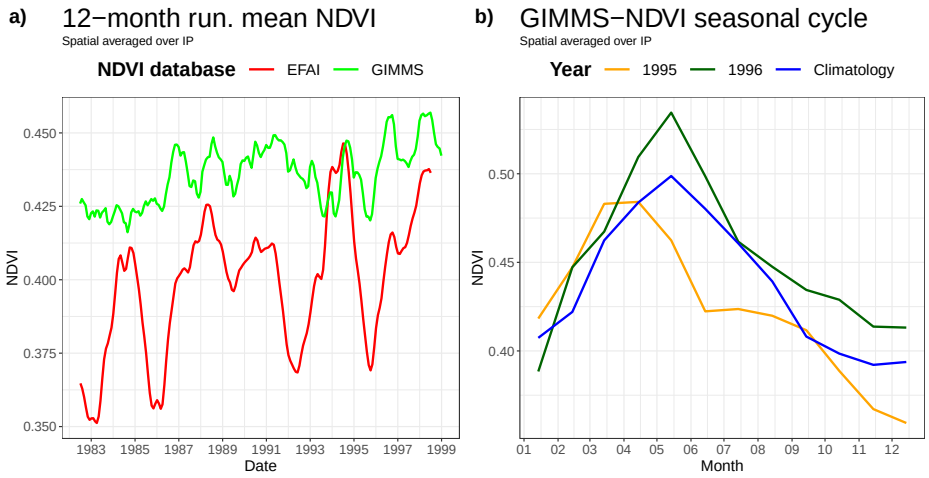

Fig. 3.3: a) NDVI 12 month run mean of the spatially averaged series for the IP derived from the EFAI-NDVI (red line) and GIMMS-NDVI (green line) b) GIMMS-NDVI monthly values for a wet year (1996, green line), a dry year (1995, orange line) and climatology (blue line). Source: Jiménez-Gutiérrez et al. (2019).

calculated on a 7 year period (1985-1991) with the monthly evolution on a specific dry (1995) and wet year (1996) (Figure 3.3b). The biggest NDVI differences between the dry and wet year are observed in spring, when the maximum of vegetation productivity occurs, prevailing these NDVI differences in a lesser way the rest of the year. The spatial average NDVI difference between wet and dry years is about 5% reaching values up to 15% in some areas. This elucidates that taking into account the interannual variability could be important when implementing these data in RCMs.

3.3.1 Analysis of FVC retrieval methods

FVC data were obtained for the 25 year of available NDVI data using the three methods. Figure 3.4a shows the temporal evolution of the FVC data spatially averaged over the IP and Figure 3.4b the temporal means of FVC values over the domain. Since the three methods use the same NDVI, there is a very good agreement in the temporal variation of FVC, however some important differences appear. The most remarkable difference comparing the magnitude of FVC is that WETZEL method presents FVC values 10% greater than the others. The ZENG and GUTMAN methods only differ around a 3% in

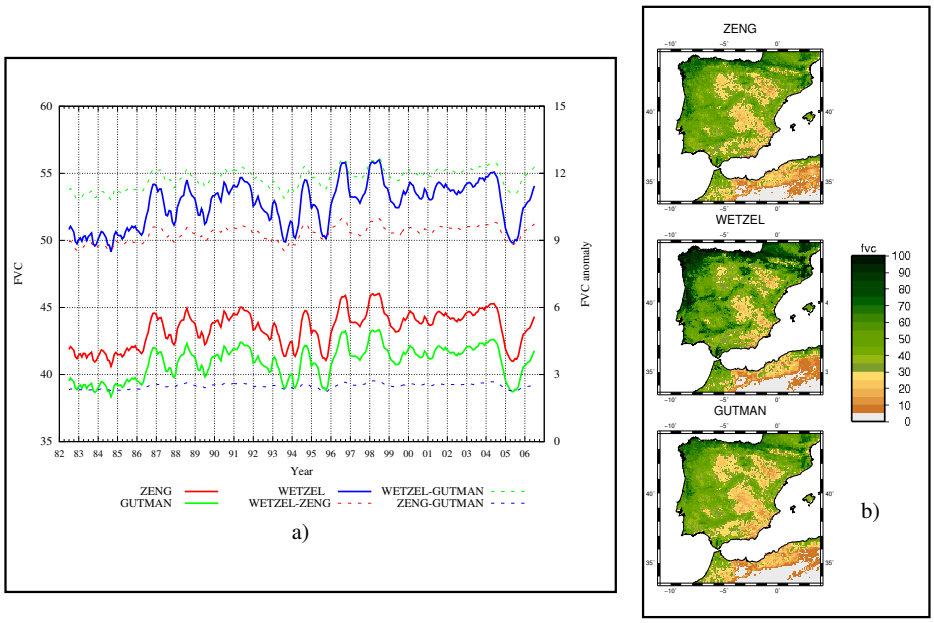

Fig. 3.4: a) FVC spatial averaged time series (solid lines) and differences between them (dashed lines) for the whole IP calculated by the WETZEL (blue line), GUTMAN (green line) and ZENG (red line) methods. b) FVC temporal averaged over the whole period (1982-2006) for the IP for the ZENG, WETZEL and GUTMAN methods. Source: Jiménez-Gutiérrez et al. (2019).

magnitude. This large difference is due to the fact that when applying WETZEL method the frequency distribution of NDVI was not taken into account. Regarding the spatial variability, the ZENG and GUTMAN show very similar patterns although the ZENG method achieves a larger range of FVC values, reaching values near 10% and over 80% more frequently.

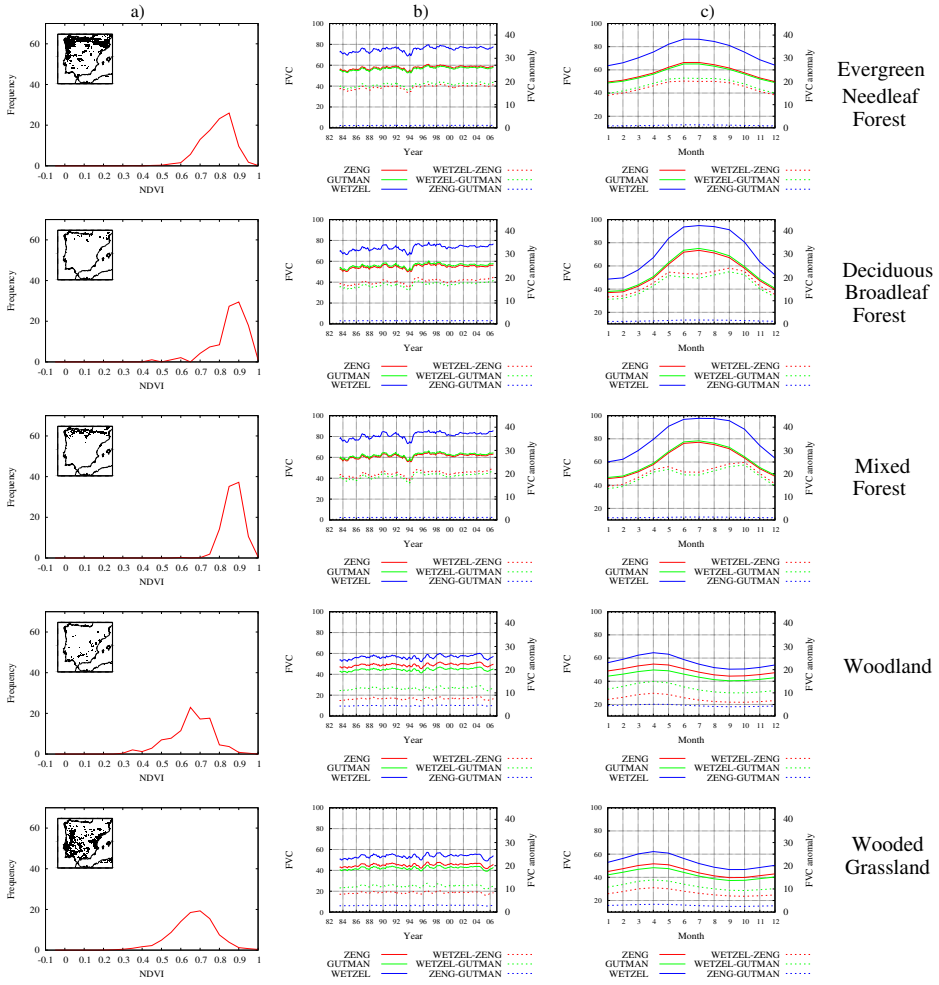

Fig. 3.5: a) Area covered by land type. Relative frequency distributions of NDVI in the IP by land types according to UMD global landcover. b) FVC time series in forest land types calculated with the GUTMAN (green solid line), WETZEL (blue solid line) and ZENG (red solid line) methods (spatial average by land type). Differences between FVC methods: WETZEL-ZENG (red dashed line), WETZEL-GUTMAN (green dashed line), GUTMAN-ZENG (blue dashed line). c) Same as b but monthly averaged values by land type for the period 1982-2006. Source: Jiménez-Gutiérrez et al. (2019).

The differences between the methods depend on the land type by construction. Figures 3.5b and 3.6b depict the time series of the FVC spatially averaged by land types calculated with the GUTMAN (green solid line), WETZEL (blue solid line) and ZENG (red solid line) methods as well as the differences between them (dashed lines). The GUTMAN and ZENG methods show very similar FVC values in forest land types (Fig.3.5), while the WETZEL method shows significant differences of around 20 % respect to the other methods. Land types with low values of FVC, such as shrubland, cropland and grassland (Fig.3.6) present smaller differences. In the case of closed and open shrubland, the WETZEL method presents the closest values to the other methods. This can be explained because NDVI values below the rupture point of the WETZEL method are more frequent for this land types (3.6a).

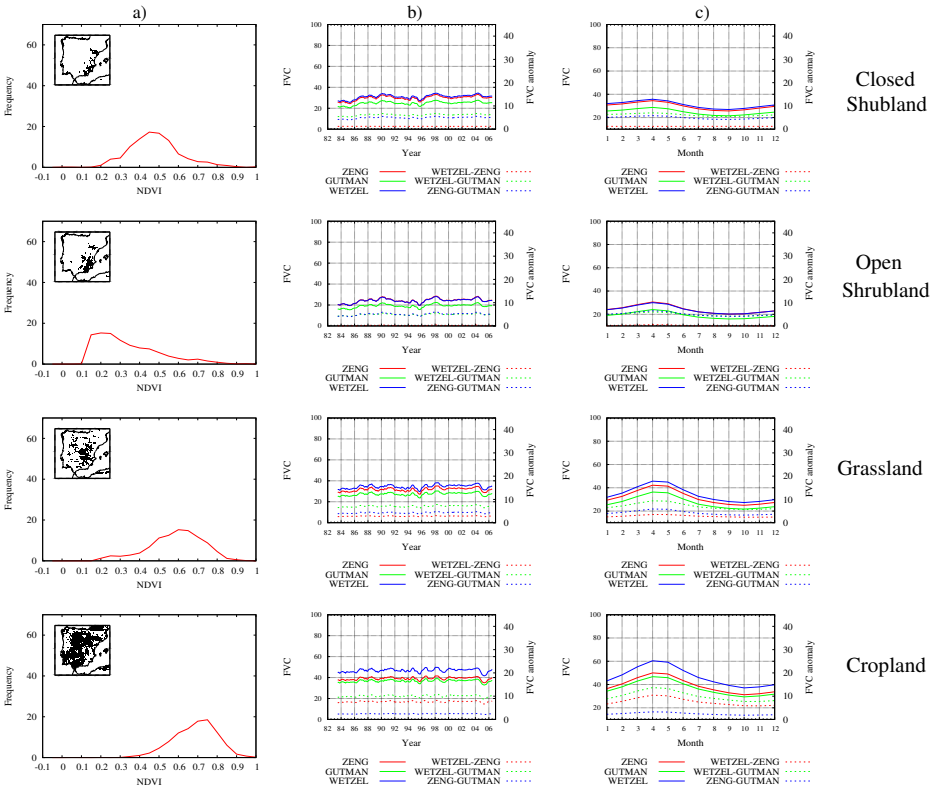

Fig. 3.6: As Figure 3 but for closed and open shrubland, grassland and croplands. Source: Jiménez-Gutiérrez et al. (2019).

Therefore, in general places with high FVC values exhibit a good agreement between the methods that take into account the NDVI frequency distribution (GUTMAN and ZENG), showing larger differences with the WETZEL method. While in places with medium and low values of FVC, the spread among the methods is lower.

Another interesting feature is to evaluate is the differences in phenology. Figures 3.5 and 3.6 show the relative frequency distribution if NDVI (a), temporal evolution (b) and FVC annual cycle (c) for each biome and the differences between them. In the biomes where the maximum of FVC occurs in summer, forest vegetation with low hydric stress, the GUTMAN and ZENG methods have a quite similar behavior (maximum value of 60-80% in summer) while the WETZEL method gives greater values. In the rest of the biomes, the maximum of FVC occurs in spring (irrigated lands or places with summer hydric stress) and the differences between the methods are smaller than for forest land types, although there are differences that could be remarkable in cropland, grasslands and woodland areas.

3.3.2 Sensitivity to the FVC estimation method

Here we asses the sensitivity of climate simulations to the use of different FVC data presented above. For the sake of clarity, we only present the comparisons between the ZENG and WETZEL experiments, because they show the largest FVC differences. Figure 3.7a depicts the FVC monthly means of ZENG for some months representative of each season (January, April, July and October) and 3.7b the FVC differences between the ZENG and WETZEL methods. There is a clear negative difference in the FVC estimated (ZENG-WETZEL) with higher FVC values for the WETZEL data, especially in areas with the highest FVC. The biggest difference is in April, when the vegetation productivity presents the maximum rate of generation of biomass.

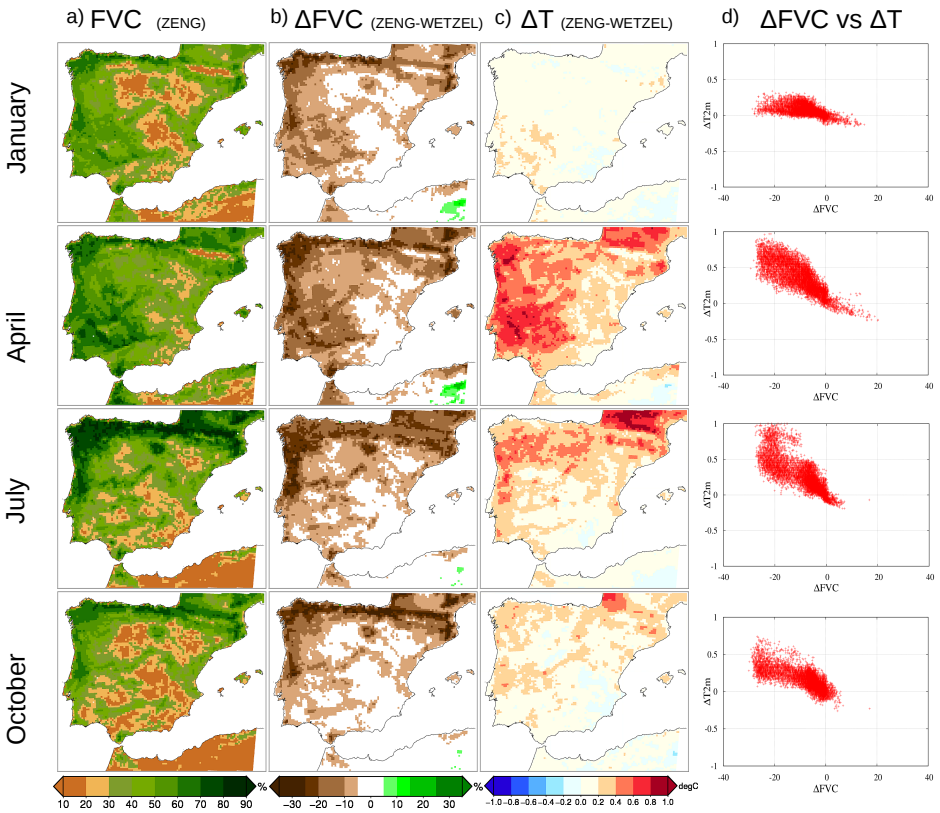

Fig. 3.7: a) Monthly means of FVC for the ZENG method. b) Differences of monthly means of FVC between the ZENG and WETZEL methods. c) Differences in monthly means of T2m between the ZENG and WETZEL regional climate simulations. d) X-Y scatter plot graph between differences of FVC (x-axis) and differences in T2m between ZENG and WETZEL methods(y-axis). Source: Jiménez-Gutiérrez et al. (2019).

The effect of such differences between the ZENG and WETZEL data on the regional climate simulations for monthly mean T2m is depicted in Figures 3.7c and 3.7d. In general, lower FVC values lead to higher temperatures, but this relationship depends on the time of the year (Figure 3.7d). This result is directly related to the sensible and latent heat partitioning (not shown). An increase/decrease of vegetation leads to a larger/lower evapotranspiration and therefore, a higher/smaller latent heat production. This leads to a reduced/intensified sensible heat manifested in a decrease/increase in T2m. Besides, there is an additional effect due to the modification of soil thermal conductivity by the

presence of a vegetation canopy. Heat flux from soil is reduced when FVC increases because of heat conductivity is diminished (Peters-Lidard et al., 1997; Ek et al., 2003). This effect is of importance mostly during night when these fluxes have a dominant role and can cause higher night temperatures with reduced FVC.

It is worth noting that T2m differences are higher in April and July than in January and October with similar FVC differences (Figure 3.7). In January differences of 30% in FVC lead to changes smaller than 0.5 ° C, while in July or April can reach 1 ° C in some places. This is mainly due to the greater availability of energy at these months. In addition, the greater dispersion in the quasi-linear relationship between changes in FVC and T2m (Figure 3.7d) for higher ΔFVC values may be relevant. Therefore, it is clear that changing the FVC database modifies the climatology reproduced by a RCM, both the spatial patterns and the amplitude of the annual cycle.

3.3.3 Sensitivity to FVC interannual variations

As mentioned above, in RCM experiments, FVC values are usually prescribed using climatologies, so they do not vary from year to year. But vegetation depends on the climate conditions as well as other factors, and it has a non negligible interannual variability. In this section we analyze the effect of varying the FVC according to the observations (real FVC) versus fixed monthly climatological/prescribed values.

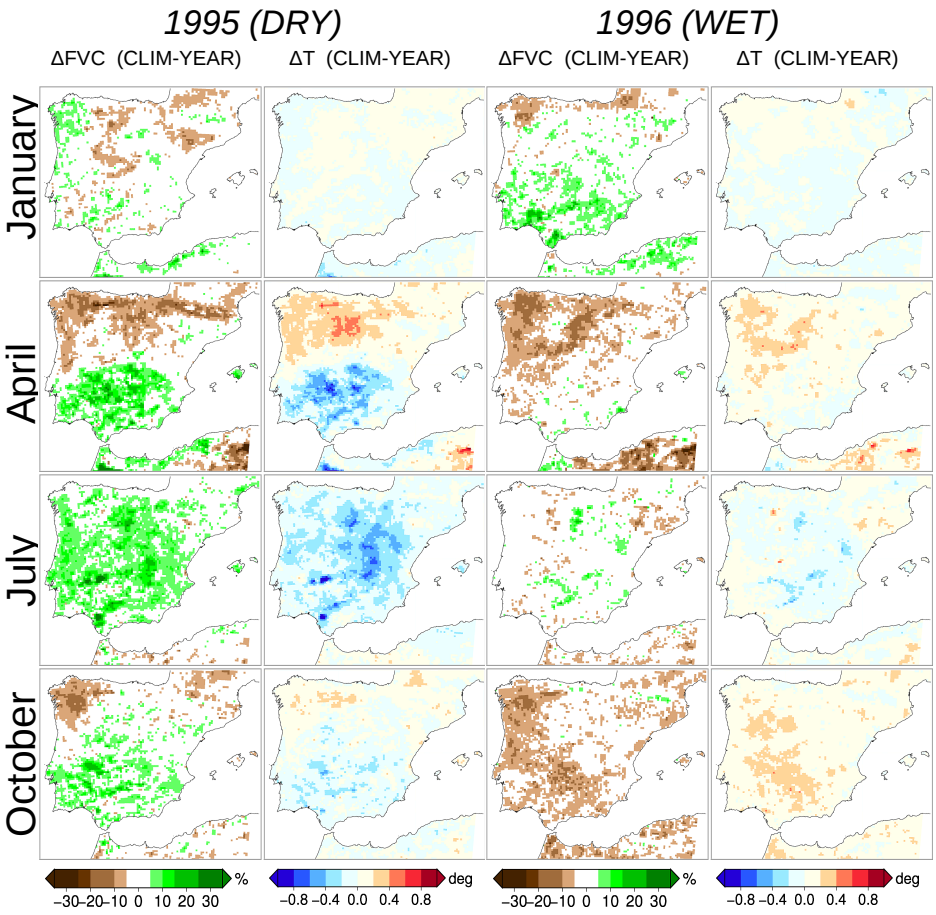

Fig. 3.8: Differences between CLIM simulation (climatology-based FVC) and YEAR simulation (inter-annual varying FVC) for FVC and T2m in a dry year (1995) and a wet year (1996). Source: Jiménez-Gutiérrez et al. (2019).

Figure 3.8 shows the differences between the FVC 5-year climatology simulation (CLIM) and the reconstructed (YEAR) for January, April, July and October for two years, the dry 1995 and wet 1996, These years were selected because of their quite different climate conditions. Dry conditions prevailed during 1995, while 1996 was characterized for abundant precipitation that favored higher biomass production.

During the dry year, the prescribed FVC is much higher that the estimated for this year, finding large areas with ΔFVC over 10%, especially in April and July that locally reaches values around 30%. The T2m temperature patterns resembles the spatial structure of ΔFVC with a clear negative bias. The largest T2m differences appear again in July and April, with values larger than 0.4 ° C in large areas that locally are over 0.8 ° C.

During the wet year the largest ΔFVC appears in April in the north-west part of the IP, and October over the South and Western Iberia. In this case differences are negative, i.e. the prescribed FVC underestimates the YEAR FVC. Interestingly, the absolute T2m differences are smaller, with slightly lower absolute ΔFVC. This is due to the fact that in July (highest sensitivity) ΔFVC is quite small, and that in April advection phenomena prevailed in the area with the largest ΔFVC.

Adding both effects at the different times suggest that interannual variability can change more that 1 ° C in some areas for a given month.

3.4 Discussion and conclusions

Three database of monthly FVC from 1982 to 2006 has been created for a domain covering the whole IP with a spatial resolution of 0.1 ° with the aim of being implemented in RCMs to improve climate simulations by providing more realistic soil physical conditions. Three different methodologies, WETZEL, GUTMAN and ZENG, were applied to the same NDVI database. The GIMMS-NDVI data was selected because it has better interannual behavior, longer record and is compatible with MODIS and SPOT-Vegetation data, which facilitates its temporal extension.

The comparison between the FVC databases reveals important differences between them that depend on the NDVI value and the biome, being especially relevant for forest land types. Methods that use the frequency distribution of NVDI (ZENG and GUTMAN) are more similar although some differences can be found between them depending of the land type. In addition, the FVC series reveal an important interannual variability, consequently prescribed FVC values can present important differences regarding the "real" FVC. These facts can be important when FVC are used in RCMs coupled to LSMs. The magnitude of the differences found causes a noteworthy impact on surface fluxes and hence modifying the regional climate.

The RCM experiments performed exhibit a not negligible effect of FVC uncertainty on the monthly climatological values. The results showed that differences of 30% of FVC, that appear in the two sensitivity experiments, can produce bias of 1 ° in T2m monthly values. Therefore, depending on the spatial structure of the FVC differences, the climatological patters are modified. In addition, the magnitude of the model response

depends on the time of the year. This implies that the annual cycle reproduced by the model is also sensible to the FVC data used. Finally, the role of the interannual variability of the FVC series can also change the interannual variability of climatological series (T2m in our study). In the experiment showed here, the differences for some times of the year, especially spring and summer could reach 1 ° C.

It is known that changes in vegetation also modifies the albedo. This was not taken into account in our experiments. Therefore, it can be expected an impact on the regional climate simulations. In fact, this impacts can be opposite to our findings since a decrease of the vegetation leads to an increase of albedo and then, less radiation is trapped by the surface and temperature could decrease. However, Crawford et al. (2001) show that the impact of changing albedo on surface heat fluxes is much smaller, an order of magnitude, than changing FVC.

In this Chapter we just analyze the sensitivity of RCM simulations to changes in FVC. A question remaining is if the RCM simulations with these new FVC datasets can better capture the climate over the IP. The sensitivity of the model to the FVC changes is much smaller than the deviations of the model respect to the observations (not shown), therefore it is difficult to find any improvement using only one or two years of data. This is not a surprising result. For example, Gómez-Navarro et al. (2012a) shows that the skill score of different RCMs depends on the data-base chosen for evaluating the model. Other example can be found in Fernández et al. (2007) and Jerez et al. (2013) where the authors did not find any combination of physical parameterizations that always reproduce better the observed climate. However, changing FVC with time instead of using climatological data should improve the simulation of inter-annual regional climate variability. For instance, the mean temperature differences between the dry and the wet year are better represented by the YEAR simulations (not shown).

In this work, just linear models have been tested for obtaining FVC from NDVI, because they have been more frequently used (for instance, in most of works cited along the work). Some examples are the NOAH Land-Surface Model and the NAM Eta model. However, some authors use quadratics models. Figure 3.1 shows the relationship between FVC and NDVI for the linear models analyzed and a quadratic model (GUTMAN Quadratic). The quadratic methodology drives to lower values of FVC. Anyway, the FVC differences obtained with linear methods covers the range of the differences in FVC that we found.

4

Temperature Response to Changes in Fraction Vegetation Cover in a Regional Climate Model∗

This chapter is focused in understand the physical processes that matter in the final response of near surface temperature through changes in fraction vegetation cover (FVC) using the Noah Land Surface Model (LSM). One of the main processes that condition the ratio between latent heat (LE) and sensible heat fluxes (H), is the bare-vegetation soil fraction determined by FVC. FVC drives the distribution of total evapotranspiration in transpiration through plants, evaporation canopy and bare soil evaporation. Plants transpiration is conditioned mainly by canopy resistance (R_c) and have an extensive treatment in this chapter. In Noah LSM, FVC is involved in another important process related with the reduction of thermal conductivity (K_t) in presence of vegetation. In this way, ground heat fluxes (G) are reduced with vegetation, inhibiting heat transport to deeper soil layers during the day and reducing ground temperature (T_g) during the night. In order of having a better understanding of this processes, a set of ideal simplified simulations with constant values of FVC have been performed.

∗ The main contents of this chapter are included in:
- J. M. Jiménez-Gutiérrez, F. Valero, J. Ruiz-Martínez, and J. P. Montávez, 2021: Temperature Response to Changes in Vegetation Fraction Cover in a Regional Climate Model. *Atmosphere*, 12(5), 599. (Jiménez-Gutiérrez et al., 2021)

4.1 Introduction

The role of FVC in numerical weather prediction and climate models is crucial, as it determines how energy is partitioned between latent (LE) and sensible (H) heat flux at surface. By means of LE, the water available in soil and vegetation is released to the atmosphere. FVC defines how total evaporation (E) is splitted into soil evaporation and plants transpiration (Jacquemin and Noilhan, 1990; Hong et al., 2009). Increasing FVC in a certain surface area results in enhancing transpiration and decreasing soil evaporation under the same soil moisture condition. In addition, FVC also has some implications in the ground heat transport since soil thermal conductivity (K_t) is moduled by FVC (Ek et al., 2003) in some land surface models (LSMs).

Matsui et al. (2005) analyze several key issues regarding the spatial and temporal variability of FVC. FVC calculation through NDVI was treated in Chapter 3 concluding that the uncertainty in the estimation of FVC can influence climate simulations (Hong et al., 2009; Refslund et al., 2014; Jiménez-Gutiérrez et al., 2019). On the other hand, some differences are also found when comparing climatological FVC datasets (constant monthly values, Gutman and Ignatov (1998)) with those that account for temporal evolution. In the latter, the wet-dry year variability provides a substantial temporal and spatial FVC heterogeneity. This issue has been treated profusely on regional climate modeling (Hong et al., 2009; James et al., 2009; Meng et al., 2014; Refslund et al., 2014; Crawford et al., 2001). Therefore, there are several key points related to the FVC data employed in regional climate modeling that introduce some uncertainties in climate simulations.

Thus, it is relevant to quantify how the variations of the FVC affect the prediction of the regional climate models (RCMs) as well as to identify the main physical factors involved. This quantification must be carried out under ideal conditions for a simpler explanation of physical processes and trying to cover both different times of the year and soil moisture conditions that allow addressing a wide range of cases. Therefore, it is desirable that the study situation and area include a high range of soil moisture conditions. For this reason the Iberian Peninsula (IP), as was treated in Section 1.4, is a suitable framework in which accomplish this regional climate simulations.

The main goal of this study is to analyze the impact of changing FVC in a RCM. The work focuses on the sensitivity of temperature to changes in FVC, by means of two one-year long simulations with different values of constant FVC in time and space.

4.2 Methods and Data

4.2.1 Land Surface Model

LSMs provide the boundary conditions at the land-atmosphere interface (see Section 1.1 for more details of land surface atmosphere interactions). Their role is partitioning available energy at the surface into sensible and latent heat flux components and rainfall into runoff and evaporation. In addition they update state variables which affect surface fluxes (e.g., snow cover, soil moisture, soil temperature). They are key component of climate models. Section 1.1.3 gives more insight about LSMs.

As commented in Section 2.2 Noah LSM is the chosen one in the MM5 simulations and a detailed explanation of the physics of the model is given in Sections 2.2.2 and 2.2.3.

4.2.2 Experiments Description

The description of the model configuration and the simulated domains is given in Section 2.3. The physics model parameterizations chosen are detailed in Section 2.3.3. The experimental design consist of two one-year long runs (plus spin-up) where FVC has a constant value in time and space of 90% (FVC90) and 30% (FVC30). For the sake of simplicity, land use has been set to constant (Cropland-Woodland mosaic) in both experiments. In this manner, the physical parameters such as albedo, roughness length, emissivity and thermal inertia, remains the same in both experiments, making easier the attribution of changes to FVC.

The runs have been performed for the year 1995 (considered as a dry year) with 4 additional months of spin-up period as has been described in the regional climate simulation strategy in Section 2.3.2.

4.3 Results

The analysis of differences (FCV90 - FVC30) of the averaged minimum, mean and maximum temperature over the whole year (see Figure 4.1) shows that the temperature in the simulation with the highest FVC is always colder. The differences range from 0.2 to 2.2 °C. The pattern of differences reveals that the greatest changes occurs in the valleys of the great rivers and inland flat areas. In the case of maximum temperatures, the differences present a spatial pattern characterized by a positive change in the south-east

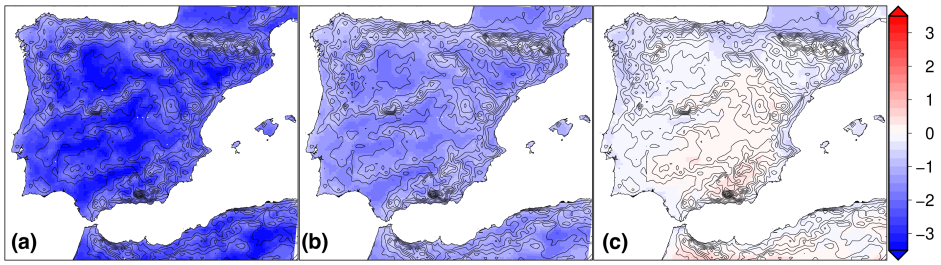

Fig. 4.1: Differences between FVC90-FVC30 experiment for (**a**) minimum, (**b**) mean, and (**c**) maximum daily temperature (°C) averaged over the whole period. Black contours denote the topography. Source: Jiménez-Gutiérrez et al. (2021).

half of the domain and a negative change in the North of the domain, with differences ranging between −0.5 and 0.5 °C.
For minimum temperatures, the spatial pattern of the differences is very similar to that of mean temperatures but much more intense, with differences reaching 4 °C. The spatial pattern of minimum temperature differences is related with the places where the denser cold air accumulates by gravity drainage. Meanwhile, the pattern of maximum temperature differences fits wet and dry areas. However, there is a large spatial variability along the year of such patterns. In summer, coastal Mediterranean areas show negative differences instead of the expected positive differences. This can be due to the enhancement of sea-breeze circulation related to the higher maximum temperatures inland. It is worth mentioning that the model has an idealized homogeneous land cover (cropland), which also explains the reasonably homogeneous patterns of the differences.

Below, we analyze the sensitivity to FVC for different times of the year and hours of the day. Figure 4.2 shows the air temperature at 2 m (T2m) at noon (12 UTC) (Figure 4.2a) and midnight (00 UTC) (Figure 4.2b) for each experiment and their differences for the central month of each season.

At night the difference patterns are almost the same along the year. They are coincident with the minimum temperature pattern shown above. However, the intensity depends on the time of the year, being much larger in summer (up to 5 °C) that in winter (up to 1 °C). On the other hand, the temperature difference patterns at midday strongly change along the year. In winter, temperature differences are small, in Spring are negative in all areas, while in Summer and Autumn some important differences appear between the north (negative) and south (positive) of the domain. Therefore, the effect of changing FVC on temperature is quite variable and depends on the time of day and season as well as on the surface properties.

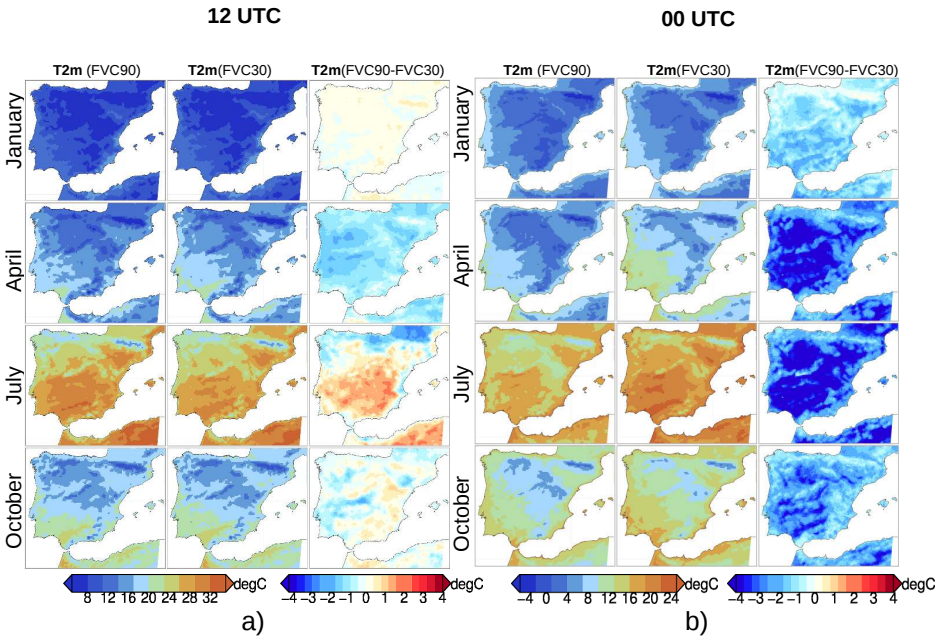

Fig. 4.2: T2m (°C) for experiments FVC90 and FVC30 and their differences at 12 UTC (**a**) and at 00 UTC (**b**) for January, April, July and October. Source: Jiménez-Gutiérrez et al. (2021).

4.3.1 Analysis of Surface Energy Fluxes

During the day, the temperature variations depend on the partitioning between H and LE. Figure 4.3a shows the differences between FVC90 and FVC30 for LE, H and EF at midday. During January and specially in April, LE is higher in FVC90, leading to lower values of H in most parts of the domain. However, this behaviour reverses in July and October in all areas of the domain but in the North. The obtained patterns correlate well with the changes obtained for maximum temperature (Figure 4.2a) and temperature at mid-day (Figure 4.2b). The spatial correlations with the differences of the sensible heat fluxes are 0.0 for January, 0.89 for April 0.89, 0.87 for July and 0.65 for October.

During the night, temperature changes depend on the availability of the soil for providing energy through G . Figure 4.3b depicts the surface fields of G at midnight. At first glance, it is clearly noticeable that upwards fluxes of this variable are always greater in the FVC30 experiment, primarily in July, with differences around 30–40 W/m^2. As men-

tioned before, this difference in the ground heat fluxes comes from the lower K_t values in vegetated surfaces. During the day, the ground catches more energy (higher soil temperature) and during the night there is more heat available, besides heat can be released more easily to the atmosphere.

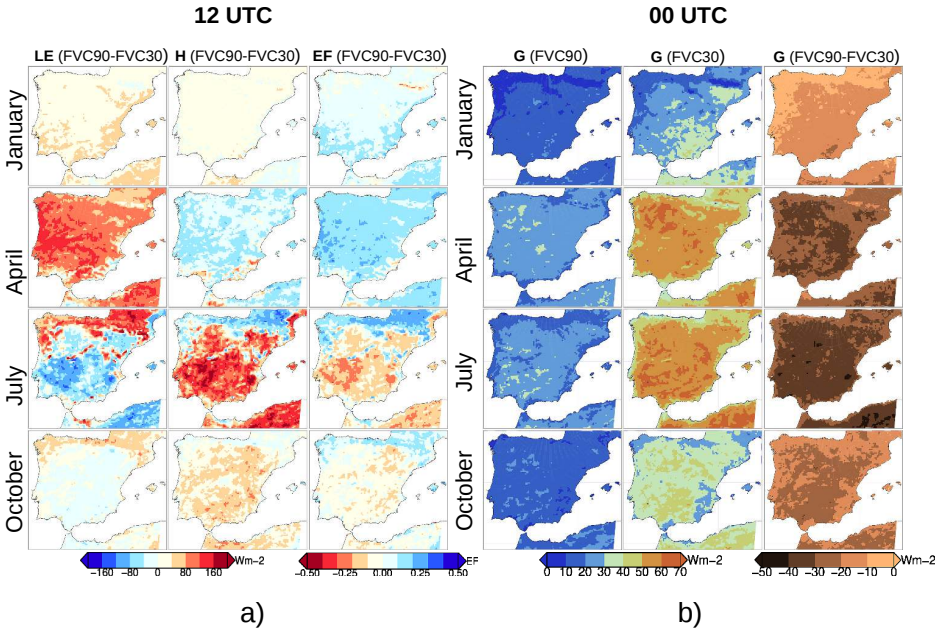

Fig. 4.3: (**a**) Differences of LE (W/m^2), H (W/m^2) and EF between experiments FVC90 and FVC30 at 12 UTC. (**b**) G (W/m^2) for experiments FVC90 and FVC30 and its differences at 00 UTC. Monthly means of January, April, July and October. Source: Jiménez-Gutiérrez et al. (2021).

4.3.2 Canopy Resistance and Soil Moisture

As commented before, the main differences in maximum temperatures are related to the evaporative fraction. Let's analyse them the canopy resistance as well as the soil moisture.

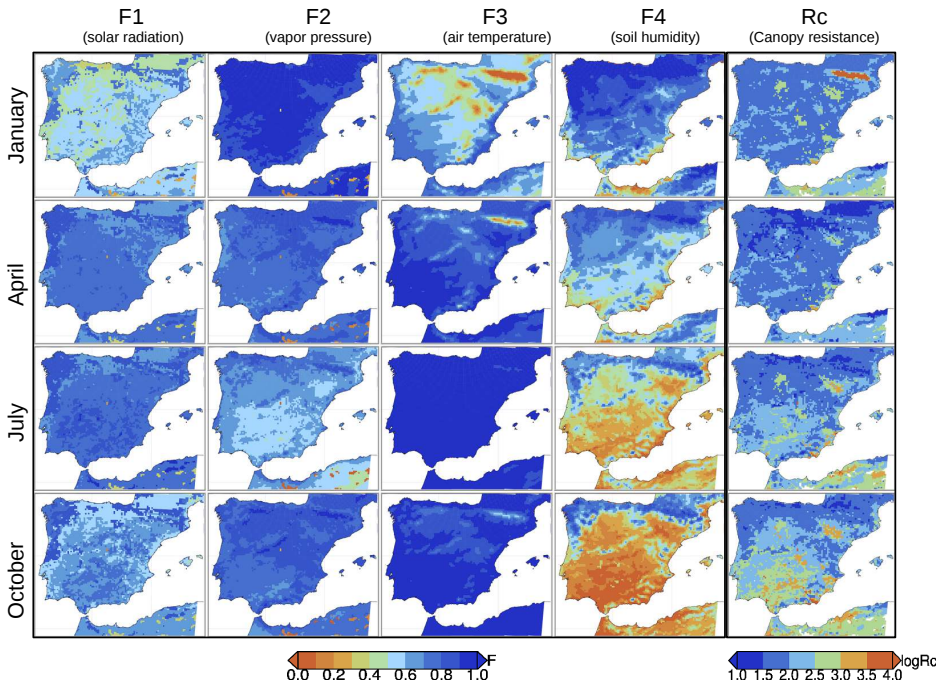

Fig. 4.4: Experiment FVC30. Deficit factors F1, F2, F3, F4 and R_c. Monthly means of January, April, July and October. Source: Jiménez-Gutiérrez et al. (2021).

Figure 4.4 show the R_c (expressed as logarithmic values) and the factors implied in its calculation for FVC30 experiment. The main contribution clearly comes from SM deficit (F4) with values very close to 0, showing a great difference respect the other factors. The FVC90 experiment presents a similar behaviour, being F4 lower, and therefore larger values of R_c (not shown). The analysis of the R_c (logarithmic) for FVC30, FVC90 and their differences (Figure 4.5a) displays that R_c evolves along the year with a minimum in Spring and a maximum in October. R_c is always higher in FVC90 and the differences are greater in summer, being the spatial pattern quite similar to the temperature differences at noon.

Regarding the SM, Figure 4.5b displays the monthly means for experiments FVFC30 and FVC90, and their differences for January, April, July and October for the second layer (from 0.1 to 0.4 m depth). In this year, the soil moisture is decreasing along the year in both experiments reaching the wilting point in a large portion of the domain (see Figure 4.6). However, the drying of soil is faster in FVC90 condictions. Negative differences of SM appears everywhere along the whole year. Greater FVC (FVC90)

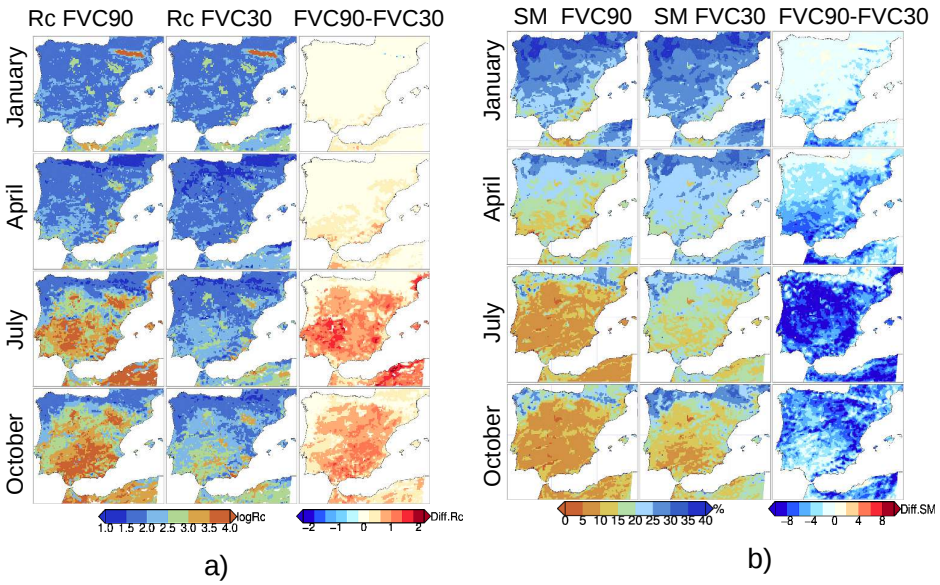

Fig. 4.5: (**a**) R_c for experiments FVC90 and FVC30 and its differences. (**b**) SM (%) (0.1-0.4 m depth) for experiments FVC90 and FVC30 and its differences. Monthly means of January, April, July and October. Source: Jiménez-Gutiérrez et al. (2021).

leads to a higher extraction of SM for E_t in the root zone layers. These differences reach its maximum in Summer (till 10%). Therefore the wilting point (WP), starting point when transpiration stops (Figure 4.6), is reached earlier and in wider areas in FVC90 experiment. In addition, there is a reduction of the SM differences in October. This can be attributed to the fact that FVC90 experiment reaches before the WP and FVC30 can continue extracting water from soil.

Therefore, the changes in temperature related to FVC mainly depend on the time of day and the availability of soil water. Figure 4.7 shows a clear example of this. We analyze the daily cycles of temperature and heat fluxes for the two simulations at two points (N1 and S1, see Figure 4.7) with very different water regimes. N1 is located in one area where there is not SM deficit along the year and there is just a slightly difference in R_c between FVC90 and FVC30. The location of S1 presents a SM deficit and R_c is much greater in FVC90 experiment.

Concerning nightime temperature, T2m is consistently minor in FVC90 for both locations, as a result of G being lower throughout the night in this experiment. This is linked

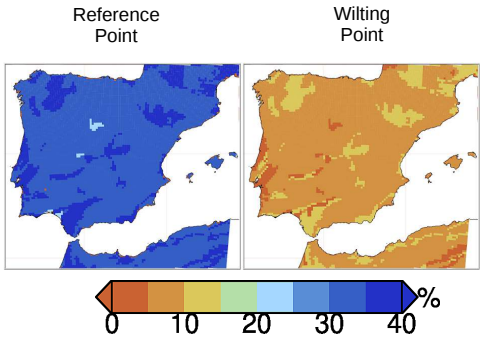

Fig. 4.6: Wilting point and Reference Point for SM (%). Source: Jiménez-Gutiérrez et al. (2021).

with the reduction of K_t in presence of vegetation, inhibiting the release of energy from soil layers to surface.

In N1, FVC30 T2m is always higher, but in winter, when temperature in both experiments is almost equal during the day. In this case, although LE flux is higher, H flux is also higher, due to the greater availability of energy due to the lower absorption by the soil. The differences in the heat transferred to the soil are quite similar along the year, while the amount of available energy is quite different depending on the season. This causes that H to be larger in FVC30 in the rest of seasons, leading to higher temperatures. It is also interesting that temperature differences between the experiments occur late in the afternoon and early at night. This is coincident with the maximum differences of upward ground heat flux.

In S1, the behaviour is similar while R_c difference is small (Winter and Spring). However, in Summer, LE is smaller in FVC90, leading to larger H and therefore to higher temperature. This LE depletion is associated to the SM deficit and R_c in FVC90 experiment. The effect of the higher vegetation coverage in FVC90 is a greater transpiration (LE fluxes) when SM is not a limiting factor. This greater evaporation entails a greater SM extraction from soil layers. Thereby, the WP is reached before in FVC90 that in FVC30 and this leads to a reversion of the cooling effect of vegetation (see Figure 4.8). Therefore, FVC90 shows higher temperature during the day, and lower temperatures during the night when soil moisture is scarce and transpiration is inhibited, leading to a bigger temperature daily range.

The different behaviour of both locations along the year at midday is presented in Figure 4.8. N1 is characterized by almost saturated soil in winter that evolves along the year with a minimum around September. The values for FVC90 are always lower but SM is always far from the WP. Temperature differences are negative, i.e., FVC90 shows

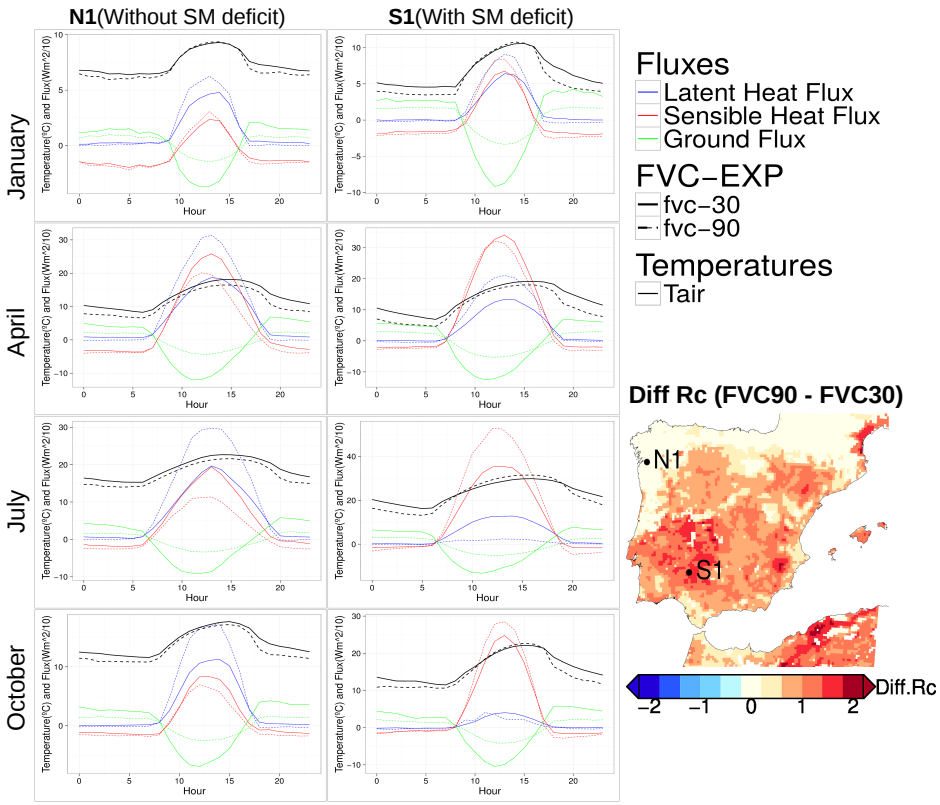

Fig. 4.7: Hourly means averaged for January, April, July and October. T2m (black line), H (red line), LE (blue line) and G (green line) for experiments FVC90 (dashed line) and FVC30 (solid line). Representative locations without SM deficit (N1) and with SM deficit (S1). Source: Jiménez-Gutiérrez et al. (2021).

lower temperatures, specially in summer, when differences reach 1.5 °C. The colder temperature is due to the higher *LE* in FVC90 because the larger capacity for extracting water from soil. The behaviour in S1 is similar to N1 during the first months (from January to May). However, after May SM of FVC90 experiment reaches the WP. At this point, *LE* strongly decays leading to higher *H* that carries out higher temperatures. Note that in both locations, *G* flux is always larger in FVC30 leading to (*G*–*H*) differences perfectly fits to *LE*.

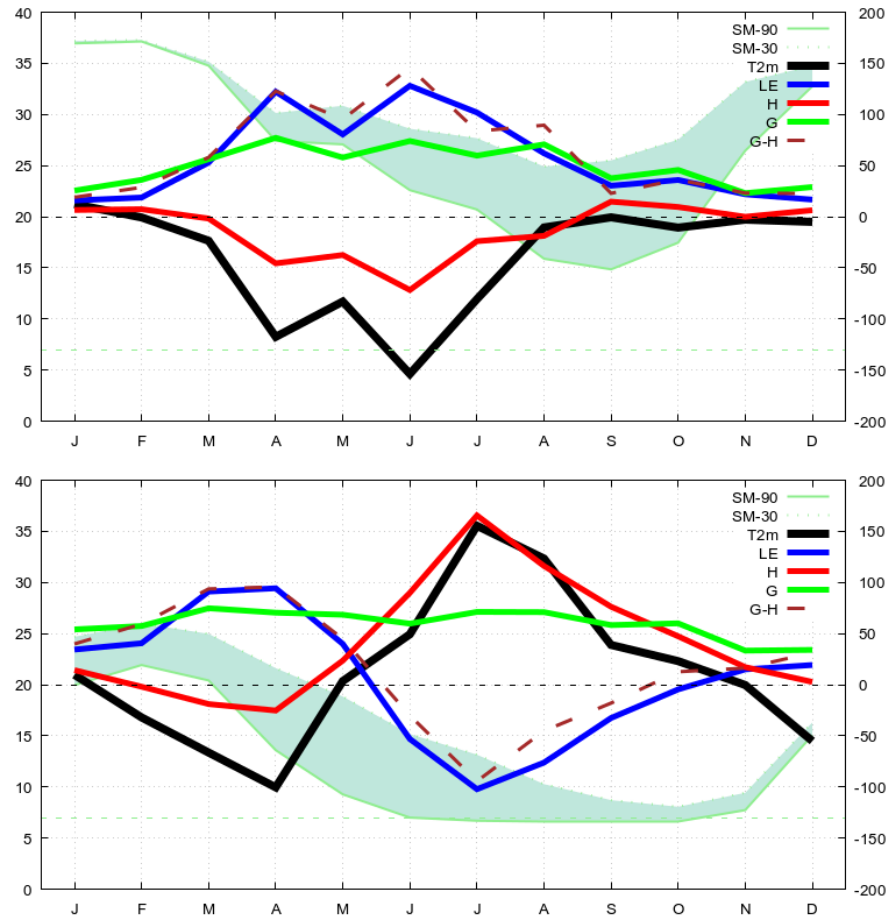

Fig. 4.8: Monthly mean differences at midday between FVC90 and FVC30 experiments for temperature ($°C \times 10^2$) and latent, sensible and ground heat fluxes (W/m^2, left y-axis) . Shaded green area represents the differences of the soil moisture at the third layer of the soil model (%, right y-axis). FVC90 has always the lower value. The constant dashed green-light line represents the wilting point. Left (right) panel shows the results for N1 (S1). Source: Jiménez-Gutiérrez et al. (2021).

4.4 Discussion

In this work the sensitivity of temperature to changes of the FVC has been studied in a RCM coupled to the Noah LSM. The analysis was performed by carrying out two identical simulations of one full year with constant FVC (90% and 30%) for all land points of the domain and times of the year. Our results, show how temperature is modified by changes in FVC depending on the time of the year, the time of the day and soil moisture availability.

Increasing the FVC leads to decrease the thermal soil conductivity (Ek et al., 2003). This implies a reduction of ground heat fluxes. During the day the soil absorbs less heat and therefore more sensible heat is available to warm the air. The final effect on temperature will depend on the portion of such sensible and latent heat fluxes ratio and will be discussed later. During the night the upward ground heat flux is diminished having as consequence a faster cooling of the air. Therefore, during the night a larger FVC always causes cooling.

When soil moisture is available, an increased FVC causes higher latent heat release through evapotranspiration. Therefore, during the day a larger FVC cools the air. The final effects on temperature will depend on the excess of sensible heat related to the soil thermal conductivity. On the other hand, changes in FVC leads to changes of a stress term in the canopy resistance parameterization Jacquemin and Noilhan (1990) mainly trough the soil moisture availability. Under high moisture stress, soil moisture near the WP, the latent heat released by evapotranspiration is strongly diminished, therefore such cooling effect almost disappears. This originates that an increase of FVC does not modify latent heat flux in such conditions.

As mentioned before, larger FVC leads to a faster drying of soil which implies larger effects on canopy resistance. High canopy resistance values inhibits water flux transpiration. In a situation of scarce precipitation, a soil with higher FVC reaches the Wilting Point before a less vegetated soil. This leads to have less latent heat, occasioning higher diurnal temperatures.

This response was also analyzed by Matsui et al. (2005) while comparing simulations with fixed and dynamic FVC studying North American monsoons. They also indicate the relevance of soil moisture factor in their simulations and the fact that higher FVC not always enhances EF and E_t. Other authors also highlight the importance of canopy resistance physics in controlling evaporation (Kurkowski et al., 2003; Marshall et al., 2003).

4.5 Conclusions

Summarizing, increasing FVC always entails lower temperatures at night. The maximum cooling occurs in places where cold air is accumulated (valleys, plane areas, etc). If soil moisture is available, increasing FVC leads to a drop in temperature when the excess of latent heat by evapotranspiration is larger that the excess of sensible heat due to the lesser thermal soil conductivity. In winter months both almost compensate and diurnal temperatures do not suffer great changes. However, in the rest of the year latent heat flux is larger and air temperature decreases. In case of dry soils, latent heat becomes small and temperature increases. In addition, more vegetation leads to faster drying of the soils, reaching the WP before and provoking higher temperatures.

Note that this behavior is related with an increase of the daily temperature range. In the case of our experiments, the mean annual differences over land are larger than 2 °C, reaching some specific places at some months values above 5 °C when changing FVC from 30 to 90%. It is worth mentioning that results can be model dependent, therefore it would be desirable to perform more experiments using other LSMs based on varied physical approaches.

Thus, we find a remarkable sensitivity of temperature to FVC. The FVC variations imposed in our experiments could serve as an upper limit to the common differences that can be found due to different factors such as inter-annual variability, reconstruction method of FVC, NDVI databases, etc. Therefore, a correct estimation of FVC values is crucial in order to improve temperature representation in RCMs. Moreover, the canopy resistance parameterization is critical in understanding the final effect of FVC (Matsui et al., 2005), then a correct representation of canopy resistance parameters like R_{cmin} (Kumar et al., 2014) or parameters dependent of soil type could have a non-negligible impact on RCM experiments.

Another important aspect may be the impact that the imposition of future vegetation values may have on climate change scenarios. An excess of vegetation in areas where future projections tend to give drier climates may amplify the estimates of increase in maximum temperatures, with the consequent effect on heat waves. One interesting question may be related to a better understanding of compound events such as droughts and fires. Areas with large vegetation in situations of water stress can cause temperatures to rise more and in turn make droughts more extreme increasing the probability of fires. On the other hand, a future reduction of vegetation might lead to an increase of temperature, specially the minimum ones, favoring extreme events such as raising the number of tropical nights.

5

Spatial and temporal variability of FVC and their effects on regional climate experiments

In the previous chapters, have been analyzed the effect that variations of fraction vegetation cover (FVC) can have in the simulation of near surface temperature in regional climate simulations. Values that FVC can take in a regional model are subject to variations that may have different sources. As shown in Chapter 3, the FVC calculated value depends on satellite database, as well as of the calculation method of FVC from satellite values (NDVI). On the other hand, most of the regional climate simulations with regional climate models (RCMs) consider FVC climatological values, that is to say, include an intra-annual variability but not and interannual variability.

This chapter deals with the role that intra-annual and interannual variations of FVC can have in near surface temperature simulated by RCMs. In this way, a set of regional climate simulations have been performed using near-real time (COP-YEAR) and monthly averaged values (COP-CLIM) from Copernicus FVC data, and another considering the default climatological values of FVC in the Noah LSM (GUT-CLIM).

5.1 Introduction

The Land surface (LSM) component of a numerical weather prediction model needs to have information about the vegetation covering the ground. This information is essential in order to correctly simulate the exchange of heat, moisture and momentum fluxes between the ground and the atmosphere. Vegetation is usually approximated by

three parameters; the green vegetation fraction (FVC), the leaf area index (LAI), and the vegetation type or class Stensrud (2007). Depending on the soil-vegetation-atmosphere parameterization used, FVC can be used once LAI is set. This occurs in the Noah LSM. On the other hand, FVC values are often prescribed to a climatology, with values varying from month to month. Depending on the database (NDVI) and the methodology used, FVC can have different values for the same area Jiménez-Gutiérrez et al. (2019).

Some previous works Jiménez-Gutiérrez et al. (2019, 2021) (for the thesis, previous chapters), have shown that there is a relevant sensitivity of temperature to FVC variations. Temperature changes are different for maximum and minimum temperatures. While for minimum temperature there is a clear linear relationship between temperature changes and FVC, for maximum temperatures it is not so clear. Furthermore, the slope of the relationship depends on the season of the year, mainly due to the amount of energy put into play.

Climate variability, specially precipitation, implies temporal and spatial FVC heterogeneity that can lead to a non negligible effect in numerical simulations (Matsui et al., 2005). For this reason, extensive research has been carried out across different spatial and temporal scales to study the sensitivity of LSMs to the implementation of FVC datasets obtained from NDVI data with high temporal and spatial resolution, particularly with the Noah LSM. In the field of mesoscale modelling with high-resolution domains and with several days of evaluation, several examples of real-time FVC data incorporation can be found (Kurkowski et al., 2003; James et al., 2009; Hong et al., 2009; Kumar et al., 2013; Li et al., 2014; Vahmani and Ban-Weiss, 2016). These works clearly show the impact of using satellite-derived land cover parameters compared to model simulations that use prescribed climatological values to describe land cover characteristics. In the field of regional climate simulations, several examples can be found with the Noah LSM using realistic FVC data instead of default data. With simulated periods of 1-3 months some works are also available in the literature; cases of heat waves in Europe (Refslund et al., 2014) and oasis-desert systems in China (Zhang et al., 2017) with improved model performance, and with inconclusive results studying the effect on droughts in southern South America (Müller et al., 2014b), with inconclusive results. Other examples of relatively long, full-year, simulations with improved FVC data (He et al., 2017; Yan et al., 2020a) in China show a more realistic behavior of the simulated T2m and humidity fields but less clear improvements in precipitation. Finally, other works with multi-year simulations (15-30 years) (Ge et al., 2014; Yan et al., 2019) find relationships between vegetation changes and temperature trends, improving the representation of extreme events such as heat waves, although it seems they may introduce new biases in simulations.

In this context, it is interesting to study the sensitivity of climate simulations both to the use of different databases and to the introduction of realistic spatio-temporal variability of vegetation. The Iberian Peninsula (IP) is an ideal domain for such tests. The

IP is characterized by a strong spatial climate variability, with Mediterranean, continental, high mountain, oceanic and near-desert climates and a strong intra-annual and inter-annual variability (Tullot, 2000) that is reflected in its high vegetation variability.

The main objective of this work is to analyze the sensitivity of climate simulations to spatial and temporal variability of vegetation in long term periods. For this purpose, a series of long simulations will be carried out using different FVC databases, and the effects on statistical moments of the maximum and minimum temperature will be analyzed as well as the possible connection between changes in vegetation and temperature trends.

5.2 Data and Experiments

In order to accomplish the objectives of this chapter three long term simulations have been performed, using different FVC data. First, a simulation was carried out using the default FVC data in MM5, based on the Gutman method Gutman and Ignatov (1998). Secondly a simulation using the high resolution data provided by Copernicus, including the temporal variability of the observed data. And finally a simulation using the climatological values of the previous case. Following, these data and experiments are detailed.

5.2.1 Vegetation data

As mentioned in previous chapters the Land Surface Model used in this work is the NOAH model Niu et al. (2011). NOAH needs FVC as information of vegetation, while LAI is kept constant.

Noah LSM in MM5 and WRF model uses a default FVC monthly climatological data (GUT). This commonly used database is described in Gutman and Ignatov (1998) . More details can be found in Sections 2.3.4.4 and 3.2.2.

On the other hand, Version 2 of global FVC from Copernicus Global Land Service at 1 km resolution (∗) is used (COP). This database ranges from 1999 until june of 2020. The input data are the daily Top of the Atmosphere reflectances measured with the sensors of SPOT-VGT and PROBA-V satellites. The calibrated reflectances in visible, near-infrared and shortwave infrared are used to calculate instantaneous estimates of the products using a neural network trained with MODIS and CYCLOPES products. Moreover, a temporal smoothing and gap filling is made using climatology information from version 1 to ensure continuity and consistency. In a second stage, these instanta-

∗ http://www.land.copernicus.eu/global

neous first guess of products are composited for obtaining values every 10 days (Verger et al., 2014).

For assimilating Copernicus FVC data into the Noah LSM, it was necessary to perform a preprocesing of the original data. This previous work consisted of creating monthly values and interpolate them from the original spatial resolution (1 km) to the 10 km resolution of our experiments. For this task some modification of MM5 preprocesing routines were carried out.

In addition, the climatological values (yearly values of each month) of Copernicus FVC data was constructed. Note that all FVC data are interpolated by the pre-processing tools to the 10km domain.

5.2.2 Experiments description

All regional climate simulations have been performed using the climate version of the MM5 described in Section 2.3.2, and widely used in climate experiments (Gómez-Navarro et al., 2012b; Jerez et al., 2012; Lorente-Plazas et al., 2015, among many others). The experiments performed in this work span the period from 2000 to 2017 following the strategy explained in Section 2.3.2. The spatial configuration and model physics are detailed in Sections 2.3.1 and 2.3.3. All experiments are driven by era Interim reanalysis (Dee et al., 2011) using boundary conditions every 6 hours. The spin-up time is four months, time enough to forget the effects of initial conditions (Jerez et al., 2020). Therefore, all experiments performed only differ in the FVC data used.

As mentioned above, one objective of this chapter is to analyze the role of using two different FVC databases with different resolution and methodology. For this purpose, two simulations (CLIM) have been carried out in which the temporal variability of FVC is the same (CLIM) but the climatological values are different (Gutman method and Copernicus). On the other hand, we are interested in the role of including the role of temporal (interannual) variability of FVC. For this purpose, we will perform experiments using the FVC Copernicus values reconstructed for every month of the particular period of our simulation (YEAR). Therefore, three long climate simulations using two different data sets; GUT-CLIM and COP-CLIM that use FVC monthly climatological data, and COP-YEAR that uses montly FVC data. Table 5.1 presents a summary of the experiments performed.

Case	FVC dataset	Resolution	Temporal average
GUT-CLIM	NDVI from AVHRR	0.15 °	Climatology 1985-1991
COP-CLIM	Copernicus	0.1 °	Climatology 2000-2017
COP-YEAR	Copernicus	0.1°	Yearly values 2000-2017

Table 5.1: Summary of the simulations performed using default FVC of model MM5 and Copernicus FVC.

5.3 Results

5.3.1 Analysis of FVC data

As a first step, we analyzed the differences between the climatological values of FVC in GUT and COP experiments. Evidently, the mean climatological data of COP-YEAR are identical to COP-CLIM by construction. Figure 5.1 presents the mean monthly values of GUT-CLIM and COP-CLIM for the months of January, April, July and October as well as their differences. These months have been chosen as representative months for each season and will be used throughout the chapter.

We note that the two databases realistically present the spatiotemporal variability of FVC. In the southern areas of the IP, the vegetation peaks occur in April, while in the north they occur in summer. On the other hand, the databases capture in an acceptable way the vegetation gradients that appear between the north of the IP with values close to 100% and the south with values below 20% in large areas. The spatial correlation of the two data-bases for each month is always over 0.93. This means that the spatial pattern is almost identical, although, as can be seen in the figure, the structure obtained by COP is much finer as expected.

However, we obtain that there is a significant difference in the value of FVC in them. GUT-CLIM always presents much higher values, which on average are around 18% and vary in the range of 5 to 25%. The analysis of the differences shows that they are significantly correlated with the mean values. The largest differences appear in places with high, but not maximum, vegetation. For example, in the case of summer and autumn, the northern faces of the main mountain ranges show the greatest differences.

These differences may be due to several factors. On the one hand, the periods with which the climatologies have been calculated are different, and on the other hand, both the satellite data and the methodologies used for the calculation of FVC are very different.

Therefore, we observe that there is some structure in the spatial differences and that these are dependent on the time of year. An interesting question is is whether these

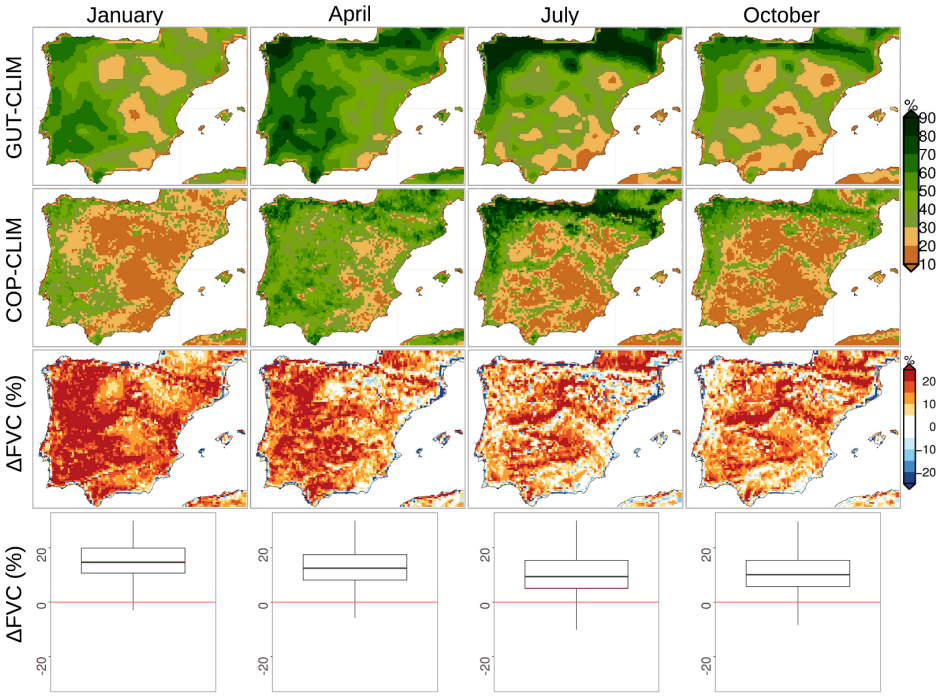

Fig. 5.1: Monthly average of FVC in January, April, July and October for the period 2000-2017 in GUT-CLIM (first row) and COP-CLIM (second row) experiments and their spatial and box-plot differences (third row and fourth).

patterns of differences can be related to the land use. Figure 5.2 shows the average annual cycles for the different land uses.

In general, the differences are greater in winter and smaller in late summer and early autumn. This behavior is quite similar in all types except for agriculture, where these differences are more constant throughout the year. Differences are minimal in summer in closed forest areas. Another interesting feature is the delay between peaks, i.e. in the period of highest productivity. This seems to occur later in most of the types in the COP-CLIM.

One of the main motivations of this work is to study the role of interannual variability of vegetation on climate reproduction by a RCM. Let us analyze the variability of the FVC in our simulations. Figure 5.3 plots the mean, standard deviation, and range, calculated as the maximum and minimum of FVC in the COP-YEAR experiment. As before, we present only the values for four representative months of the year.

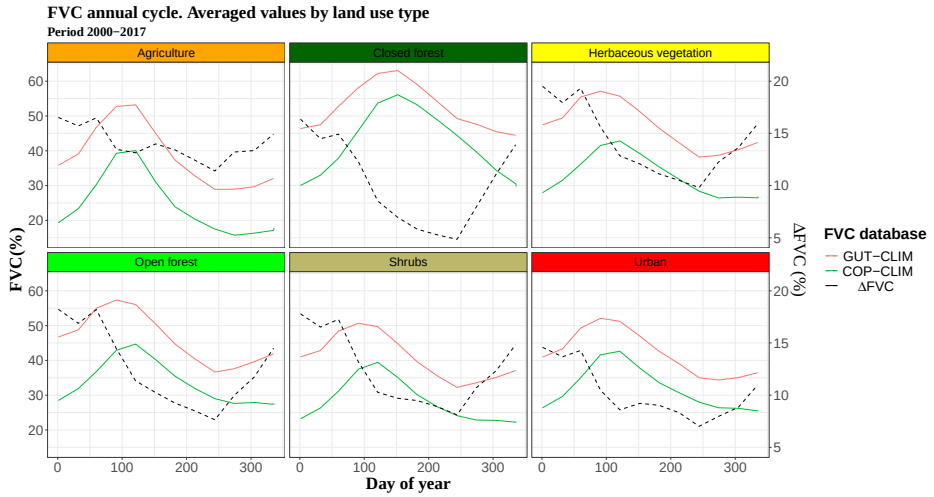

Fig. 5.2: Annual cycle of FVC for the period 2000-2017 by land use type in GUT-CLIM and COP-CLIM simulations.

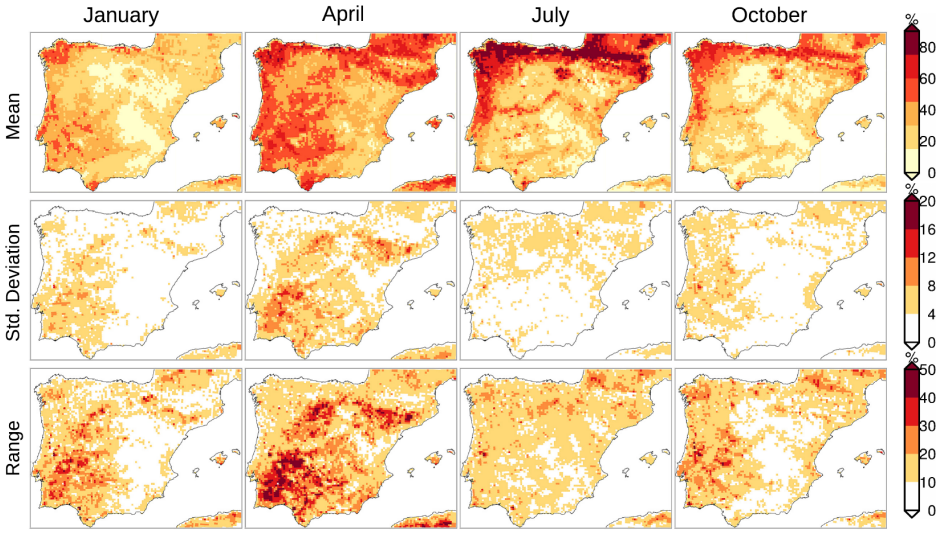

Fig. 5.3: Mean, standard deviation and range (between maximum and minimum values) of Copernicus FVC for the period 2000-2017 in the months of January, April, July and October.

The results show that the greatest variability of FVC occurs in winter in the west of the IP. In spring the pattern is similar but extends to the south, and the Ebro valley and it is stronger that in winter. However, this pattern is different in summer where the variability, although lower, is more evident in the north. In the other hand, it is similar to the winter pattern but extends to the east of the Peninsula. The differences (range) reach values of more than 40% in large areas in the south and center of the IP. Note, however, that areas in the north, where vegetation values are maximum, show little inter-annual variability. The variability pattern is well correlated with the mean field, the spatial correlation ranges from 0.71 in May to 0.90 in September.

This variability must be closely related to the precipitation regimes in the IP. The western area is strongly influenced by the NAO, while the eastern area is more related to autumn precipitation. However, in the north, precipitation variability does not seem to affect vegetation variability in a notable way, possibly because there is always enough moisture available for the development of the vegetation cover.

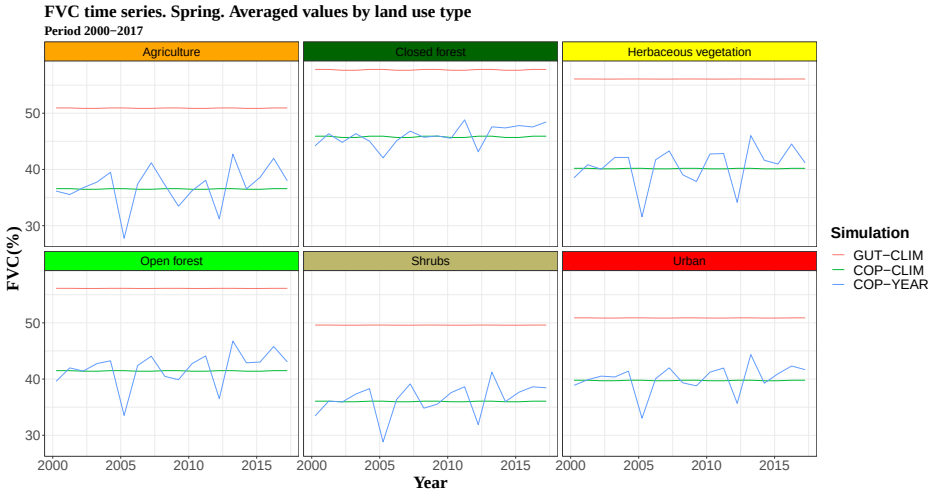

Fig. 5.4: Yearly values of FVC in spring for the period 2000-2017 by land use type. GUT-CLIM, COP-CLIM and COP-YEAR experiments.

Analyzing again the series grouped by land use in spring, where the plant productivity is larger in most of places (Figure 5.4) we observe several interesting aspects. In general, the variability of the series never reaches the GUT-CLIM values. This could imply that the years chosen for the climatology are not determinant, but that the methodology is the most important factor to explain the differences between both databases. On the other

hand, the lower temporal variability correspond to the closed forest land use, that is the one with the largest FVC mean value. This correspond to the northern areas. The rest of land types present similar behavior. In addition, all series show a positive trend, i.e. the vegetation is growing along the time. At this point, and taking into account the results of previous chapters, we can anticipate that this will cause a change in the variability of the temperature series in both the short and long term. This feature will be addressed later.

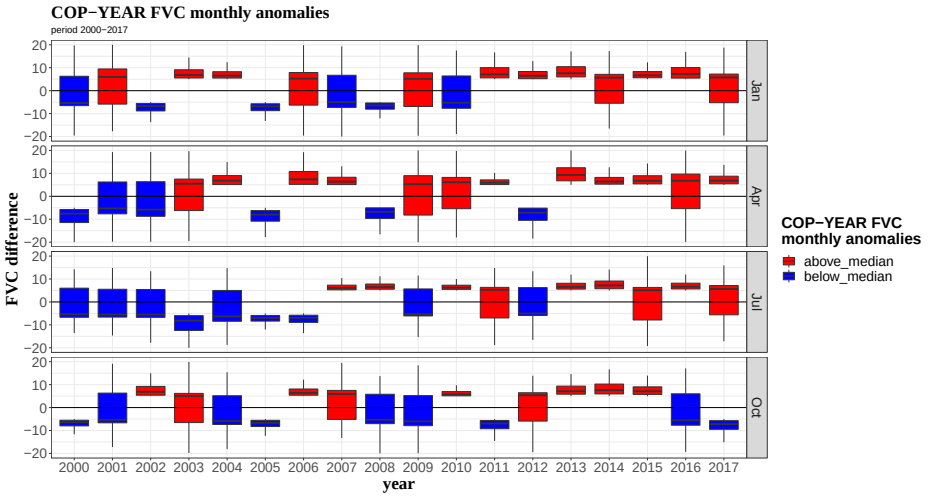

Fig. 5.5: Boxplot of yearly mean anomalies of COP-YEAR FVC simulations in January, April, July and October for the period 2000-2017. All points of the simulation domain are considered.

Figure 5.5 represents the boxplot of the FVC differences between the COP-YEAR and COP-CLIM simulations, or just the COP-YEAR anomalies, in January, April, July and October for the period 2000-2017 considering all the points of the simulation domain. The years in which the median is above 0 are marked with red color (more vegetated years) and those with vegetation below median (less vegetated years) are marked with blue.

Although in some years differences of FVC show a great spatial variability, in others differences are more unifom leading to a mean pattern of more/less vegetation covered years. Regarding the behaviour between months, there are years in which the pattern can be reversed or remains the same during the same year. This will depend of the spatial variability and distribution of precipitation along the year.

The positive trend of all series except for October is again striking. We also observe how the FVC anomaly has a differente pattern in different years. In some cases the vegetation anomaly affects all places in all months, for example the years 2013 (excess) and 2005 (defect). While in others, both the excess and the defect of vegetation is unevenly distributed in the points of the domain, for example the year 2003 or 2016. Figure 5.6 and 5.7 show the spatial patterns of these anomalies for years with vegetation defect, 2005 and 2012 (Figure 5.6) and for cases with excess vegetation; 2013 and 2016, (Figure 5.7).

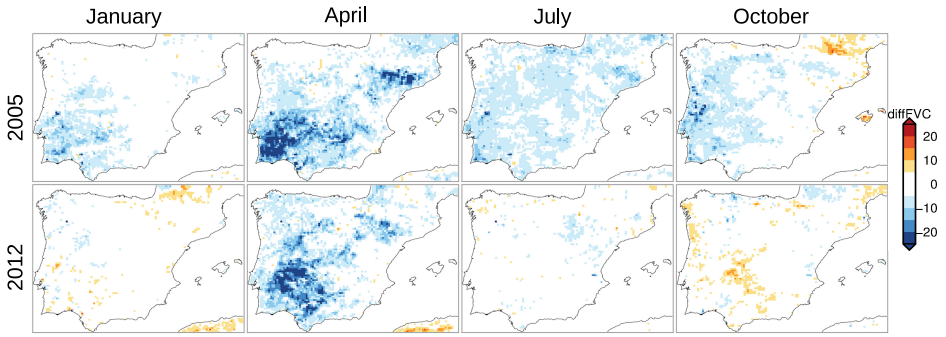

Fig. 5.6: FVC Copernicus anomalies in sample years with FVC values below the median for the period 2000-2017.

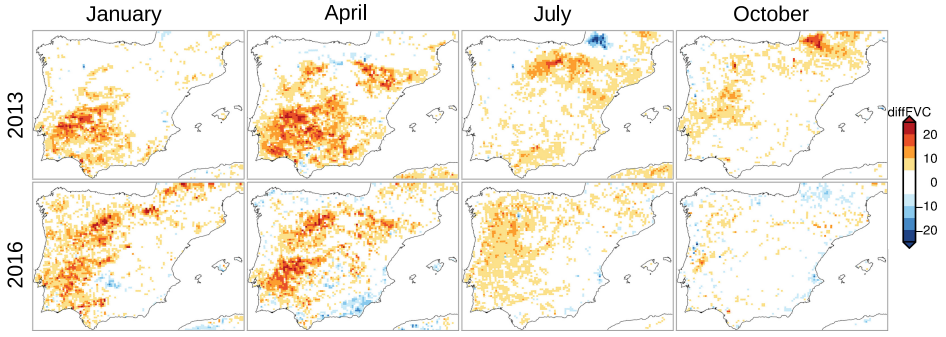

Fig. 5.7: Same as Figure 5.6 but with FVC values over median.

Year	2000	2001	2002	2003	2004	2005	2006	2007	2008	2009	2010	2011	2012	2013	2014	2015	2016	2017
Precipitation anomaly (mm)	52	9	60	107	-43	-187	8	-76	75	16	209	-76	-85	110	59	-121	47	-166

Table 5.2: Precipitation anomalies for the period 2000-2017 calculated from AEMET 5km precipitation dataset. Spatial average in the 10 km simulated domain

Considering spatial precipitation anomalies from AEMET 5km precipitation dataset for the whole simulated domain (Table 5.2), it should be noted that in the selected years with generally lower FVC values (Figure 5.6), there seems to be a relationship with drier years from the hydric point of view, with a more pronounced effect in 2005 throughout all the months. For the years with a higher FVC (Figure 5.7), 2016 has a less clear relationship with precipitation than 2013, observing an opposite pattern (lower FVC) in the southwest of the Iberian Peninsula (IP) more appreciable in April. Hence, the relation with precipitation needs to be deeper analyzed, specially at local scale.

5.3.2 Temperature response to constant changes in FVC

Firstly, the effect of changes in FVC on 2 meter temperature (T2m) fields has been analyzed by comparing regional climate simulations GUT-CLIM and COP-CLIM. Figure 5.8 shows monthly means differences between GUT-CLIM and COP-CLIM experiments averaged over the period 2000-2017 for mean, maximum and minimum T2m.

As expected from the results of previous chapters, there are always negative temperature differences, i.e. the GUT-CLIM simulation is colder, since it is the one in which the vegetation fraction was higher.

The differences are greater for minimum temperatures and practically null for maximum temperatures. The mean temperature shows an intermediate behavior. Although the patterns of temperature differences roughly follow those of vegetation, there are notable deviations depending on the area. For example, the northern areas of the peninsula show smaller differences. We also note that such pattern seems to be modulated by the orography and by the base vegetation itself, especially for the minimum temperature.

On the other hand, it can be seen that the greatest differences appear in summer and the smallest in winter. In addition, the effect on spring is much greater than in autumn. In summer, these differences reach 2 °C while in the winter they barely reach 0.8 °C. This is remarkable, since the maximum departures of the vegetation occur in the winter months. This behavior must be related to the greater amount of energy to be partitioned into sensible and latent heat fluxes.

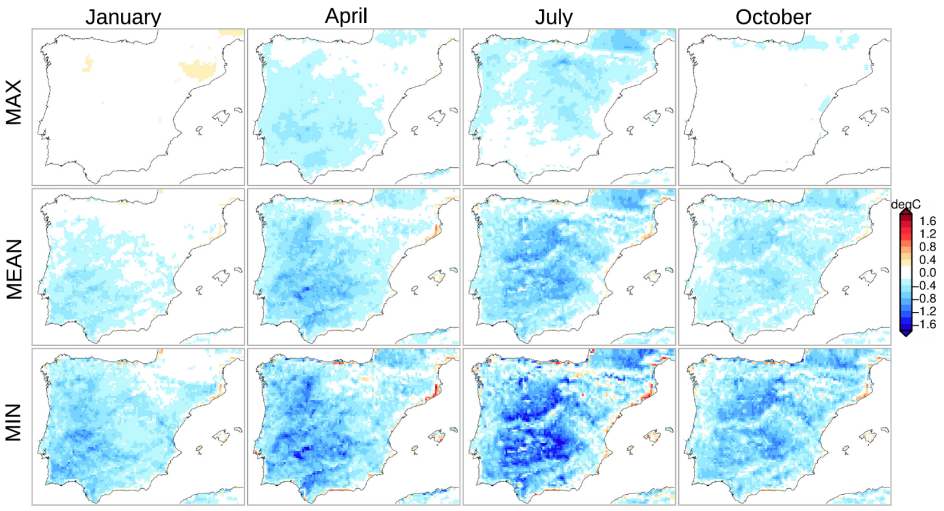

Fig. 5.8: Monthly means differences between GUT-CLIM and COP-CLIM simulations averaged over the period 2000-2017 for mean, maximum and minimum T2m for the months of January, April, July and October.

However, the role of the modification of the climatological FVC on the variance of the series, i.e. the inter annual variability of temperature, is very different. Figure 5.9 shows the differences in the standard deviation between COP-CLIM and GUT-CLIM.

In this case, the greatest differences appear for the maximum temperature, and their sign depends on the place and time of the year. Similarly, we highlight the different behavior of minimum and maximum temperatures throughout the year. For the winter months, the maximum temperature decreases its variability for practically all the IP. However, the minimum temperature increases its variance for the two Plateaus (Tagus and Douro valleys) and the Ebro valley. In the case of spring, a strong decrease in variance is observed for the maximum temperature while there is no clear pattern for the minimum. In summer the opposite happens to winter; the variance of the maximum temperature decreases in the north, while it increases very significantly in the south with values higher than 0.2 °C. Autumn presents a behavior similar to winter in minimum temperatures but more attenuated.

Attending to soil moisture differences (soil level between 0.1 and 0.4 m) of GUT-CLIM and COP-CLIM simulations, lower soil moisture levels are achieved in GUT-CLIM simulation motivated mainly for the highest values of FVC considered in this simulation. These differences as much stronger in summer and Autumn. This results

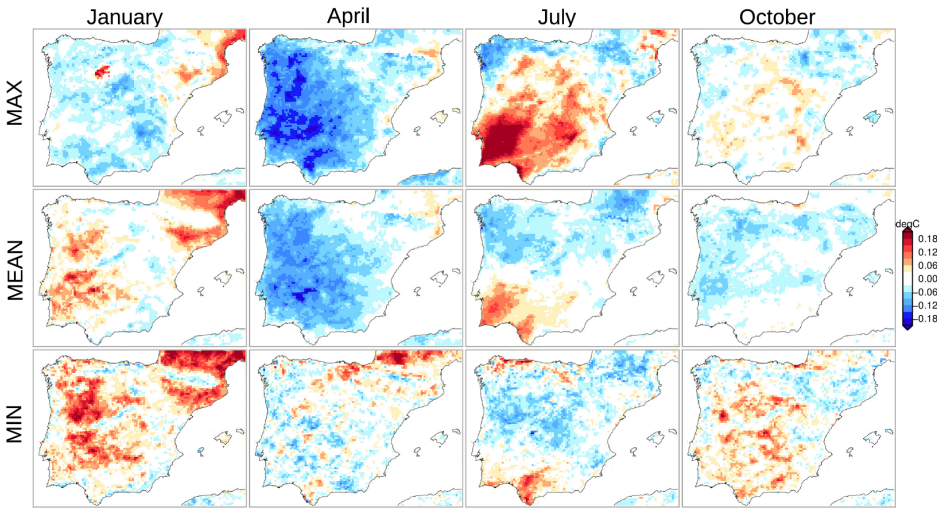

Fig. 5.9: Monthly standard deviations differences between GUT-CLIM and COP-CLIM simulations averaged over the period 2000-2017 for mean, maximum and minimum T2m for the months of January, April, July and October.

agree with those founded in Section 4.3.2, where the drying of soil was faster in the experiment with 90 % of FVC.

In summary, we found that the effects of increasing vegetation is to decrease temperature, especially the minima. However, the variability is affected in a very differently way, with maximum temperature specially affected. In situations with sufficient water availability the variance decreases, whereas situations of dry soils the variance rises.

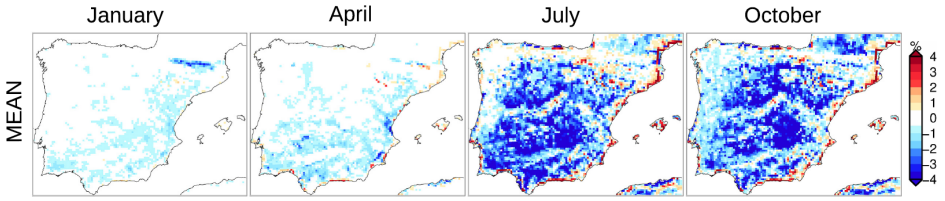

Fig. 5.10: Monthly differences of soil moisture between GUT-CLIM and COP-CLIM simulations averaged over the period 2000-2017 for the months of January, April, July and October.

5.3.3 Temperature response to temporal changes of FVC

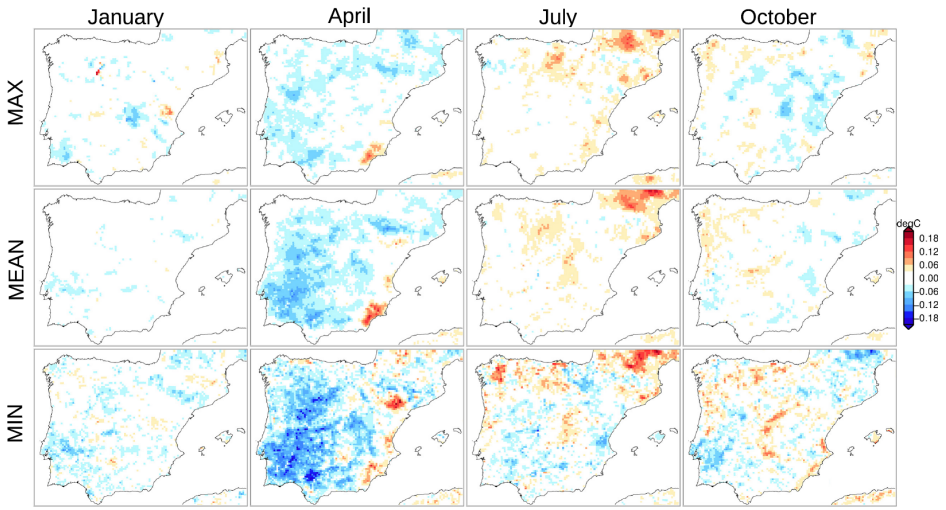

Fig. 5.11: Monthly standard deviations differences between COP-YEAR and COP-CLIM simulations averaged over the period 2000-2017 for mean, maximum and minimum T2m for the months of January, April, July and October.

First, we analyzed the differences in mean temperatures between COP-CLIM and COP-YEAR. As the vegetation has been constructed in COP-CLIM (monthly average of COP-YEAR) the differences in mean temperature of the whole period are null (not shown). As seen in previous chapters, the response of temperature to vegetation change is practically linear. Therefore, the differences that may appear in the interannual variability cancel out when integrating the whole period.

Having said this, we move directly to the analysis of the standard deviation of the series. Figure 5.11 presents the differences in standard deviation of maximum, mean and minimum temperature for the representative months of the year. The changes are greater in spring, and for the minimum temperature. The general behavior indicates that the higher the variance in the vegetation fraction, the lower the variance in temperature. However, there is a differential behavior in some areas where there is an increase in the variance.

The relationships between vegetation changes and temperature deviations are practically linear. Figure 5.13 shows the scatter plots of the relationships for maximum and minimum temperature and its linear fit. For the maximum temperatures, a significant

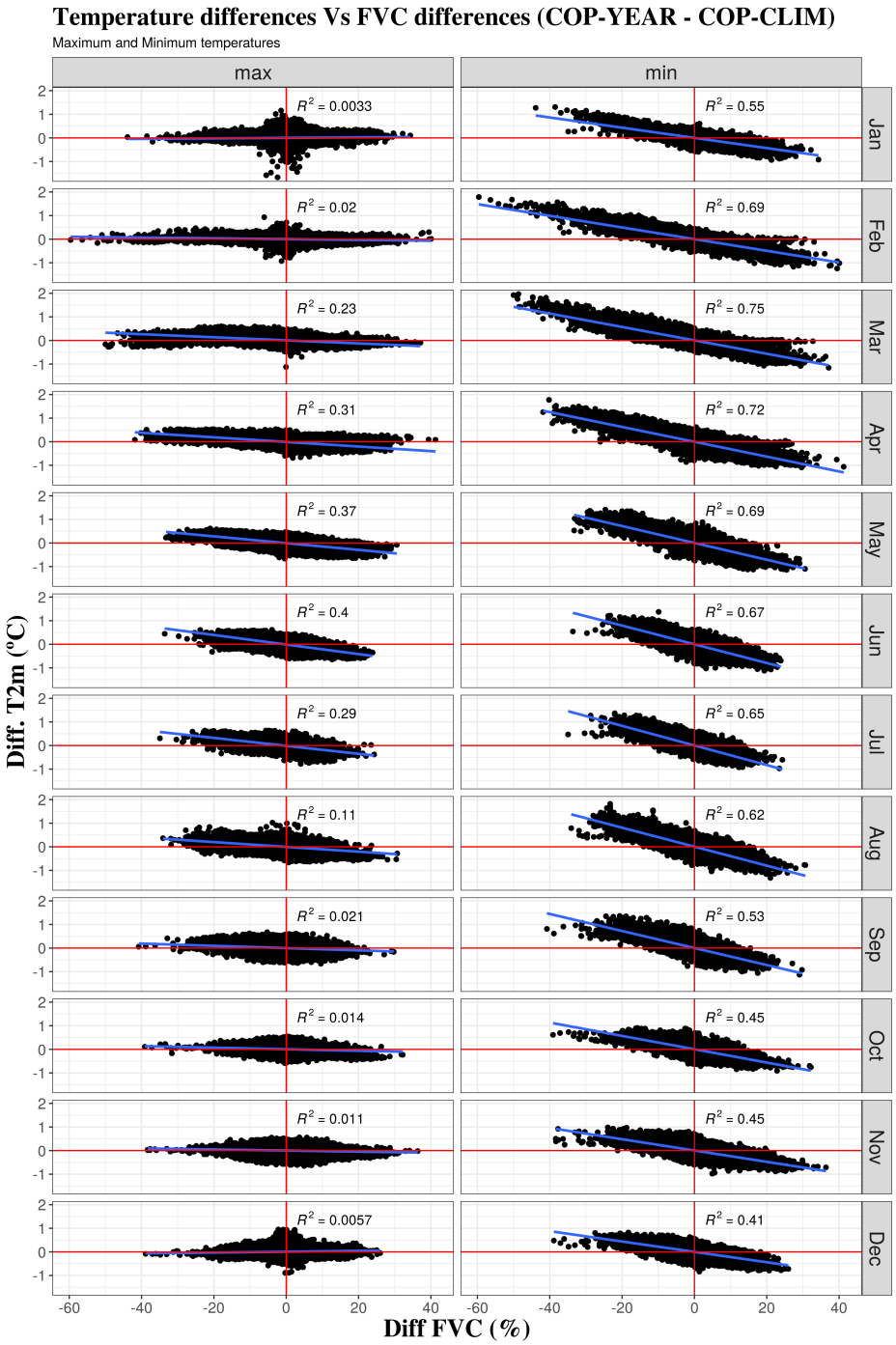

Fig. 5.12: X-Y plots of differences in FVC and T2m between COP-YEAR and COP-CLIM simulations for the period 2000-2017. Maximum and minimum temperatures for all the months of the year.

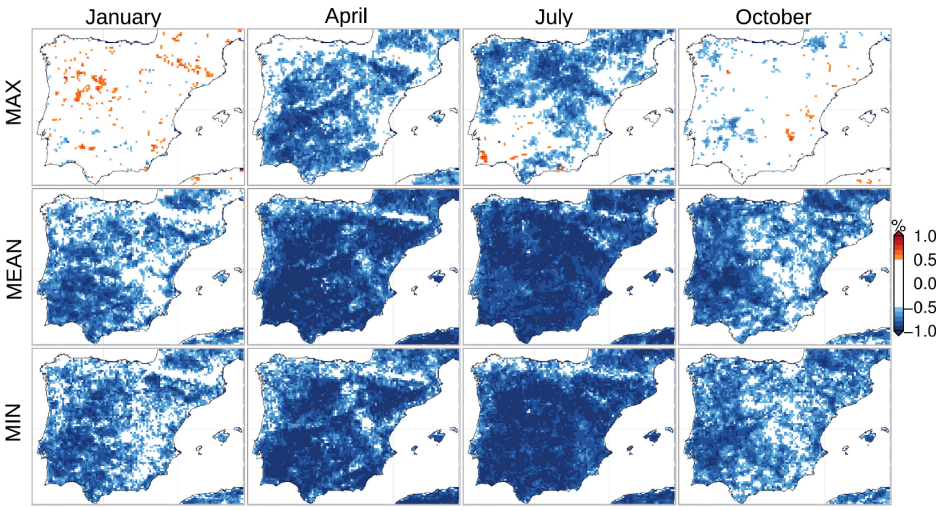

Fig. 5.13: Monthly temporal correlations of the differences of T2m against the differences of FVC between COP-YEAR and COP-CLIM simulations averaged over the period 2000-2017 for mean, maximum and minimum T2m for the months of January, April, July and October.

linear relationship only appears from April to July. These relationships are not very robust, reaching a maximum R^2 of 0.4. However, for the minimum temperature there is a significant relationship throughout the year, which is more robust in the spring and summer months. The relationships are always inverse, i.e., an increase in FVC produces a decrease in temperature and viceversa. The slope of the fitted line is greater in the spring and summer months.

This same relationship can be represented point to point (Figure 5.13). As we can observe the correlations at the local level are especially high in spring and summer for the minimum temperature. Practically significant relationships appear throughout the Iberian Peninsula except for some northern areas in summer and high mountain areas in spring. In winter and autumn, the relationships prevail in the west of the PI becoming weaker or even disappearing in the east and southeast of the peninsula.

From the sample of years with FVC below and above the median (see Figures 5.6 and 5.7), in Figures 5.14 and 5.15 are showed the differences in T2m between the COP-YEAR and COP-CLIM simulations following the same calculation criteria that in Figure 5.12. In general, the tendency observed for the maximum and minimum T2m in both figures and in Figure 5.12 is that with higher (lower) FVC, lower (higher) simulated air temperatures occur. In the case of the minimum T2m, this effect is more defined

and is related to the fact commented in Section 2.2.2 about the shadowing effect of FVC modifying soil conductivity (Eq: 2.10). With higher FVC values, there is a greater insulation of the soil and therefore a lower contribution of G from the soil to the surface, causing less heating of the air in contact with such surface (lower T2m). In the map of differences of minimum T2m (Figure 5.14), it can be seen how the effect on T2m is quite remarkable, reaching differences in the monthly means around 1.5 ° C with FVC differences around 20 % (see Figures 5.6 and 5.7). The differences in the monthly T2m between the sample of dry and wet years seem more extreme in the dry years starting from similar differences in FVC between both cases.

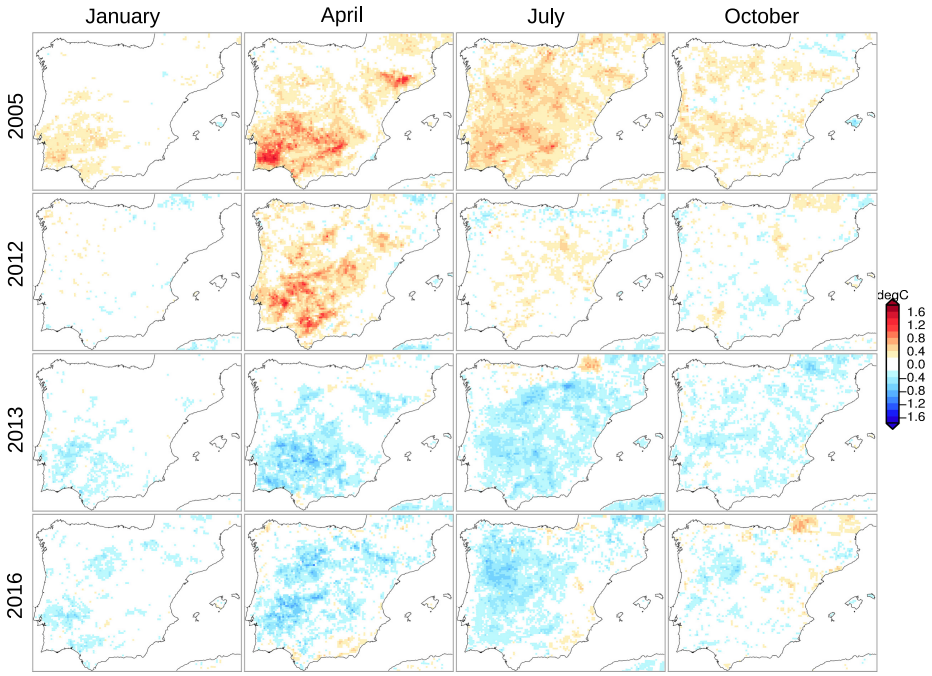

Fig. 5.14: Differences in minimum T2m between COP-YEAR and COP-CLIM simulations in sample years with FVC values below (2005;2012) and over (2013;2016) the median for the period 2000-2017 for the months of January, April, July and October.

For maximum T2m, the response to FVC changes is less intense as outlined in Figure 5.12. In this case, the effect of FVC in modulating the E of the model is the main driver (equations 2.16, 2.17, 2.19 and 2.20). In this way, a higher FVC will favor higher LE

and lower H, and therefore a lower heating of the surface air (lower T2m) since the energy is mainly invested in evaporating the available moisture from the soil. This effect can be modulated by the canopy resistance in conditions of hydric stress, with less soil moisture available, especially in the summer months, which can lead to situations of higher H with higher FVC (see Section 4.3.2 for more details). In fact, in Figure 5.15 in the southwestern part of the IP for July 2005 an opposite pattern is observed than expected, with lower temperatures in the COP-YEAR simulation despite having lower values of FVC than COP-CLIM.

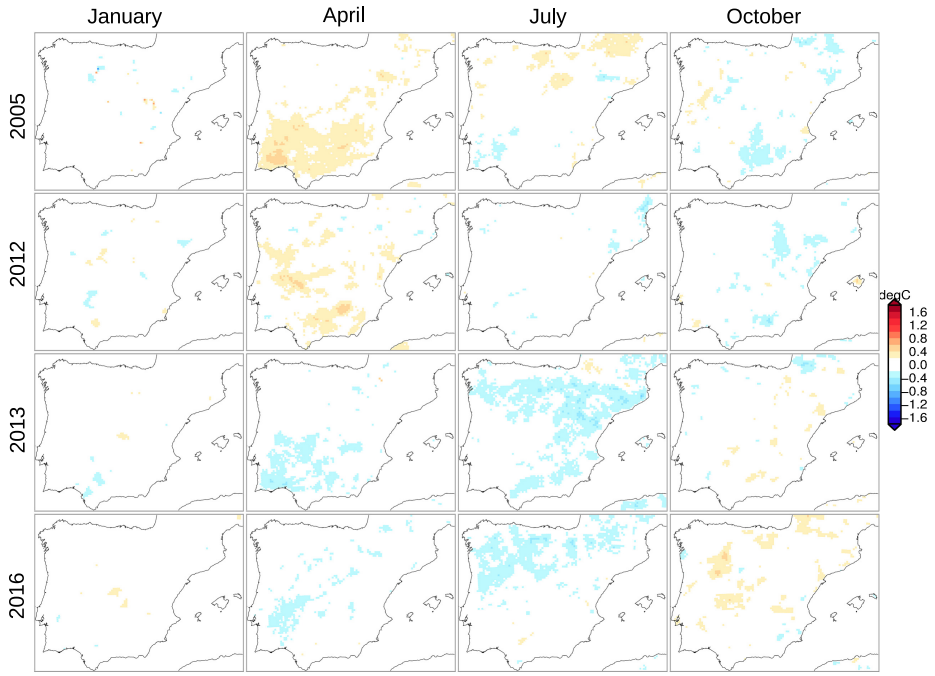

Fig. 5.15: Differences in maximum T2m between COP-YEAR and COP-CLIM simulations in sample years with FVC values below (2005;2012) and over (2013;2016) the median for the period 2000-2017 for the months of January, April, July and October.

If vegetation were independent of temperature, the linearity relationship discussed above would have to make the changes in variance between the two simulations integrated over the years zero. The effects would be counteracted. Therefore, if differences in the variance of the series appear, it is because there must be a relationship between

temperature and vegetation. For example, if vegetation is increased with temperature, a warmer period would suffer a temperature attenuation due to more vegetation. Thus, in areas with this type of response, the variance of the series would decrease, since the minimums (colder periods) of the series would be higher with less vegetation and the maximums (warmer periods) would be lower with more vegetation. On the other hand, if vegetation decreases with temperature a warmer period would be more extreme due to the lack of vegetation.

This relationship between temperature and vegetation can be direct or indirect. In places with sufficient precipitation and hence low hydric stress, temperature can be a determining factor in plant productivity. In this conditions, warmer temperatures are expected to stimulate primary productivity and example of this are the studies that indicate that plant growth has already increased across northern latitude (Myneni et al., 1997; Zhou et al., 2001; Hudson and Henry, 2009). In other areas, where precipitation is the determining factor in the growing of vegetation due to the prevalence of long periods of hydric stress, precipitation (cold events) is associated with more vegetation production.

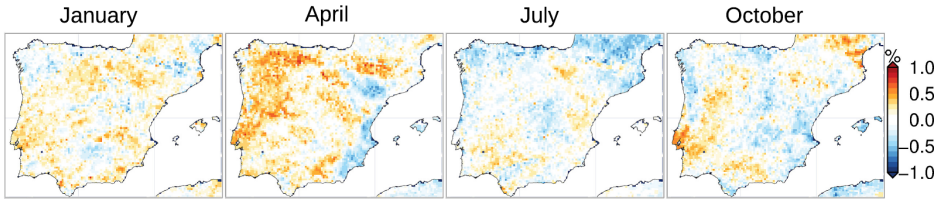

Fig. 5.16: Monthly temporal correlation of the minimum temperature anomaly and FVC change in COP-YEAR, for January, April, July and October.

In order to verify this hypothesis we calculated the correlation between the minimum temperature anomaly and the vegetation fraction anomaly (see Figure 5.16). It is clearly observed that the obtained patterns are very similar to the standard deviation differences presented in Figure 5.11. In fact, the correlation between the spatial patterns is always higher than 0.6 reaching 0.75 in May. Therefore, the relationship between temperature and FVC explains the behavior of changes in the temporal variability of the temperature series.

Let's analyze the case of the changes in the standard deviation in April. It is striking that while in the west of the IP, basically in all the Atlantic watershed and in the southern slope of the Pyrenees, there is a decrease in variability, in the Mediterranean watershed, the Ebro valley and the east of the peninsula there is an increase in variance. In situations of zonal or south-west flow, positive temperature anomalies appear in practically all the Iberian Peninsula, however precipitation remains in the areas with a decrease in variability. This leads to a different vegetation development between these areas. And therefore

the inclusion of realistic vegetation leads to very different results on the variability of the series.

5.3.4 *Trends in vegetation and their effects on long-term temperature*

As we have seen above, there is a linear response of temperature, especially minimum temperature, to changes in vegetation. The question is what happens to the long-term variability of temperature when trends in the vegetation fraction appear.

We first analyze the FVC trends for the period 2000-2017 (see Figure 5.17). In general, a positive trend is evident in different areas of the IP, which at some points can reach 2 % annually (34 % for the entire period). These trends are greater for April and are striking in the Ebro valley. In scattered areas such as the northwest (Galicia) and the southwest, very localized areas of negative FVC trend are observed.

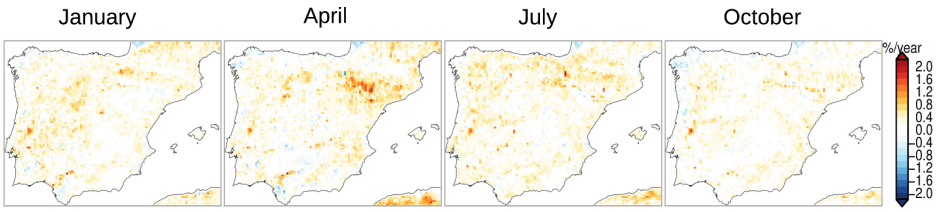

Fig. 5.17: FVC trends calculated for the period 2000-2017 (trend by year). January, April, July and October.

In order to see the signal that the evolution of the FVC implies throughout the simulated years, temperature trends simulated by the COP-CLIM and COP-YEAR are analyzed (Figure 5.18). These trends have been calculated assuming a linear adjustment and are expressed as the trend for all the simulated period. First of all, the asymmetry between winter and the rest of the seasons is noteworthy. In winter, the trends are lower, and affect mainly the northeastern quadrant, while in the rest of the seasons the warming is greater in the areas of the Atlantic basin and the Pyrenees. While the trends are greater in October for maximum temperatures, it is in summer when the trends are greater for minimum temperatures.

The simulated trend patterns are very similar between both simulations and are much more pronounced in October reaching 4 ° C. Attending the minimum temperatures, there are slight differences between both simulations above all in April and July. These differences occur mainly in the Ebro valley area, where the positive trends diminish in July

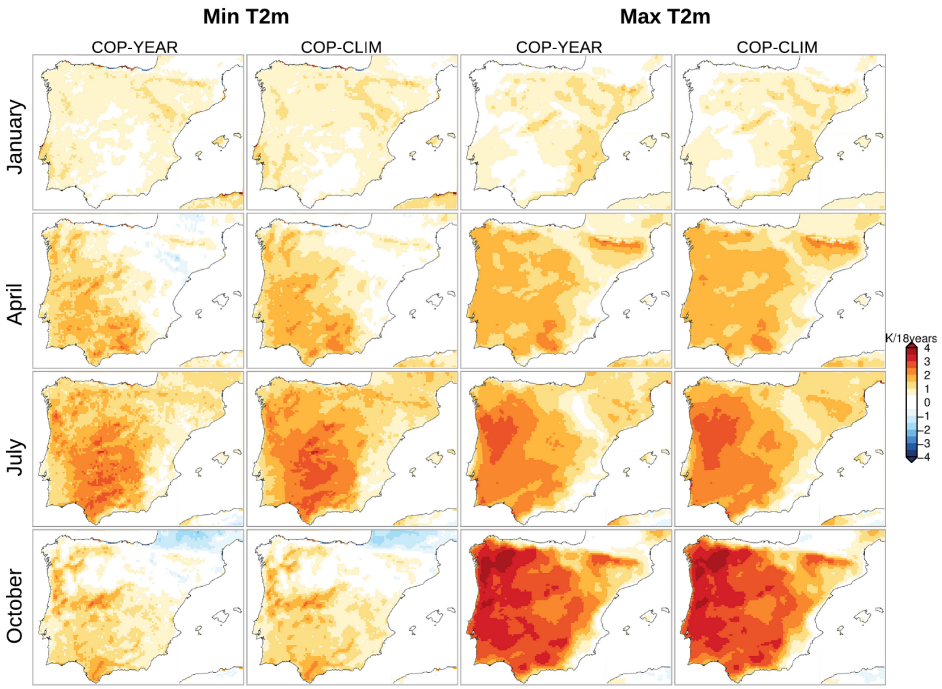

Fig. 5.18: Trends for the period 2000-2017 for COP-CLIM and COP-YEAR (°C/18years) for maximum and minimum temperature in the months of January, April, July and October.

and become negative in April, that is, the effect of vegetation may even cause trends to reverse in some areas for some months. This can be more easily observed in Figure 5.19 where the trends of the differences COP-YEAR minus COP-CLIM are shown. The Ebro valley area is an area with a marked positive trend for FVC and the COP-YEAR model translates this signal into a negative temperature trend. As expected, there is a direct relationship between FVC trends and trend differences in the simulations. Table 5.3 shows the spatial correlation between de trend patterns of FVC and trend differences. In the case of minimum temperature correlation reachs 0.9 in April being correlation always over 0.7. For maximum temperature correlations are only significant in spring and summer.

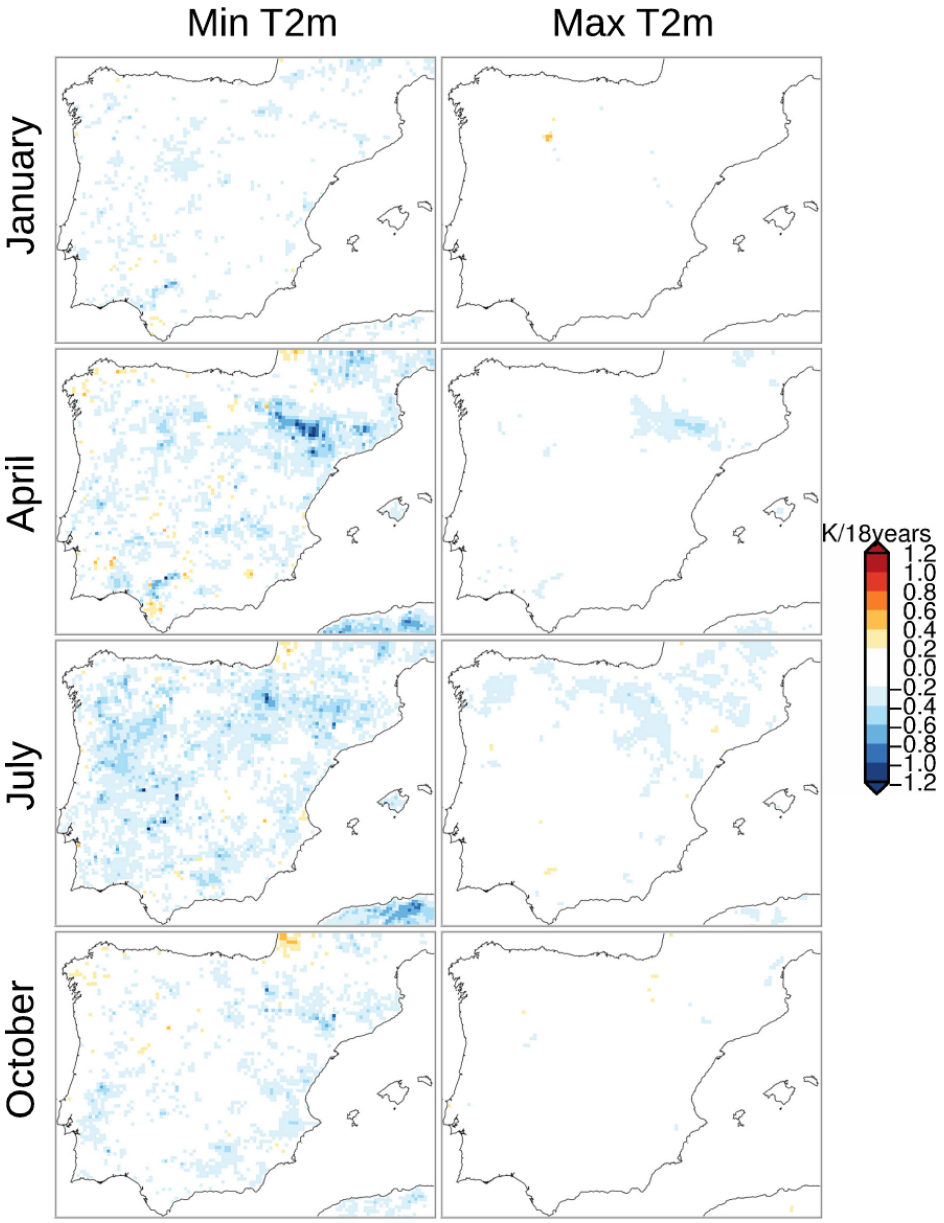

Fig. 5.19: T2m trends attributed to changes in FVC in the period 2000-2017 (trend in 18 years) for maximum and minimum T2m in the months of January, April, July and October.

Correlation	**Jan**	**Apr**	**Jul**	**Oct**
Min T2m	-0.78	-0.90	-0.86	-0.70
Max T2m	0.18	-0.65	-0.54	0.06

Table 5.3: Correlation between trends differences (COP-YEAR minus COP-CLIM) of maximum and minimum temperature and FVC during the simulated period 2000-2017.

5.4 Discussion and conclusions

In this chapter we have analyzed the effects that differences in FVC that can be introduced in regional climate simulations, due to the use of different databases and incorporating their interannual variability, can have on the simulated climate, focusing on temperature.

The comparison of two climatological databases of FVC; the Gutman (Gutman and Ignatov, 1998) climatology (GUT-CLIM) used in many works and the modern Copernicus database (COP-CLIM), shows differences of 15-20% in our study area. Obviously, these deviations can be very different depending on the database used, as already studied in previous chapters.

On the other hand, differences in FVC due to interannual variability (comparison of COP-YEAR and COP-CLIM) can reach values of 5-10%, due to long-term trends (growth of new forests, abandonment of farmland, forest fires, etc.) or higher plant productivity related to climatic factors such as precipitation and temperature.

In both cases the differences are important and can have a non-negligible effect on the climatology described by a numerical model.

It has been shown, both in this chapter and in previous chapters, that the response of temperature is practically linear to changes in vegetation, with cooler temperatures occurring in situations of greater vegetation. This response is very extensive, although there are some places where this relationship does not hold true, with temperature being almost independent of vegetation variations. These effects are greater in the spring and summer months where the energy available to distribute into sensible and latent heat fluxes is greater. This occurs in a univocal way for the minimum temperature. However, for the maximum temperature there are notable exceptions, and the response is much weaker. The changes are negligible in winter and at other times of the year, especially in summer, they depend on the available humidity in the soil, even producing the opposite effect (warming).

The comparison of GUT-CLIM and COP-CLIM shows that such changes in vegetation can lead to changes in temperature averaged over the entire period of more than one degree for minimum temperature to 0.5 for maximum temperature. Although the differences are constant over the years, they introduce a change in interannual variability, the

variance of the series. This effect is now more noticeable for maximum temperatures. Variability decreases drastically in spring when more vegetation is included, especially throughout the Atlantic basin. However, in the summer a north-south dipole appears, in which the variance decreases in the north and increases in the south. This is intimately related to the humidity contained in the soil. Places with more vegetation and low precipitation lose moisture quickly, so that the cooling due to sensible heat fluxes decreases more.

The analysis of the role of introducing the interannual variability of vegetation has shown us that there is no a priori modification of the mean properties, no doubt due to the linearity of the relationship between temperature and vegetation. However, there is an interesting sign of change in the variance of the series. This is due to the fact that there is a relationship between temperature and vegetation productivity. The places and times when higher temperatures cause higher plant productivity the variance decreases, and increases otherwise. This relationship could be direct or indirect and a deeper study of this issue would be interesting.

Finally, we observed that trends in FVC cause trends of opposite sign in temperature, especially in minimum temperatures. We obtain that in some places this underlying trend can even reverse the trend due to other causes. Note that although the period studied here is not sufficient to speak of trends at the climatological level, it does give us an idea of how long-term changes in vegetation cover can significantly modify temperature trends.

6

Evaluation of regional climate simulations using different vegetation cover databases

The previous chapters have analyzed the role of changes of frcation vegetation cover (FVC) on temperature in experiments with regional climate models. Temperature basically responds linearly to changes in FVC, affecting not only the mean of the series but also its variance. The question that arises now is, does using more realistic FVC databases lead to a better reproduction of the observed climate. In this chapter we try to answer this question.

6.1 Introduction

Vegetation has a large impact in weather and climate directly by means of biophysical processes, interacting in the exchange of moisture, energy and momentum fluxes with the atmosphere (Charney, 1975; Shukla and Mintz, 1982; Dickinson, 1984; Sellers et al., 1986; Bonan et al., 1992; Dickinson, 1993; Pielke et al., 1998; Heck et al., 2001; McPherson, 2007; Notaro et al., 2017). Moreover, there is a crucial and indirect effect of vegetation in climate due to biogeochemical processes related with CO_2 and carbon storage (McGuire et al., 2001). There is strong evidence that this impact influences weather and climate at a range of time scales, from seconds to thousand of years (Pielke et al., 1998; Pitman, 2003). Furthermore, the effect of vegetative properties on land surface-atmosphere interactions can result on atmospheric circulation changes (Pielke and Avissar, 1990; Copeland et al., 1996) that can range from local scales (Ookouchi et al., 1984;

Anthes, 1984; Mahfouf et al., 1987; Yan and Anthes, 1988; Segal et al., 1988). to regional and global scales (Reale and Dirmeyer, 2000; Chase et al., 2000; Gedney and Valdes, 2000; Cotton and Pielke Sr, 2007)

The evidence to support that changing vegetation influence climate from regional to global scales, comes from sensitivity studies that explore the impact of modifying the land surface characteristics (Pitman, 2003). The representation of vegetation in regional climate models (RCMs) is given by different physical parameters such as albedo, fraction vegetation cover (FVC), leaf area index (LAI), stomata1 resistance, soil conductivity, root depth, roughness length or vegetation types. Sensitivity studies of regional and global climate with surface albedo and its feedbacks via vegetation were prevailing initially, and key works with global circulation models (GCMs) were performed by Charney (1975), Charney et al. (1977), Lofgren (1995) and Reale and Dirmeyer (2000). Works related with the relevance of surface roughness length through vegetation can be found in Sud and Smith (1985) and Chen et al. (2012). Another examples of research can be found in the case of LAI (Chase et al., 1996; Kang et al., 2007) or root depth (Rosnay and Polcher, 1998; Feddes et al., 2001).

It would be expected, that an improved partitioning of surface sensible and latent heat fluxes can occur when incorporating near-real-time vegetation fractions into RCMs and in this manner to enhance the prediction of near surface variables (James et al., 2009). Hong et al. (2009) noted that it was difficult to conclude if more realistic FVC data resulted in better simulations and the model behaviour is not reliable with improved vegetation parameters. What is clear, is that despite decades of improvement, RCMs still suffer from large systematic biases, and one of the most promising way forward for reducing these biases is to tackle deficiencies in modelled land-atmosphere processes (Davin et al., 2016).

This chapter evaluates the ability of a set of regional climate simulations to reproduce the observed climate of the Iberian Peninsula. The simulations differ in the FVC database used; GUT-CLIM, COP-CLIM and COP-YEAR (see Chapter 5 for more details of this simulations). The first objective of this study is to analyze the possible added value of a high spatial resolution FVC dataset (COP-CLIM) as well as to add temporal variability (YEAR-CLIM) synchronously over a sufficiently long period that includes a multitude of climate conditions. The analysis of the simulations skill focuses on the ability to reproduce the 2-meter air temperature (T2m). The second objective tries to evaluate the effect of using a variable FVC data set on the low frequency variability (trends). The third objective is to study the sensitivity of the model's skill in reproducing the temperature field in relation with the thermal conductivity of the soil.

6.2 Data and methods

6.2.1 RCM experiments

The experiments used are the same as those described in Section 5.2.2. Two experiments using a prescribed climatology but with different original spatial resolution, different period, satellite data and FVC construction methodology; GUT-CLIM and COP-CLIM. And a third experiment in which the interannual variability of the FVC is included; COP-YEAR. Recall that COP-CLIM is obtained from COP-YEAR.

The description of the LSM was presented in Chapter 2. As mentioned in this chapter, the Noah LSM for the calculation of heat fluxes in soils covered by vegetation, uses a thermal conductivity that depends on the vegetation itself (Section 2.2.3, equation 2.10). The relationship between the conductivity in bare soil and soils covered by vegetation depends exponentially on the FVC. In this relationship, the parameter β appears, which indicates the magnitude of the relationship. β is preset to a value of 2. Some authors (Rosero et al., 2010; Zheng et al., 2015) point out the importance of this value and that it is usually overestimated. Note that the modification of this value would lead to a modification of soil heat fluxes, and therefore of temperatures, especially minimum temperature (see Chapter 4 for more details).

To test the sensitivity to this parameter, a series of experiments have been carried out in which the parameter β has been modified using values 2 (default), 1, and 0.5. The FVC values taken are those of the COP-YEAR experiment. The rest of the parameters are identical to the previous simulations. For simplicity, only the extreme years 2005,2012,2013 and 2016 have been simulated. In other words, a total of 12 new one-year simulations have been performed.

6.2.2 Observational data

Two databases of maximum and minimum temperature have been used. One consists on an observational grid (AEMET5K) and the other is composed of direct data from different observatories of the AEMET network (AEMET-OBS).

AEMET5K database has been generated using a total of 1800 thermometric stations from the National Climatological Data Bank of AEMET for the period 1951-2019. In its construction, a climatology based on the historical analysis of the numerical prediction model HIRLAM operating in AEMET has been used as first estimation, which is corrected by the observations (Peral-García et al., 2017; Amblar-Francés et al., 2020). AEMET5K has a spatial resolution of 5km, with daily data of minimum and maximum temperature, and covers the Spanish part of the Iberian Peninsula as well as Balearic Is-

lands. In order to compare the AEMET5K data and our simulations, all data were interpolated to a common mesh, the AEMET5K grid, using a bilinear interpolation method.

AEMET-OBS is a set of 60 automatic stations of the Spanish State Meteorological Agency (AEMET). Maximum and minimum temperature are available for the period 2000-2017. Figure 6.1 shows the geographical distribution of the meteorological stations. Model data are interpolated using a bilinear to the spatial location of the meteorological stations using a bilinear interpolation for comparison purposes.

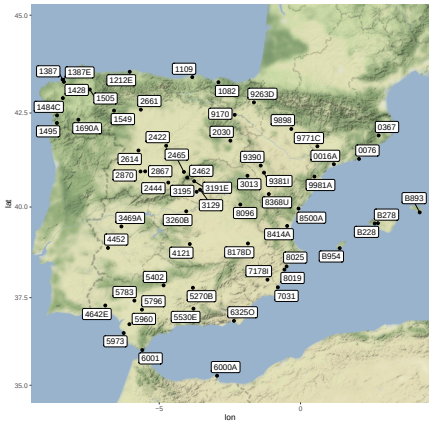

Fig. 6.1: Geographical distribution of the 60 automatic meteorological stations from AEMET.

6.3 Results

6.3.1 Skill of experiments in reproducing the mean fields

We first analyzed the bias climatological errors considering monthly averages for the reference months of January, April, July and October considering the entire study period (2000-2017) for both minimum and maximum temperature (Figure 6.2). Only the results for GUT-CLIM and COP-CLIM are shown, since the COP-CLIM and COP-YEAR simulations are indistinguishable for mean values.On the other hand, figure 6.3 shows the boxplot for all months of the year stratified by FVC values. The stratification has been done according to the values of the COP-CLIM simulation.

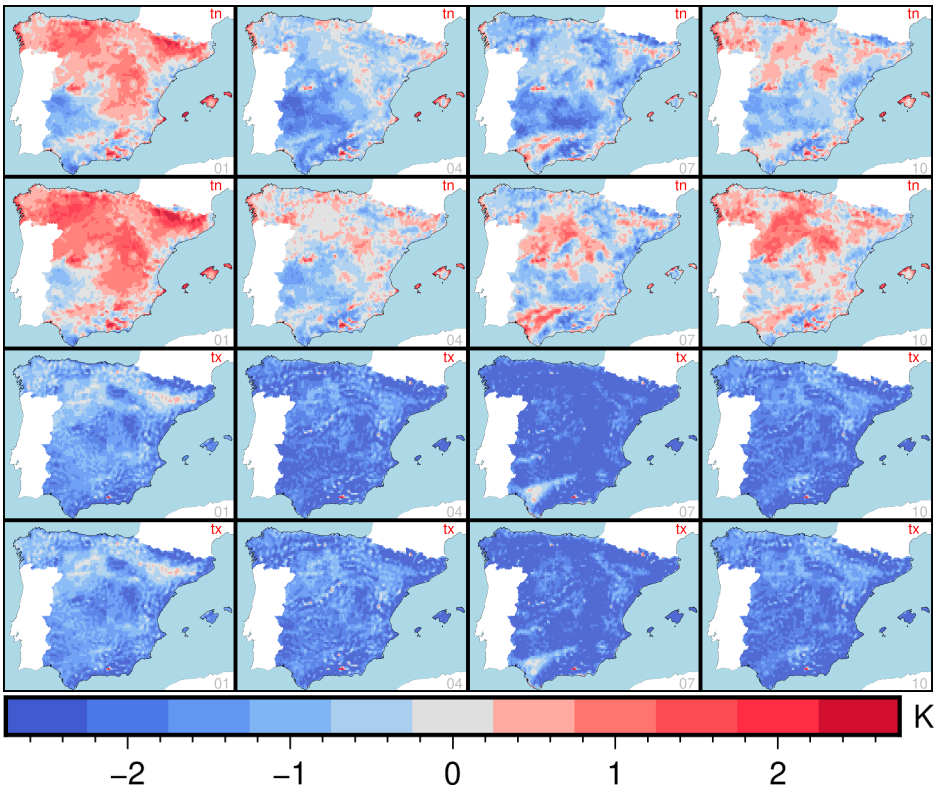

Fig. 6.2: Bias of simulations GUT-CLIM (rows 1,3) and COP-CLIM (rows 2,4) respect AEMET5K for January, April, July and October (columns 1,2,3,4) and minimum (rows 1,2) and maximum (rows 3,4) temperature.

The maximum temperature is underestimated by all experiments, all months of the year and most points. Errors ranges from 1 to almost 3 degrees. Bias errors are larger in summer and smaller in winter for both simulations. Only in some areas such as the Ebro valley in winter and the Guadalquivir valley in summer do they show good results. The COP-CLIM simulation presents smaller bias errors in some areas and times of the year, generally in the months from March to July. In the rest of the year the error statistics are very similar. The spatial patterns of error are very similar (correlation above 0.97). This could mean that actually the error pattern cannot be attributed to the change of FVC database. On the other hand, there does not seem to be a site-specific FVC-dependent differentiation of errors. The annual distribution of errors is similar across all FVC strata.

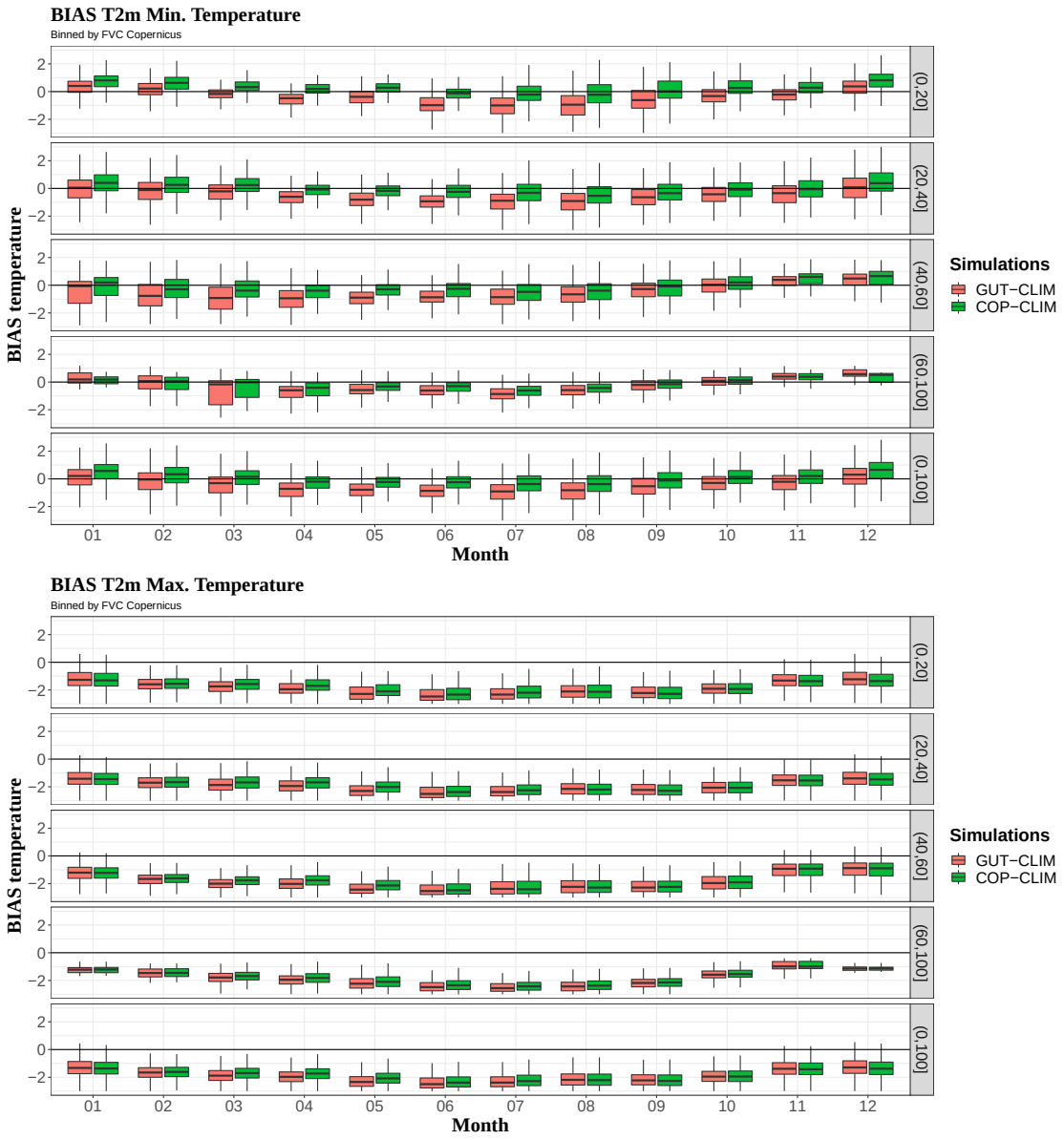

Fig. 6.3: Boxplot of monthly bias respect AEMET5K for all points and stratified by FVC for minimum (top panel) and maximum temperature (bottom panel).

Minimum temperature has a differential behaviour across regions and seasons of the year. In winter, GUT-CLIM overestimates the temperature in the north and center-east of the IP, reaching values of more than two degrees, and underestimates it in some areas of the south-east, especially in Extremadura. COP-CLIM reproduces higher temperatures, due to its lower average vegetation, as seen in the previous chapter. This makes that in the places where GUT-CLIM overestimates, the errors are higher, and where it underestimates the errors decrease. In general, during these months the biases are higher in COP-CLIM. However, from March to October the results are better for COP-CLIM. In general, in both experiments there is a bias error that depends on the time of the year. This annual dependence explains the variation in skill of the simulations (which is better) explained above. The boxplot analysis indicates that, although not very noticeable, the dispersion of GUT-CLIM is higher in several strata and months. This could be indicative of the role played by the spatial resolution of the FVC in reproducing climatology. The errors appear to be larger. Thus, in this case one can generally say that COP-CLIM introduces noticeable improvements in mean errors. These improvements are more noticeable in places with a low level of vegetation.

Secondly, we analyze the skill of the simulations to reproduce the intra-annual variability of monthly averaged temperatures. For this, we calculate the percentage error in the variance (Figure 6.4) showing the magnitude of the temperature variability. It will be shown later that the temporal correlation is very high. The error patterns are practically indistinguishable between experiments. This means that the modifications that the FVC introduces in the variance of the series, which we saw in the previous chapter, is of a smaller magnitude than the errors in the variance estimation. In the case of winter, the patterns for both maximum and minimum temperature have a very marked orographic character. The variance in high mountain areas is underestimated for maximum temperature and overestimated for maximum temperature. And there seems to be an overestimation for the area of the Strait of Gibraltar. In spring, a more complex pattern of overestimation of variance appears for minimum temperatures in western areas and slopes exposed to the westerly flow. For maxima, the variance of the simulated series is in most places underestimated. In summer, the variability of the temperature is overestimated in all places except in the peninsular center. As for the maximums, the differences present an irregular pattern. In autumn the behavior is very similar to that of spring.

As a summary we plot the Taylor diagrams of the simulations. They represent the ability of the experiments to reproduce the spatial patterns of mean averaged monthly temperature and its standard deviation (Figure 6.5.) All simulations represent very well the spatial field of temperature, both maximum and minimum. The same is not true for the spatial pattern of variance. The experiments reproduce the minimum temperature acceptably but the same is not true for the maximum. The minimum temperature patterns are not captured for the winter months. For the rest of months results do show some

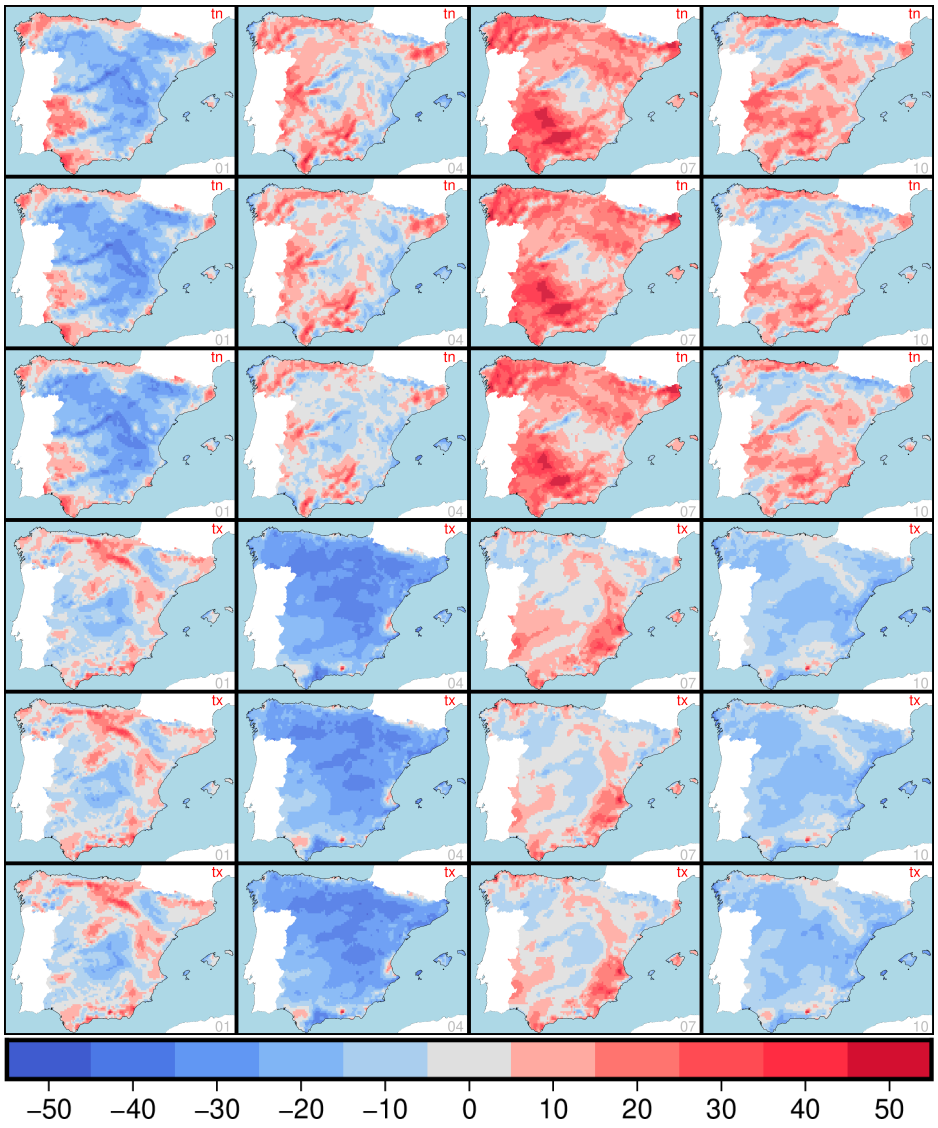

Fig. 6.4: Standard deviation percentage error. Simulations GUT-CLIM (rows 1,4), COP-CLIM (rows 2,5) and COP-YEAR (rows 3,6) respect AEMET5K for January, April, July and October (columns 1,2,3,4) considering minimum (rows 1,2,3) and maximum (rows 4,5,6) temperature.

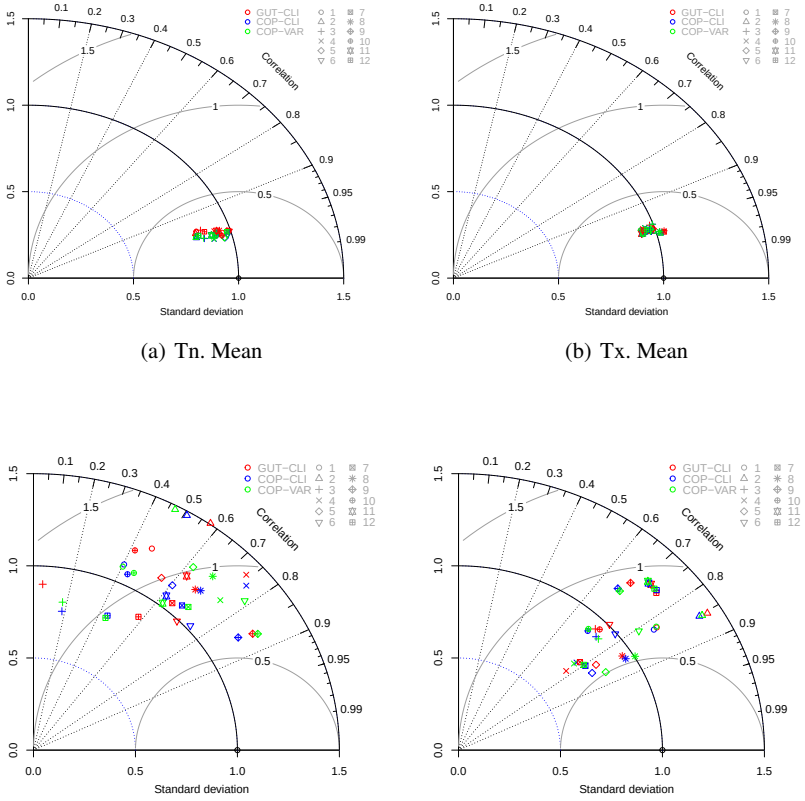

(a) Tn. Mean (b) Tx. Mean

(c) Tn. Variance (d) Tx. Variance

Fig. 6.5: Taylor Diagrams of minimum (Tn) and maximum (Tx) temperature field representation, mean and variance by experiments.

ability to reproduce these fields, but they are not very good. In any case, no experiment is found to have a higher skill in reproducing the monthly mean fields.

Fig. 6.6: Temporal correlation of monthly series of minimum and maximum temperature. Simulations GUT-CLIM (rows 1,4) , COP-CLIM (rows 2,5) and COP-YEAR (rows 3,6) respect AEMET5K for January, April, July and October (columns 1,2,3,4) considering minimum (rows 1,2,3) and maximum (rows 4,5,6) temperature.

6.3.2 Interannual variability

In the previous section we analyzed the skill of the simulations to reproduce the observed fields, based on the AEMET5k grid. Next, we present the ability of the experiments to reproduce the interannual variability. Figure 6.6 shows the temporal correlation of the monthly series. The correlation coefficient is always above 0.75 with the average being above 0.93 in all experiments, variable and time of year. The least good results are given for the minimum temperatures in winter, as expected, due to the poor variance reproduction seen in the previous section. Again, the differences between experiments are practically indistinguishable. However, we do observe some improvement, although not statistically significant, for COP-CLIM and COP-YEAR experiments with respect to GUT-CLIM.

In order to study in more detail the possible effect of introducing temporal variability of the FVC on the skill of the experiments we focused on the study of extreme years and temporal variability on a daily scale. We compare COP-CLIM and COP-YEAR simulations focusing on specific years where vegetation covers were abnormally low (2005 and 2012) and high (2013 and 2016). In this way, we have calculated the MAE (Mean Absolute Error) for the COP-YEAR and COP-CLIM simulations and analyzed their percentage differences. In Figure 6.7 we plot in percent change of MAE (YEAR-CLIM) for maximum and minimum temperature as well as differences in FVC and FVC climatological fields. We focus on the month of April. For the year 2005 (dry year) there is a lower FVC, with respect to the climatology, in practically all the IP reaching differences of the order of 20%. The largest changes, up to 20%, appear in the south of the IP, and in this case the differences are negative, which means an improvement of COP-YEAR with respect to COP-CLIM in most of the IP for both maximum and minimum temperatures. For the year 2012, something similar happens but in this case we have a slight worsening in some different areas. For wet years the opposite happens, introducing more vegetation leads to a worse reproducibility of the observations. With this we cannot say that introducing the variability of the FVC always leads to an improvement. The results considering data from AEMET-OBS are depicted in Figure 6.8 and show a similar behaviour than using AEMET5K.

From the above results, the distribution of temperature errors as a function of FVC values was further investigated. In Figure 6.9, the MAE differences between the COP-YEAR and COP-CLIM simulations are plotted stratifying by FVC values from the COP-YEAR experiment for dry and wet years. The pattern of smaller errors is observed in the COP-YEAR simulation with smaller FVC values for dry years where most of the FVC values are less than 40%. For wet years, the opposite behavior is observed, with a considerable jump from the 40-60% to the 60-100% level, where the errors in the COP-YEAR simulation are considerably higher. For maximum temperatures, where the

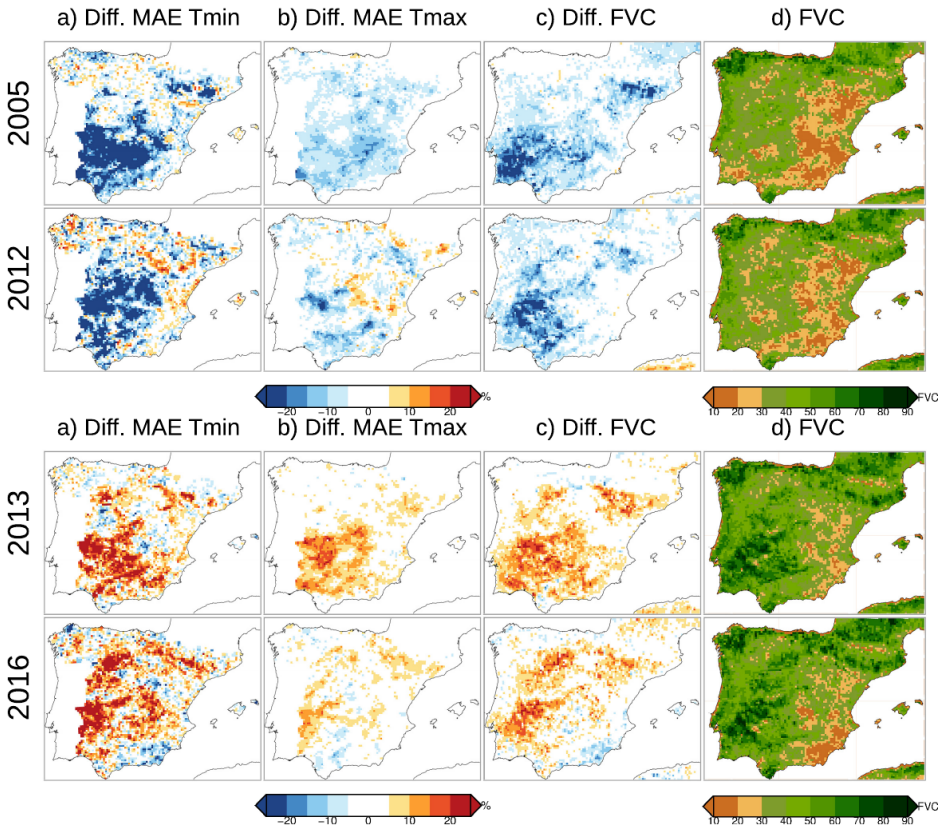

Fig. 6.7: Percentage difference of MAE in April for minimum (a) and maximum (b) temperatures between COP-YEAR and COP-CLIM simulations with AEMET5K. Difference of FVC between COP-YEAR and COP-CLIM (c). FVC of experiment COP-YEAR (d).

impact of changes in the FVC on the errors is lower, the effect of the magnitude of the FVC on the error differences is also observed.

Another interesting question is whether changes in the intranannual spatial distribution of vegetation can lead to an improvement of the reproduced spatial temperature field. In Figure 6.10 the differences between the year-to-year spatial correlation coefficient for April and minimum temperature are presented. The results are presented by levels of the FVC in COP-YEAR. The spatial correlations have always very high values as presented above, higher than 0.93 in all cases. The differences in the simulations point

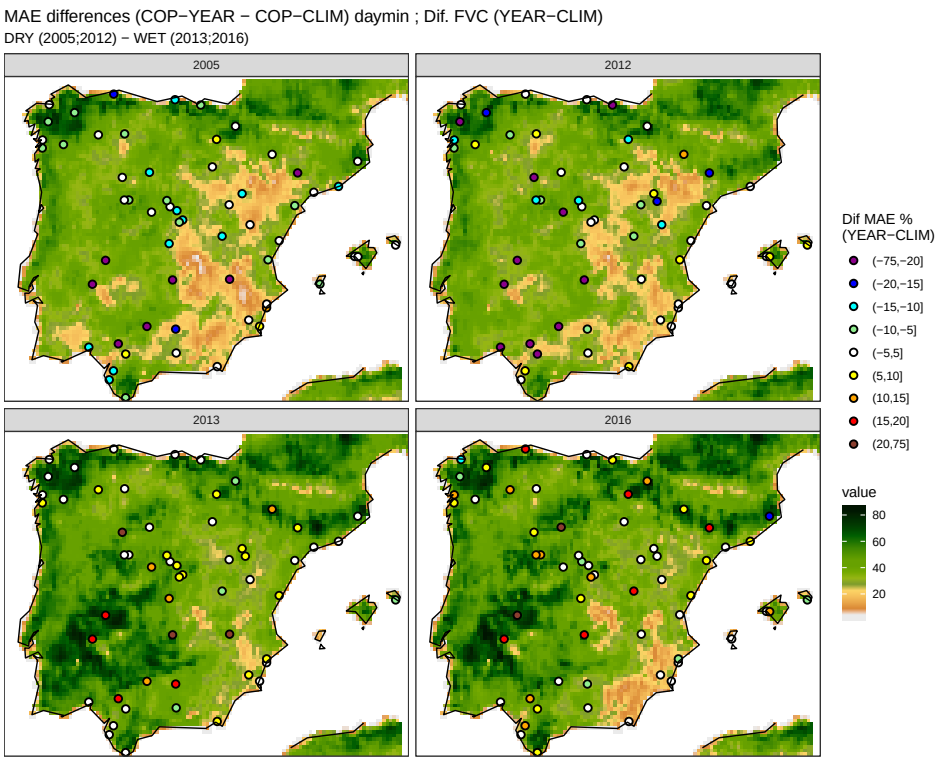

Fig. 6.8: Percentage difference of MAE in April for minimum temperature with AEMET-OBS in extreme dry years (2005 and 2012) and wet years (2013 and 2016) for minimum temperature. FVC of COP-YEAR experiment

out that for low values of FVC, COP-YEAR always enhance the spatial representation of the temperature fields. However, for large values of FVC the effect may be the opposite. In any case, the differences are small, which does not allow us to clearly confirm this result.

Thus, although the signal of possible improvement is weak, we have observed that there is some signal in the errors related to the baseline FVC values. We discuss this in more detail below. For minimum temperatures, the role of FVC comes into play primarily in the parameterization of soil conductivity as already commented in Section 6.2.1. The question we can ask ourselves and will address in the next section is whether the *insulation* effect of the FVC may be overestimated. Let us now discuss in detail the effect of the FVC on these temperatures to try to better understand the differential be-

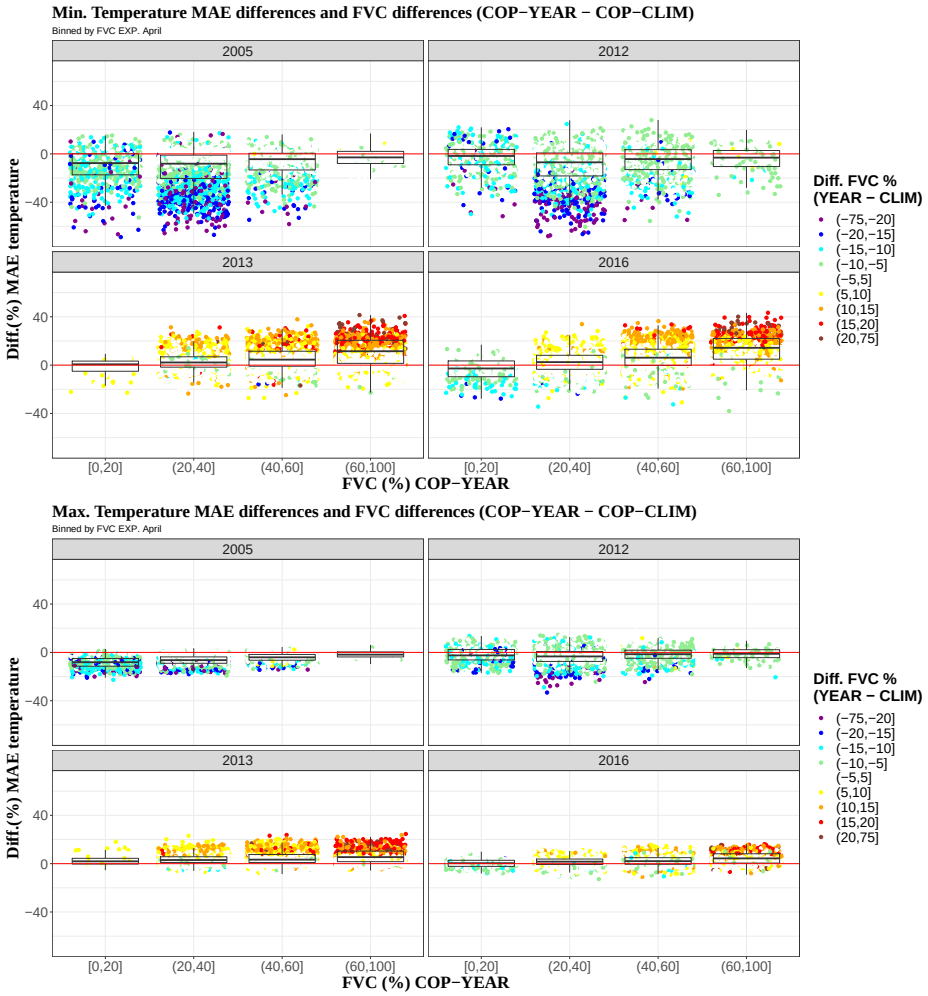

Fig. 6.9: Boxplot of differences of MAE between COP-YEAR and COP-CLIM experiments, for minimum temperature (Top panel) and maximum (Bottom panel). Differences of FVC between experiments in extreme dry years (2005-2012) and wet years (2013-2016). Results binned by FVC COP-YEAR experiment.

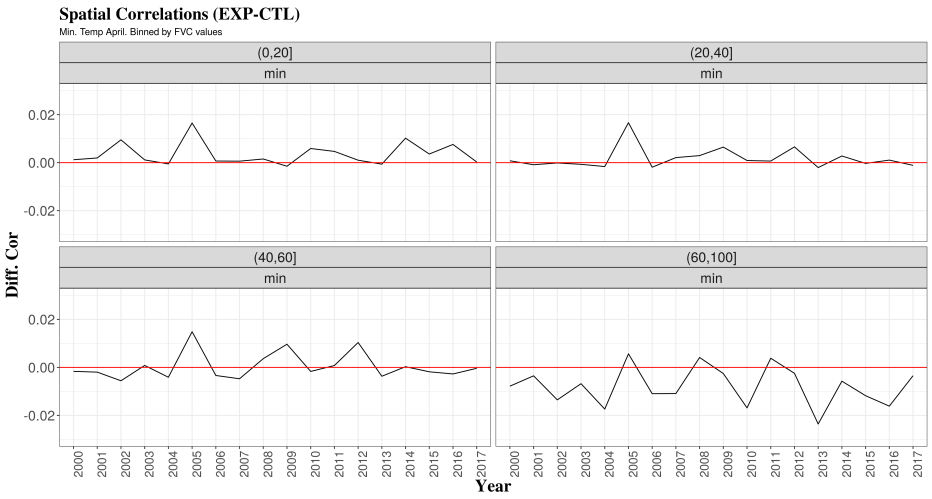

Fig. 6.10: Differences of spatial correlations between COP-YEAR and COP-CLIM experiments binned by FVC values. Calculation made for minimum temperature of April.

havior in the errors as a function of the presence of vegetation that has already been seen throughout the previous sections. Figure 6.11 represents for the month of April and stratifying by FVC values from the COP-YEAR simulation, the differences in temperature and FVC between COP-YEAR and COP-CLIM. When there is a higher FVC in the COP-YEAR experiment (green dots), lower temperatures are produced. The opposite is observed, i.e. higher temperatures when vegetation is less dense (brown dots). The slope of the relationship between temperature differences and FVC changes is greater in April, due to the fact that in general in this month the maximum plant productivity occurs as already seen in figures 5.1 and 5.2.

One aspect to note, is the asymmetric distribution observed between temperature and FVC differences depending on the sign of the FVC changes. For example, in the month of April, temperature differences close to 1.5 ° C are reached when the FVC is more dispersed, while they do not reach 1 ° C when it is denser. It can be seen that for high FVC values (60-100 %), the response in temperature differences is limited by a certain threshold, which as we have seen before reaches up to 1 ° C for FVC differences of the order of 20 %. The degree of this limitation is imposed by the empirical coefficient of thermal conductivity reduction in the presence of vegetation, which reaches almost 90% for FVC values of 100%.

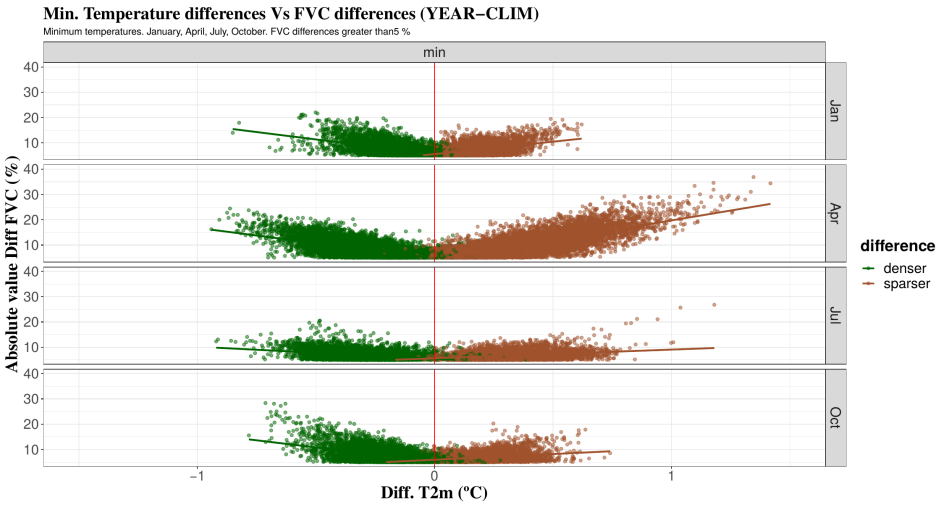

Fig. 6.11: Scatter plots of the absolute differences of minimum temperature and FVC changes for COP-YEAR and COP-CLIM for the period 2000-2017.

6.3.3 Effects of thermal conductivity on climate simulations

As we have seen in the previous section, the errors have a certain dependence on both the time of year and the base amount of vegetation. As we have seen in previous chapters, the thermal conductivity of the soil can play a very important role in temperature reproduction, especially of minimum temperatures. The thermal conductivity of the soil depends on the vegetation. Increasing the FVC leads to a decrease in the thermal soil conductivity. This implies a reduction of ground heat fluxes. During the day the soil absorbs less heat and therefore more sensible heat is available to warm the air. At night the upward ground heat flux is diminished having as consequence a faster cooling of the air. Therefore, during the night a larger FVC always causes cooling.

The relationship between the conductivity in bare soil and soils covered by vegetation depends on the inverse of the exponential on the FVC. That is, the more vegetation the soil contains, the more isolated it is. In this relationship, the parameter β appears, which indicates the magnitude of the relationship. β is preset to a value of 2. The question that arises in this section is whether this factor may be exaggerating the reduction in thermal conductivity and therefore introducing an error factor that depends critically on the base FVC.

First, the sensitivity of temperature, both maximum and minimum, to this parameter is tested. For this purpose, we use the annual simulations for the chosen years, two

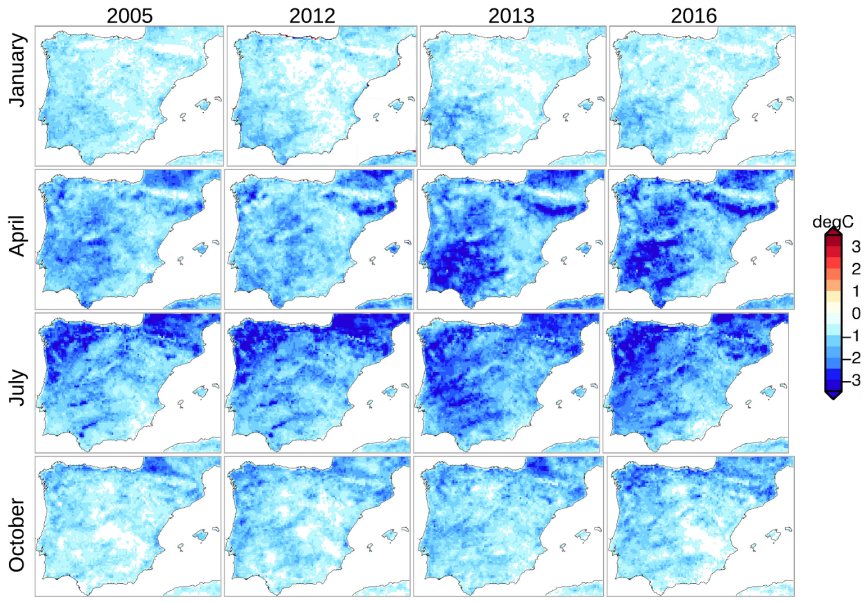

Fig. 6.12: Difference of minimum temperature in monthly means for the years 2005, 2012, 2013 and 2016 comparing simulations COP-YEAR (β = 2) and COP-YEAR-0.5 (β = 0.5) (COP-YEAR - COP-YEAR-0.5).

with positive vegetation anomaly (2005 and 2012) and two with negative anomaly (2013 and 2016) using COP-YEAR simulations as a basis. Figure 6.12 presents the differences between the simulations COP-YEAR with β = 2 and β = 0.5. We note how decreasing β increases the minimum temperature, the effect being more noticeable in months with higher available energy and in areas with more vegetation. The differences in the simulations can locally reach 3 ° C in the summer months. Note that this effect is not constant over the years, the years with more vegetation are logically affected to a greater extent. This can be seen for example in the large differences that can appear between April 2013 or 2016 and the same month of 2005 and 2012. The behavior for β = 1 is intermediate (not shown). This expected behavior can be observed by studying the stratified differences in the simulations (figure 6.13). The changes for soils with little vegetation are practically null, while in soils with higher FVC they reach an average of more than one degree in the months of April and July. In the winter months these differ-

ences barely exceed half a degree in areas with dense vegetation. Thus, the modification of the thermal conductivity will depend on the vegetation and the season. Therefore, this parameter will affect the reproduction of the annual cycle, the intraannual variation of the vegetation and will be a function of the base vegetation of each zone.

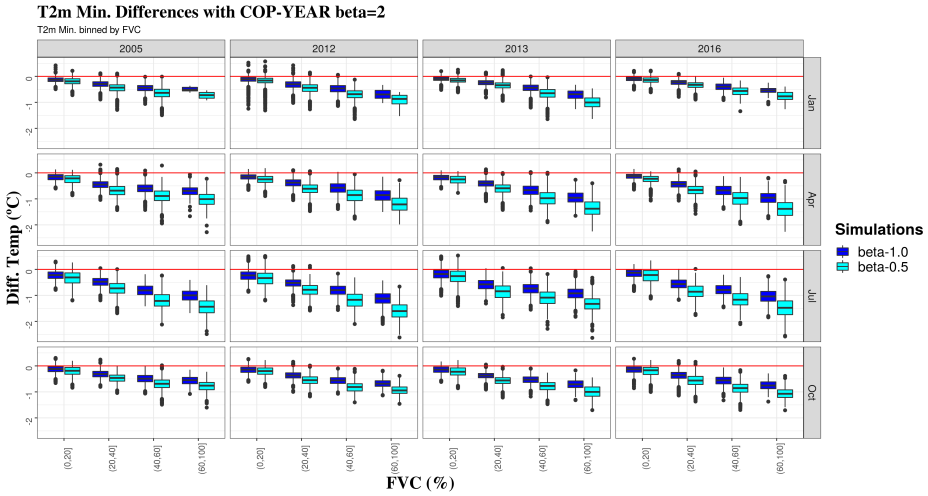

Fig. 6.13: Boxplot of minimum T2m differences in monthly means for the years 2005, 2012, 2013 and 2016 comparing COP-YEAR ($\beta = 2$) simulations with COP-YEAR-1.0 ($\beta = 1$) and COP-YEAR-0.5 ($\beta = 0.5$)). Stratified by FVC values.

After the sensitivity analysis, the next question that arises is whether this can really lead to an improvement in the reproduction of the temperature fields. Let us first analyze the impact on the minimum temperature fields in April for the years studied. Figure 6.14 presents the bias errors of the simulations taking AEMET5K as reference. The impact of modifying β is quite significant considering the temperature differences seen above. The effect of $\beta = 0.5$, seems to be very aggressive with respect to COP-YEAR since while in some areas the BIAS are reduced, in other areas they become more significant than in the COP-YEAR simulation. For $\beta = 1$, the effect on bias erros seems to be more moderate, and apparently a slight improvement over COP-YEAR can be suggested, although there are areas where there is some worsening. In figure 6.15 in which the BIAS for the three simulations are stratified, it can be seen how the differences in BIAS are progressively greater with higher values of FVC between the COP-YEAR and COP-YEAR-0.5 simulations. The simulation using $\beta = 1$ has an intermediate behavior reducing rather the bias error.

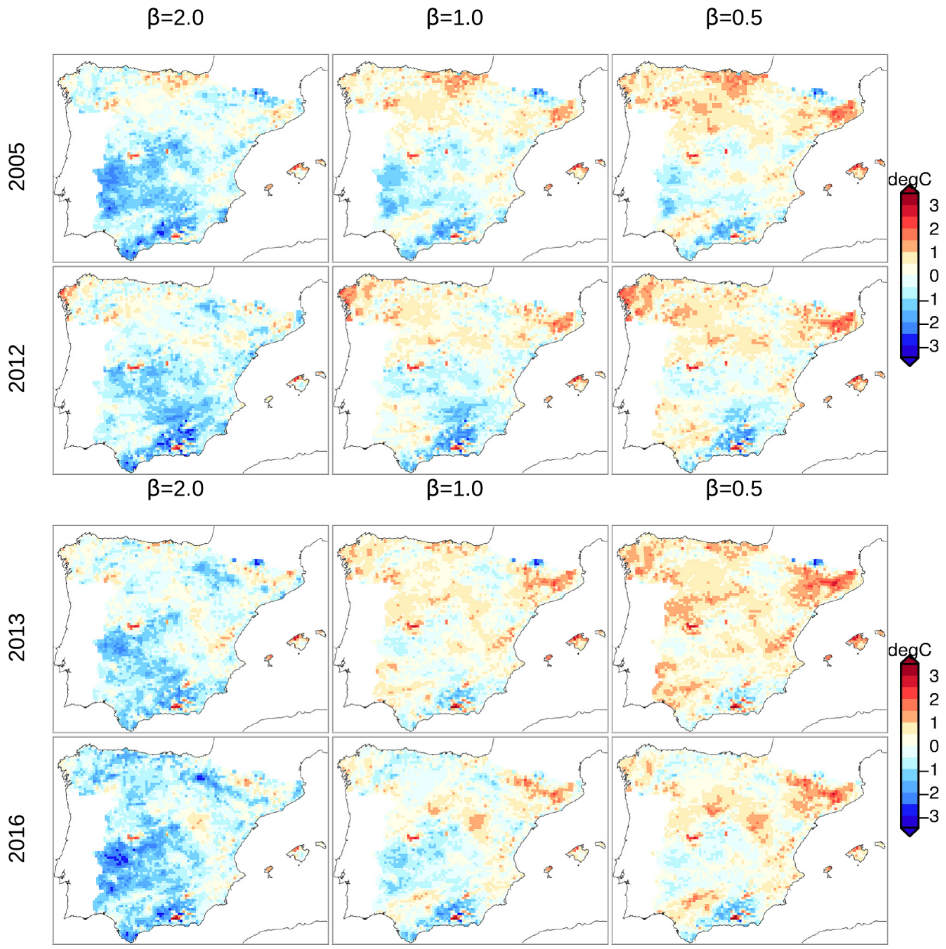

Fig. 6.14: Bias error for dry years (2005 and 2012) and wet years (2013 and 2016) for the simulations COP-YEAR ($\beta = 2$) , COP-YEAR-1.0 ($\beta = 1$) and COP-YEAR-0.5 ($\beta = 0.5$).

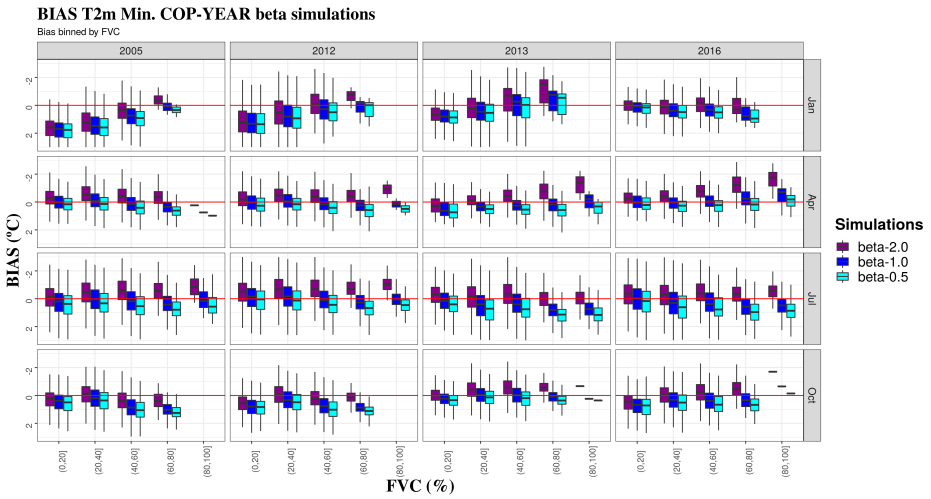

Fig. 6.15: Boxplot of BIAS of minimum T2m differences in monthly means for the years 2005, 2012, 2013 and 2016 comparing COP-YEAR ($\beta = 2$) simulations with COP-YEAR-1.0 ($\beta = 1$)) and COP-YEAR-0.5 ($\beta = 0.5$)). Stratified by FVC values.

6.3.4 Observed and simulated trends

In the previous chapter, the trends in the various simulations were presented. One striking factor was the lower trends observed in COP-YEAR associated with the trends observed in the vegetation databases. In this section we compare the trends observed in the observations and compare them with those modeled. Figure 6.16 shows the trends calculated with AEMET5K for both maximum and minimum temperature. In general, the reproduced trends are in agreement with the simulated ones. The highest trends are obtained for the maximum temperature in the summer and autumn months, with a differentiating pattern between the eastern and western peninsular zones. However, the distributions are not equal. This means that we cannot conclude anything about the added value of the incorporation of the variable FVC.

6.4 Discussion and conclusions

In this chapter we have tried to find the added value for the reproduction of climatology that can have the inclusion of FVC databases, a priori better, with higher resolution, and

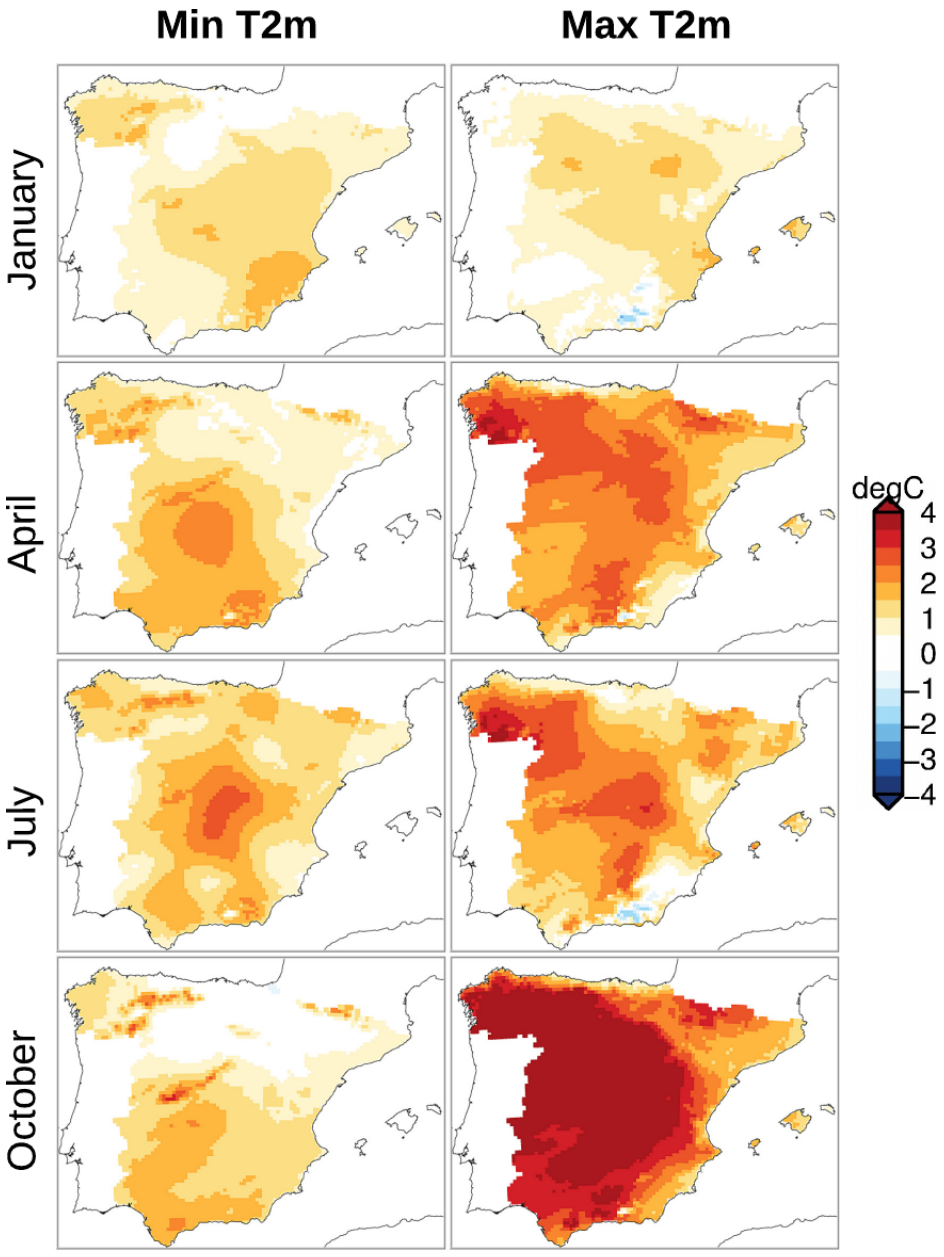

Fig. 6.16: Temperature trends (° C/18years) for maximum (right panel) and minimum (left panel) temperatures for January, Abril, July and October.

in addition to including its interannual variability. Due to the structure of some errors, it was decided to study the role of the modification of thermal conductivity linked to vegetation. The main conclusions that can be drawn from the study are presented and discussed below.

The effect of the modification of the FVC databases on the skill of the simulations is small. Errors probably associated with other factors mask the possible enhancement that could be introduced by these databases. Only slight improvements associated with the reproduction of the minimum temperature field are achieved. On the other hand, this opens an interesting debate about the databases used in the evaluation of the experiments. As mentioned in Gómez-Navarro et al. (2012a) this type of data has its problems since the intercomparison of different grid of observations can have a magnitude of errors similar to those recorded when comparing with simulations. In fact, although we have not included the results, a comparison has been made with data from the Spain02 database (Herrera et al., 2012) and the differences between the two databases are larger than the sensitivity of the model to changes in the FVC databases. On the other hand, the error patterns that present some structure related to orography may be related to the interpolation methodology used in the construction of the gridded databases, or even to the interpolation processes for grid comparison. The evaluation study presented here has also been carried out using station data (AEMET-OBS) and despite of the facts commented previously the results are similar than using AEMET5K. Probably, it would be desirable to use another type of comparison methodologies for local data that would allow to find the point or area in the model that be more significant when carrying out the evaluation as other works do.

There is an annual signal in the errors, as well as some dependence of the density of vegetation, especially in the minimum temperatures that indicate that the FVC adjustments throughout the year should be reconsidered. In a second part of the work, a series of experiments have been carried out in which the β parameter of the thermal conductivity equation that regulates the insulating effect of the FVC has been modified. The results show us that the adopted parameter $\beta = 2$ may be exaggerating the insulating effect of vegetation on surface heat transport. A somewhat lower parameter seems to give better results. Another question that can raise is whether the relationships between FVC and NDVI established in different works should be a function of the time of the year, or alternatively the parameter β.

7

Conclusions

This thesis focuses on understanding the role of the variable fraction vegetation cover (FVC) in the Noah Land Surface Model (LSM) coupled to a climate version of the MM5 model. Firstly, have been evaluated different sources of variability that can be found in FVC datasets due to the original NDVI dataset employed, the methodology of calculation and the time aggregation of the data (climatologies or near-real time values). Then, the sensitivity of the Noah LSM to changes in FVC have been studied considering the different sources of variability afforementioned and more broadly with ideal simulations, attempting to understand the main physical processes involved with FVC changes. At last, the high temporal and spatial resolution Copernicus FVC dataset have been ingested in regional climate simulations from 2000 to 2017 with the aim of elucidate the added value that a dataset of this kind can brings comparing with observations.

The interest and motivation of this study is justified by the relevance that land surface processes have in weather and climate. In the context of climate change, the knowledge of a variable that represents vegetation cover is considered of paramount importance due to its variability can act as a climate forcing in local, regional and global scales. Furthermore, this kind of studies are scarce in the Iberian Peninsula (IP) where vegetation variability can be remarkable due to its precipitation regime, deforestation or afforestation processes. Due to the fact that IP has been identified as an area, within the Mediterranean region, with large sensitivity to climate change, this kind of studies are needed for improving regional climate and future climate scenarios simulations.

The thesis is structured in four main parts. The first part studies the different sources of variability that can affect the calculation of FVC and how these can be tranlated in simulated fields of 2 meter air temperature (T2m) in a RCM (Chapter 3). Chapter 4 is devoted to understand the physical processes that matter in the final response of

near surface temperature through changes in FVC. In Chapter 5 has been carried out an analysis of regional climate simulations ingesting the Copernicus FVC dataset and the default climatological values of FVC in the Noah LSM. Finally, in Chapter 6 the previous simulations have been compared with observations.

Each chapter of this thesis has a specific section devoted to the conclusions of the most relevant results obtained therein. However, the main conclusions of this thesis are summarized in Section 7.1 of this chapter, providing a broader prespective of the work. Additionally, Section 7.2 presents possible future research topics.

7.1 Main conclusions

In Chapter 3, firstly the comparison of two different NDVI databases (EFAI and GIMMS) is accomplished, from which FVC can be calculated. Then, three calculation methodologies, WETZEL, GUTMAN and ZENG using the GIMMS database of NDVI (Tucker et al., 2005), have been applied to generate three different databases of FVC for the period 1982-2006. The differences between these databases and their subsequent effect on heat fluxes and temperatures were evaluated when incorporated to an annual simulation. Finally, the effect of using synchronous values of FVC for a dry and a wet year where compared with climatological values in an additional simulation. The main conclusions of this chapter are the next:

- EFAI and GIMMS NDVI presents a quite different interannual variability in a analyzed period of 17 years showing that some uncertainties can be found using NDVI datasets that can affect to the final calculation of FVC.
- The comparison between the FVC databases, WETZEL, GUTMAN and ZENG reveals important differences between them that depend on the NDVI value and the biome.
- FVC series reveal a important interannual variability, consequently climatological FVC values can present relevant differences compared with synchronous FVC values.
- The RCM experiments performed exhibit a not negligible effect of FVC uncertainty on the monthly climatological values. The results showed that differences of 30% of FVC, that appear in the two sensitivity experiments, can produce bias of 1 $^{\circ}$ in T2m monthly values. In addition, the magnitude of the model response depends on the time of the year, being greater in April and July.

In Chapter 4, a set of ideal simplified simulations with constant values of FVC of 90 % and 30 % have been performed in order of having a better understanding of the physical processes behind FVC parameterization. FVC drives the distribution of total evapotranspiration in transpiration through plants, evaporation canopy and bare soil evaporation, and determines the ratio between latent heat (LE) and sensible heat fluxes (H). In

Noah LSM, FVC is involved in another important process related with the reduction of thermal conductivity (K_t) in presence of vegetation. In this way, ground heat fluxes (G) are reduced with vegetation, inhibiting heat transport to deeper soil layers during the day and reducing ground temperature (T_g) during the night. The main conclusions reached are the next:

- There is a remarkable sensitivity of temperature to FVC in Noah LSM. This effect is more noticeable at nighttime, and in spring and summer when there is more radiative energy available in the study area.
- During nighttime, a larger FVC always causes cooling because the upward ground heat flux is diminished in presence of vegetation via thermal conductivity reduction.
- When soil moisture is available, a FVC increase causes higher LE release through evapotranspiration during the daytime. Therefore, with larger FVC less energy is available for sensible heat release and this provokes cooler T2m.
- With high moisture stress, soil moisture can reach the wilting point, and stomatal canopy resistance acts diminishing latent heat released by evapotranspiration. Under these conditions, the cooling effect of FVC almost disappears and higher values of FVC does not implies higher latent heat fluxes.
- In the experiments performed with constant FVC, larger FVC leads to a faster drying of soil which implies larger effects on canopy resistance. In a situation of scarce precipitation, a soil with higher FVC reaches the wilting point before a less vegetated soil. This leads to have less latent heat, occasioning higher diurnal temperatures.
- Canopy resistance parameterization is a relevant parameter controlling evapotranspiration. In its formulation in Noah LSM soil moisture deficit factor have a great importance in study areas like IP where there is a season with remarkable soil hydric stress.

In Chapter 5 a set of regional climate simulations during the period 2000-2017 have been carried out with the Copernicus dataset using synchronous monthly values (COP-YEAR) and climatological monthly values averaged over the time of simulation (COP-CLIM). Another simulation with the Noah LSM MM5 default FVC dataset have been performed with lesser horizontal resolution and calculated with climatological values from 1985 to 1991 (GUT-CLIM). The main conclusions reached are:

- The use of a high resolution and real time FVC is a useful tool for assessing and understanding the final role that the variable FVC has in a LSM.
- MM5 default FVC climatology (GUT-CLIM) compared with Copernicus FVC presents higher values, with differences in magnitude between 15-20 % comparing seasonilities averaged over the simulation period. On the other hand, differences in FVC due to interannual variability (comparison of COP-YEAR and COP-CLIM) can reach values of 5-10%.

- Comparison of GUT-CLIM and COP-CLIM shows that differences in vegetation between these databases can lead to changes in temperature averaged over the entire period of more than one degree for minimum temperature to 0.5 for maximum temperature. These changes are observed in the variance of the series, being more noticeable for maximum temperatures.
- Introducing the interannual variability of vegetation with COP-YEAR simulation (compared with COP-CLIM), shows a sign of change in the variance of the temperature series compared with variance of FVC.
- Trends in FVC cause trends of opposite sign in temperature especially in minimum temperatures.

Finally, in Chapter 6 the regional climate simulations of Chapter 5 have been compared with meteorological stations and a gridded dataset from AEMET centering the analysis in minimum and maximum T2m. The effect of the parameterization of soil thermal conductivity have been evaluated with several sensitivity experiments. These are the final conclusions of this chapter:

- Copernicus simulations perform better than GUT-CLIM reducing T2m BIAS and MAE, above all in minimum T2 and in the months of April and July.
- There is a difference in the response of FVC during day and night depending on its net effect in the radiative balance. For this reason, is needed to assess its role in T2m considering separetely minimum and maximum daily values. Evaluation of T2m considering daily mean values in regional climate simulations with FVC near real time data, can induce to misinterpretations of the final added value of this datasets.
- There are slightly differences in skill between COP-YEAR and COP-CLIM simulations, except in the years where there are maximum differences in FVC between COP-CLIM and COP-YEAR. In years with FVC below (above) normal values, COP-YEAR performs better (worst) than COP-CLIM simulation. These differences are attributed to the role of vegetation in the decrease of thermal conductivity.
- The role of FVC in reducing soil thermal conductivity has a noticeable impact in minimum T2m. With the results obtained, it is hypothesized that this reduction is slightly agressive in Noah LSM and therefore minimum T2m are negatively biased. Additional work assessing ground heat fluxes with observational data would be needed to assert this hyphotesis.
- It is necessary to be cautious with long term simulations including synchronus FVC data. In the trend analysis carried out in this work, uncertainties in the formulation of the Noah LSM related with FVC can lead to an exaggerated effect of climatic attribution to vegetation changes.

7.2 Future work

As a future work the following issues can be addressed:

- Analyze errors of surface fluxes is needed for a better understanding of the results of maximum T2m. Given the scarcity of surface stations of this kind in the IP, it would be interesting to use the EUMETSAT LSA-SAF evapotranspiration, H and LE satellite data products.
- Deepen in the role of FVC in thermal conductivity reduction with the help of ground flux measurements.
- Perform simulations with more complex LSMs like Noah-MP with a more realistic approach of biophysical processes related with vegetation.
- Address the study of droughts in detail and how regional climate simulations can be influenced by more realistic vegetation data.
- Assess the impact of a better spatial and temporal variability of FVC in local circulations and its effect in wind fields.
- Analyze the effect of long term simulations with realistic FVC in precipitation patterns, above all in convective precipitation.
- Considering albedo and FVC datasets together in regional climate simulations assessing its individual contribution.
- The use of satellite datasets of land surface temperature for evaluating real time FVC datasets in regional climate simulations can be interesting. Surface stations can be non representative in many cases of the vegetation cover collected by satellite data due to its location in urban areas or non natural placements. The use of land surface temperature can allow to assess model performance in forested or agricultural areas in a more proper way.

References

Amblar-Francés, M., P. Ramos-Calzado, J. Sanchis-Lladó, A. Hernanz-Lázaro, M. Peral-García, B. Navascués, M. Dominguez-Alonso, M. Pastor-Saavedra, and E. Rodríguez-Camino, 2020: High resolution climate change projections for the pyrenees region. *Advances in Science and Research*, **17**, 191–208.

Anthes, R., 1984: Enhacement of convective precipitation by mesoscale variations in vegetative covering in semiarid regions. *J. Climate Appl. Meteor.*, **23**, 541–554.

Best, M. J., G. Abramowitz, H. Johnson, A. Pitman, G. Balsamo, A. Boone, M. Cuntz, B. Decharme, P. Dirmeyer, J. Dong, et al., 2015: The plumbing of land surface models: benchmarking model performance. *J. Hydrometeor.*, **16**, 1425–1442.

Bonan, G. B., D. Pollard, and S. L. Thompson, 1992: Effects of boreal forest vegetation on global climate. *Nature*, **359**, 716–718.

Bright, R. M., E. Davin, T. O Halloran, J. Pongratz, K. Zhao, and A. Cescatti, 2017: Local temperature response to land cover and management change driven by non-radiative processes. *Nature Climate Change*, **7**, 296–302.

Buchhorn, M., B. Smets, L. Bertels, B. D. Roo, M. Lesiv, N.-E. Tsendbazar, L. Li, and A. Tarko, 2021: Copernicus Global Land Service: Land Cover 100m: version 3 Globe 2015-2019: Product User Manual. https://doi.org/10.5281/zenodo.4723921.

Campbell, P. C., J. O. Bash, and T. L. Spero, 2019: Updates to the noah land surface model in wrf-cmaq to improve simulated meteorology, air quality, and deposition. *Journal of advances in modeling earth systems*, **11**, 231–256.

Cao, Q., D. Yu, M. Georgescu, Z. Han, and J. Wu, 2015: Impacts of land use and land cover change on regional climate: a case study in the agro-pastoral transitional zone of china. *Environmental Research Letters*, **10**, 124025.

Carlson, T. N., E. M. Perry, and T. J. Schmugge, 1990: Remote estimates of soil moisture availability and fractional vegetation cover for agricultural fields. *Remote Sensing of Environ.*, **52**, 45–70.

Carlson, T. N. and D. A. Rypley, 1997: On the relation between ndvi, fractional vegetation cover, and leaf area index. *Remote Sensing of Environ.*, **62**, 241–252.

Chang, J.-T. and P. J. Wetzel, 1991: Effects of spatial variations of soil moisture and vegetation on the evolution of a prestorm environment: A numerical case study. *Mon. Wea. Rev.*, **119**, 1368–1390.

Charney, J., W. J. Quirk, S.-h. Chow, and J. Kornfield, 1977: A comparative study of the effects of albedo change on drought in semiarid regions. *J. Atmos. Sci.*, **34**, 1366–1385.

Charney, J. G., 1975: Dynamics of deserts and drought in the sahel. *Quart. J. Roy. Meteor. Soc.*, **101**, 193–202.

Chase, T. N., R. A. Pielke, T. G. Kittel, R. Nemani, and S. W. Running, 1996: Sensitivity of a general circulation model to global changes in leaf area index. *J. Geophys. Res. Atmospheres (1984–2012)*, **101**, 7393–7408.

Chase, T. N., R. Pielke Sr, T. Kittel, R. R. Nemani, and S. W. Running, 2000: Simulated impacts of historical land cover changes on global climate in northern winter. *Climate Dyn.*, **16**, 93–105.

Chase, T. N., R. Pielke Sr, T. Kittel, M. Zhao, A. Pitman, S. W. Running, and R. R. Nemani, 2001: Relative climatic effects of landcover change and elevated carbon dioxide combined with aerosols: A comparison of model results and observations. *J. Geophys. Res. Atmospheres (1984–2012)*, **106**, 31685–31691.

Chen, F., 2007: The noah land surface model in WRF: a short tutorial. *LSM group meeting*.

Chen, F. and J. Dudhia, 2001: Coupling an advanced land-surface/hydrology model with the penn state/ncar mm5 modeling system. part i: Model implementation and sensitivity. *Mon. Wea. Rev.*, **129**, 569–585.

Chen, F., Z. Janjić, and K. Mitchell, 1997: Impact of atmospheric surface-layer parameterizations in the new land-surface scheme of the ncep mesoscale eta model. *Bound. Lay. Meteor.*, **85**, 391–421.

Chen, F., K. Mitchell, J. Schaake, Y. Xue, H.-L. Pan, V. Koren, Q. Y. Duan, M. Ek, and A. Betts, 1996: Modeling of land surface evaporation by four schemes and comparison with fife observations. *J. Geophys. Res. Atmospheres (1984–2012)*, **101**, 7251–7268.

Chen, G.-S., M. Notaro, Z. Liu, and Y. Liu, 2012: Simulated local and remote biophysical effects of afforestation over the southeast united states in boreal summer. *J. Climate*, **25**, 4511–4522.

Choudhury, B., S. Idso, and R. Reginato, 1987: Analysis of an empirical model for soil heat flux under a growing wheat crop for estimating evaporation by an infrared-temperature based energy balance equation. *Agric. For. Meteor.*, **39**, 283–297.

Christensen, J. H., B. Machenhauer, R. G. Jones, C. Schär, P. M. Ruti, M. Castro, and G. Visconti, 1997: Validation of present-day regional climate simulations over europe: Lam simulations with observed boundary conditions. *Climate Dyn.*, **13**, 489–506.

Copeland, J. H., R. A. Pielke, and T. G. Kittel, 1996: Potential climatic impacts of vegetation change: A regional modeling study. *J. Geophys. Res. Atmospheres (1984–2012)*, **101**, 7409–7418.

Cosby, B. J., B. J, G. M. Hornberger, R. B. Clapp, and T. R. Ginn, 1984: A statistical exploration of the relationships of soil moisture characteristics to the physical properties of soils. *J. Hydrometeor.*, **20**, 682–690.

Costa Tenorio, M., C. Morla Juaristi, and H. Sainz Ollero, 1998: *Los bosques ibéricos. Una interpretación geobotánica*. Barcelona: Planeta.

Cotton, W. R. and R. A. Pielke Sr, 2007: *Human impacts on weather and climate*. Cambridge University Press.

Crawford, T. M., D. J. Stensrud, F. Mora, J. W. Merchant, and P. J. Wetzel, 2001: Value of incorporating satellite-derived land cover data in mm5/place for simulating surface temperatures. *J. Hydrometeor.*, **2**, 453–468.

Davies, H., 1976: A lateral boundary formulation for multi-level prediction models. *Quart. J. Roy. Meteor. Soc.*, **102**, 405–418.

Davin, E. L., E. Maisonnave, and S. I. Seneviratne, 2016: Is land surface processes representation a possible weak link in current regional climate models? *Environmental Research Letters*, **11**, 074027.

Deardorff, J. W., 1978: Efficient prediction of ground surface temperature and moisture, with inclusion of a layer of vegetation. *Journal of Geophysical Research: Oceans*, **83**, 1889–1903.

Dee, D. P., S. M. Uppala, A. Simmons, P. Berrisford, P. Poli, S. Kobayashi, U. Andrae, M. A. Balmaseda, G. Balsamo, P. Bauer, P. Bechtold, A. C. M. Beljaars, L. van de Berg, J. Bidlot, N. Bormann, C. Delsol, R. Dragani, M. Fuentes, A. Geer, L. Haimberger, S. B. Healy, H. Hersbach, E. V. Hólm, L. Isaksen, P. Kållberg, M. Köhler, M. Matricardi, A. P. McNally, B. M. Monge-Sanz, J.-J. Morcrette, B.-K. Park, C. Peubey, P. de Rosnay, C. Tavolato, T. J.-N, and F. Vitart, 2011: The era-interim reanalysis: Configuration and performance of the data assimilation system. *Quart. J. Roy. Meteor. Soc.*, **137**, 553–597.

Dickinson, R. E., 1984: Modeling evapotranspiration for three-dimensional global climate models. *Climate processes and climate sensitivity*, **29**, 58–72.

— 1993: Biosphere atmosphere transfer scheme (bats) version 1e as coupled to the ncar community climate model. *NCAR Tech. Note TH-387+ STR*.

Dudhia, J., 1989: Numerical study of convection observed during the winter monsoon experiment using a mesoscale two-dimensional model. *J. Atmos. Sci.*, **46**, 3077–3107.

Duveiller, G., J. Hooker, and A. Cescatti, 2018: The mark of vegetation change on earth's surface energy balance. *Nature communications*, **9**, 1–12.

Ek, M. and L. Mahrt, 1991: OSU 1-D PBL model user's guide. Technical report, Department of Atmospheric Sciences, Oregon State University.

Ek, M. B., K. E. Mitchell, Y. Lin, E. Rogers, P. Grunmann, V. Koren, G. Gayno, and J. D. Tarpley, 2003: Implementation of noah land surface model advances in the national centers for environmental prediction operational mesoscale eta model. *J. Geophys. Res. Atmospheres (1984–2012)*, **108**.

Eltahir, E. A., 1998: A soil moisture-rainfall feedback mechanism: 1. theory and observations. *Water resources research*, **34**, 765–776.

Feddes, R. A., H. Hoff, M. Bruen, T. Dawson, P. De Rosnay, P. Dirmeyer, R. B. Jackson, P. Kabat, A. Kleidon, A. Lilly, et al., 2001: Modeling root water uptake in hydrological and climate models. *Bull. Amer. Meteor. Soc.*, **82**, 2797–2810.

Fernández, J., J. Montávez, J. Sáenz, J. González-Rouco, and E. Zorita, 2007: Sensitivity of the mm5 mesoscale model to physical parameterizations for regional climate studies: Annual cycle. *J. Geophys. Res. Atmospheres (1984–2012)*, **112**.

Fernández-Montes, S., J. Gómez-Navarro, F. Rodrigo, J. García-Valero, and J. Montávez, 2017: Covariability of seasonal temperature and precipitation over the iberian peninsula in high-resolution regional climate simulations (1001–2099). *Global Planet. Change*, **151**, 122–133.

Fisher, R. A. and C. D. Koven, 2020: Perspectives on the future of land surface models and the challenges of representing complex terrestrial systems. *Journal of Advances in Modeling Earth Systems*, **12**, e2018MS001453.

Gallo, K., D. Tarpley, K. Mitchell, I. Csiszar, T. Owen, and B. Reed, 2001: Monthly fractional green vegetation cover associated with land cover classes of the conterminous usa. *Geophys. Res. Lett.*, **28**, 2089–2092.

Ge, Q., X. Zhang, and J. Zheng, 2014: Simulated effects of vegetation increase/decrease on temperature changes from 1982 to 2000 across the eastern china. *Int. J. Climatol.*, **34**, 187–196.

Gedney, N. and P. J. Valdes, 2000: The effect of amazonian deforestation on the northern hemisphere circulation and climate. *Geophys. Res. Lett.*, **27**, 3053–3056.

Gesch, D. B., K. L. Verdin, and S. K. Greenlee, 1999: New land surface digital elevation model covers the earth. *EOS, Transactions American Geophysical Union*, **80**, 69–70.

Godfrey, C. M., D. J. Stensrud, and L. M. Leslie, 2002: The influence of improved land surface and soil data on mesoscale model predictions. Preprints, *19th Conf. on Hydrology*, Amer. Meteor. Soc., San Diego, CA, CD–ROM, 4.7.

Gómez-Navarro, J., J. Montávez, S. Jerez, P. Jiménez-Guerrero, and E. Zorita, 2012a: What is the role of the observational dataset in the evaluation and scoring of climate models? *Geophys. Res. Lett.*, **39**.

Gómez-Navarro, J., J. Montávez, P. Jiménez-Guerrero, S. Jerez, R. Lorente-Plazas, J. González-Rouco, and E. Zorita, 2012b: Internal and external variability in regional simulations of the iberian peninsula climate over the last millennium. *Climate of the Past*, **8**, 25.

Grell, G., J. Dudhia, and D. Stauffer, 1994: A description of the fifth-generation Penn State/NCAR Mesoscale Model (mm5). Ncar tech. note, NCAR.

Grell, G. A., 1993: Prognostic evaluation of assumptions used by cumulus parameterizations. *Mon. Wea. Rev.*, **121**, 764–787.

Gutman, G. and A. Ignatov, 1998: The derivation of the green vegetation fraction from noaa/avhrr data for use in numerical weather prediction models. *Int. J. Remote Sensing*, **19**, 1533–1543.

Gutman, G., D. Tarpley, A. Ignatov, and S. Olson, 1995: The enhanced noaa global land datasets from the advanced very high resolution radiometer. *Int. J. Remote Sensing*, **76**, 1141–1156.

Hanamean Jr, J. M., R. A. Pielke Sr, C. L. Castro, D. S. Ojima, B. C. Reed, and Z. Gao, 2003: Vegetation greenness impacts on maximum and minimum temperatures in northeast colorado. *Meteor. Appl.*, **10**, 203–215.

Hanks, R. J. and G. L. Ashcroft, 1986: Applied soil physics.

Hansen, M., R. DeFries, J. R. G. Townshend, and R. Sohlberg, 1998: Umd global land cover classification. 8 kilometer. version 1.0. 1981-1994.

— 2000: Global land cover classification at 1km resolution using a decision tree classifier. *Int. J. Remote Sensing*, **21**, 1331–1365.

He, J., Y. Yu, L. Yu, N. Liu, and S. Zhao, 2017: Impacts of uncertainty in land surface information on simulated surface temperature and precipitation over china. *Int. J. Climatol.*, **37**, 829–847.

Heck, P., D. Lüthi, H. Wernli, and C. Schär, 2001: Climate impacts of european-scale anthropogenic vegetation changes: A sensitivity study using a regional climate model. *J. Geophys. Res. Atmospheres (1984–2012)*, **106**, 7817–7835.

Henderson-Sellers, A., K. McGuffie, and C. Gross, 1995: Sensitivity of global climate model simulations to increased stomatal resistance and c02 increases. *J. Climate*, **8**, 1738–1756.

Herrera, S., J. M. Gutiérrez, R. Ancell, M. Pons, M. Frías, and J. Fernández, 2012: Development and analysis of a 50-year high-resolution daily gridded precipitation dataset over spain (spain02). *Int. J. Climatol.*, **32**, 74–85.

Hong, S., V. Lakshmi, E. Small, F. Chen, M. Tewari, and K. W. Manning, 2009: Effects of vegetation and soil moisture on the simulated land surface processes from the coupled wrf/noah model. *J. Geophys. Res. Atmospheres (1984–2012)*, **114**.

Hong, S. and H. Pan, 1996: Nonlocal boundary layer vertical diffusion in a medium-range forecast model. *Mon. Wea. Rev.*, **124**, 2322–2339.

Hudson, J. M. and G. Henry, 2009: Increased plant biomass in a high arctic heath community from 1981 to 2008. *Ecology*, **90**, 2657–2663.

Hughes, J. D., 2011: Ancient deforestation revisited. *Journal of the History of Biology*, **44**, 43–57.

Jacquemin, B. and J. Noilhan, 1990: Sensitivity study and validation of a land surface parameterization using the hapex-mobilhy data set. *Bound. Lay. Meteor.*, **52**, 93–134.

James, K. A., D. J. Stensrud, and N. Yussouf, 2009: Value of real-time vegetation fraction to forecasts of severe convection in high-resolution models. *Wea. Forecasting*, **24**, 187–210.

James, M. E. and S. N. V. Kalluri, 1994: The pathfinder avhrr land dataset:an improved coarse resolution dataset for terrestrial monitoring. *Int. J. Remote Sensing*, **15**, 3347–3363.

Jerez, S., J. M. López-Romero, M. Turco, R. Lorente-Plazas, J. J. Gómez-Navarro, P. Jiménez-Guerrero, and J. P. Montávez, 2020: On the spin-up period in wrf simulations over europe: Trade-offs between length and seasonality. *Journal of Advances in Modeling Earth Systems*, **12**, e2019MS001945, doi:https://doi.org/10.1029/2019MS001945, e2019MS001945 2019MS001945.
URL https://agupubs.onlinelibrary.wiley.com/doi/abs/10.1029/2019MS001945

Jerez, S., J. Montavez, J. Gomez-Navarro, P. Jimenez, P. Jimenez-Guerrero, R. Lorente, and J. F. Gonzalez-Rouco, 2012: The role of the land-surface model for climate change projections over the iberian peninsula. *J. Geophys. Res. Atmospheres (1984–2012)*, **117**.

Jerez, S., J. P. Montavez, J. J. Gomez-Navarro, P. Jimenez-Guerrrero, J. M. Jimenez, and J. F. Gonzalez-Rouco, 2010: Temperature sensitivity to the land-surface model in mm5 climate simulations over the iberian peninsula. *Meteor. Z.*, **19**, 363–374.

Jerez, S., J. P. Montavez, P. Jimenez-Guerrero, J. J. Gomez-Navarro, R. Lorente-Plazas, and E. Zorita, 2013: A multi-physics ensemble of present-day climate regional simulations over the iberian peninsula. *Climate Dyn.*, **40**, 3023–3046.

Jiménez-Gutiérrez, J. M., F. Valero, S. Jerez, and J. P. Montávez, 2019: Impacts of green vegetation fraction derivation methods on regional climate simulations. *Atmosphere*, **10**, 281.

Jiménez-Gutiérrez, J. M., F. Valero, J. Ruiz-Martínez, and J. P. Montávez, 2021: Temperature response to changes in vegetation fraction cover in a regional climate model. *Atmosphere*, **12**, 591.

Kang, H.-S., Y. Xue, and G. J. Collatz, 2007: Impact assessment of satellite-derived leaf area index datasets using a general circulation model. *J. Climate*, **20**, 993–1015.

Kimball, J., 2014: *Vegetation Phenology*, Springer New York. 886–890.

Kumar, A., F. Chen, M. Barlage, M. B. Ek, and D. Niyogi, 2014: Assessing impacts of integrating modis vegetation data in the weather research and forecasting (wrf) model coupled to two different canopy-resistance approaches. *J. Appl. Meteor. Climatol.*, **53**, 1362–1380.

Kumar, P., B. K. Bhattacharya, and P. Pal, 2013: Impact of vegetation fraction from indian geostationary satellite on short-range weather forecast. *Agric. For. Meteor.*, **168**, 82–92.

Kurkowski, N. P., D. J. Stensrud, and M. E. Baldwin, 2003: Assessment of implementing satellite-derived land cover data in the eta model. *Wea. Forecasting*, **18**, 404–416.

Li, M., Y. Song, X. Huang, J. Li, Y. Mao, T. Zhu, X. Cai, and B. Liu, 2014: Improving mesoscale modeling using satellite-derived land surface parameters in the pearl river delta region, china. *J. Geophys. Res. Atmospheres (1984–2012)*, **119**, 6325–6346.

Li, X. and J. Zhang, 2016: Derivation of the green vegetation fraction of the whole china from 2000 to 2010 from modis data. *Earth Interact.*, **20**, 1–16.

Limei, R., R. Gilliam, F. Binkowski, A. Xiu, J. Pleim, and L. Band, 2015: Sensitivity of the weather research and forecast/community multiscale air quality modeling system to modis lai, fpar, and albedo. *J. Geophys. Res. Atmospheres (1984–2012)*, **120**, 8491–8511, 2015JD023424.

Lo, J. C.-F., Z.-L. Yang, and R. A. Pielke Sr, 2008: Assessment of three dynamical climate downscaling methods using the weather research and forecasting (wrf) model. *J. Geophys. Res. Atmospheres (1984–2012)*, **113**.

Lofgren, B. M., 1995: Surface albedo-climate feedback simulated using two-way coupling. *J. Climate*, **8**, 2543–2562.

Lorente-Plazas, R., J. Montávez, S. Jerez, J. Gómez-Navarro, P. Jiménez-Guerrero, and P. Jiménez, 2015: A 49 year hindcast of surface winds over the iberian peninsula. *Int. J. Climatol.*, **35**, 3007–3023.

Loveland, T. R., B. C. Reed, J. F. Brown, D. O. Ohlen, Z. Zhu, L. Yang, and J. W. Merchant, 2000: Development of a global land cover characteristics database and igbp discover from 1 km avhrr data. *Int. J. Remote Sensing*, **21**, 1303–1330.

Mahfouf, J., E. Richard, and P. Mascart, 1987: The influence of soil and vegetation on the development of mesoscale circulations. *J. Climate Appl. Meteor.*, **26**, 1483–1495.

Mahfouf, J. F. and J. Noilhan, 1991: Comparative study of various formulations of evaporations from bare soil using in situ data. *J. Appl. Meteor.*, **30**, 1354–1365.

Mahmood, R., R. A. Pielke, and C. A. McAlpine, 2016: Climate-relevant land use and land cover change policies. *Bull. Amer. Meteor. Soc.*, **97**, 195–202.

Mahrt, L. and M. Ek, 1984: The influence of atmospheric stability on potential evaporation. *J. Appl. Meteor.*, **23**, 222–234.

Mahrt, L. and H. Pan, 1984: A two-layer model of soil hydrology. *Bound. Lay. Meteor.*, **29**, 1–20.

Malinowski, R., S. Lewinski, M. Rybicki, E. Gromny, M. Jenerowicz, M. Krupinski, A. Nowakowski, C. Wojtkowski, M. Krupinski, E. Krätzschmar, and P. Schauer, 2020: Automated production of a land cover/use map of europe based on sentinel-2 imagery. *Remote Sensing*, **12**, doi:10.3390/rs12213523.
URL https://www.mdpi.com/2072-4292/12/21/3523

Manabe, S., 1969: Climate and the ocean circulation: I. the atmospheric circulation and the hydrology of the earth's surface. *Mon. Wea. Rev.*, **97**, 739–774.

Marshall, C. H., K. C. Crawford, K. E. Mitchell, and D. J. Stensrud, 2003: The impact of the land surface physics in the operational ncep eta model on simulating the diurnal cycle: Evaluation and testing using oklahoma mesonet data. *Wea. Forecasting*, **18**, 748–768.

Matsui, T., V. Lakshmi, and E. E. Small, 2005: The effects of satellite-derived vegetation cover variability on simulated land-atmosphere interactions in the nams. *J. Climate*, **18**, 21–40.

McGuire, A. D., S. Sitch, J. S. Clein, R. Dargaville, G. Esser, J. Foley, M. Heimann, F. Joos, J. Kaplan, D. W. Kicklighter, R. A. Meier, J. M. Melillo, B. Moore III, I. C. Prentice, N. Ramankutty, T. Reichenau, A. Schloss, H. Tian, L. J. Williams, and U. Wittenberg, 2001: Carbon balance of the terrestrial biosphere in the twentieth century: Analyses of co2, climate and land use effects with four process-based ecosystem models. *Global Biogeochemical Cycles*, **15**, 183–206.

McPherson, R. A., 2007: A review of vegetation-atmosphere interactions and their influences on mesoscale phenomena. *Progress in Physical Geography*, **31**, 261–285.

Meng, X. H., J. P. Evans, and M. F. McCabe, 2014: The impact of observed vegetation changes on land–atmosphere feedbacks during drought. *J. Hydrometeor.*, **15**, 759–776.

Miller, J., M. Barlage, X. Zeng, H. Wei, and K. Mitchell, 2006: Sensitivity of the ncep/noah land surface model to the modis green vegetation fraction data set. *Geophys. Res. Lett.*, **33**, 237–250.

Mlawer, E., S. Taubman, P. Brown, M. Iacono, and S. Clough, 1997: Radiative transfer for inhomogeneous atmospheres: Rrtm, a validated correlated-k model for the longwave. *J. Geophys. Res.*, **102**, 16663–16682.

Montandon, L. M. and E. E. Small, 2008: The impact of soil reflectance on the quantification of the green vegetation fraction from ndvi. *Remote Sensing of Environ.*, **112**, 1835–1845.

Müller, O. V., E. H. Berbery, D. Alcaraz-Segura, and M. B. Ek, 2014a: Regional model simulations of the 2008 drought in southern south america using a consistent set of land surface properties. *J. Climate*, **27**, 6754–6778.

— 2014b: Regional model simulations of the 2008 drought in southern south america using a consistent set of land surface properties. *J. Climate*, **27**, 6754–6778.

Myneni, R. B., F. G. Hall, P. J. Sellers, and A. L. Marshak, 1995: The interpretation of spectral vegetation indexes. *IEEE Transac. Geosc. Rem. Sens.*, **33**, 481–486.

Myneni, R. B., C. D. Keeling, C. J. Tucker, G. Asrar, and R. R. Nemani, 1997: Increased plant growth in the northern high latitudes from 1981 to 1991. *Nature*, **386**, 698–702.

Niu, G. Y., Z.-L. Yang, K. Mitchell, F. Chen, M. Ek, M. Barlage, A. Kumar, K. Manning, D. Niyogi, E. Rosero, M. Tewari, and Y. Xia, 2011: The community noah land surface model with multiparameterization options (noah-mp): 1. model description and evaluation with local-scale measurements. *J. Geophys. Res. Atmospheres (1984–2012)*, **116**.

Noilhan, J. and S. Planton, 1989: A simple parameterization of land surface processes for meteorological models. *Mon. Wea. Rev.*, **117**, 536–549.

Notaro, M., G. Chen, Y. Yu, F. Wang, and A. Tawfik, 2017: Regional climate modeling of vegetation feedbacks on the asian australian monsoon systems. *J. Climate*, **30**, 1553–1582.

Oke, T. R., 1987: *Boundary layer climates*. Routledge.

Ookouchi, Y., M. Segal, R. Kesller, and R. Pielke, 1984: Evaluation of soil moisture effects on the generation and modification of mesoscale circulation. *Mon. Wea. Rev.*, **112**, 2281–2292.

Overgaard, J., D. Rosbjerg, and M. Butts, 2006: Land-surface modelling in hydrological perspective–a review. *Biogeosciences*, **3**, 229–241.

Pan, H.-L. and L. Mahrt, 1987: Interaction between soil hydrology and boundary-layer development. *Bound. Lay. Meteor.*, **38**, 185–202.

Patil, M., M. Kumar, R. Waghmare, T. Dharmaraj, and N. Mahanty, 2014: Evaluation of noah-lsm for soil hydrology parameters in the indian summer monsoon conditions. *Theor. App. Clim.*, **118**, 47–56.

Penman, H. L., 1948: Natural evaporation from open water, bare soil and grass. *Proceedings of the Royal Society of London. Series A. Mathematical and Physical Sciences*, **193**, 120–145.

Peral-García, C., B. Navascués, and P. Ramos-Calzado, 2017: Serie de precipitación diaria en rejilla con fines climáticos. nota técnica 24 de aemet. Technical report, AEMET.

Peters-Lidard, C. D., M. S. Zion, and E. F. Wood, 1997: A soil-vegetation-atmosphere transfer scheme for modeling spatially variable water and energy balance processes. *J. Geophys. Res. Atmospheres (1984–2012)*, **102**, 4303–4324.

Pettorelli, N., V. J. Olav, M. Atle, J. M. Gaillard, C. J. Tucker, and N. C. Stenseth, 2005: Using the satellite-derived ndvi to assess ecological responses to enviromental change. *IEEE Transac. Geosc. Rem. Sens.*, **20**, 503–510.

Pielke, R. A., 2005: Land use and climate change. *Science*, **310**, 1625–1626.

Pielke, R. A. and R. Avissar, 1990: Influence of landscape structure on local and regional climate. *Landscape Ecology*, **4**, 133–155.

Pielke, R. A., R. Avissar, M. Raupach, A. J. Dolman, X. Zeng, and A. S. Denning, 1998: Interactions between the atmosphere and terrestrial ecosystems: influence on weather and climate. *Global change biology*, **4**, 461–475.

Pielke Sr, R. A., 2002: Overlooked issues in the us national climate and ipcc assessments. *Climatic Change*, **52**, 1.

Pielke Sr, R. A., A. Pitman, D. Niyogi, R. Mahmood, C. McAlpine, F. Hossain, K. K. Goldewijk, U. Nair, R. Betts, S. Fall, M. Reichstein, P. Kabat, and N. de Noblet, 2011: Land use/land cover changes and climate: modeling analysis and observational evidence. *Wiley Interdisciplinary Reviews: Climate Change*, **2**, 828–850.

Pinzon, J., 2002: Using hht to successfully uncouple seasonal and interannual components in remotely sensed data. *Conference Proceedings Jul 14-18*, SCI, Orlando, Florida.

Pitman, A. J., 2003: The evolution of, and revolution in, land surface schemes designed for climate models. *Int. J. Climatol.*, **23**, 479–510.

Price, J. C., 1992: Estimating vegetation amount from visible and near infrared reflectances. *Remote Sensing of Environ.*, **41**, 29–34.

Reale, O. and P. Dirmeyer, 2000: Modeling the effects of vegetation on mediterranean climate during the roman classical period: Part i: Climate history and model sensitivity. *Global Planet. Change*, **25**, 163–184.

Reale, O. and J. Shukla, 2000: Modeling the effects of vegetation on mediterranean climate during the roman classical period: Part ii. model simulation. *Global Planet. Change*, **25**, 185–214.

Refslund, J., E. Dellwik, A. Hahmann, M. Barlage, and E. Boegh, 2014: Development of satellite green vegetation fraction time series for use in mesoscale modeling: application to the european heat wave 2006. *Theor. App. Clim.*, **117**, 377–392.

Rosero, E., Z.-L. Yang, T. Wagener, L. Gulden, S. Yatheendradas, and G.-Y. Niu, 2010: Quantifying parameter sensitivity, interaction, and transferability in hydrologically enhanced versions of the noah land surface model over transition zones during the warm season. *J. Geophys. Res. Atmospheres (1984–2012)*, **115**.

Rosnay, P. d. and J. Polcher, 1998: Modelling root water uptake in a complex land surface scheme coupled to a gcm. *Hydrology and Earth System Sciences*, **2**, 239–255.

Sagan, C., O. B. Toon, and J. B. Pollack, 1979: Anthropogenic albedo changes and the earth's climate. *Science*, **206**, 1363–1368.

San-Miguel-Ayanz, J., J. M. Moreno, and A. Camia, 2013: Analysis of large fires in european mediterranean landscapes: Lessons learned and perspectives. *Forest Ecology and Management*, **294**, 11–22, the Mega-fire reality.

Sato, H., A. Ito, A. Ito, T. Ise, and E. Kato, 2015: Current status and future of land surface models. *Soil science and plant nutrition*, **61**, 34–47.

Schaake, J. C., V. I. Koren, Q.-Y. Duan, K. Mitchell, and F. Chen, 1996: Simple water balance model for estimating runoff at different spatial and temporal scales. *J. Geophys. Res. Atmospheres (1984–2012)*, **101**, 7461–7475.

Schmuck, G., J. San-Miguel-Ayanz, A. Camia, T. Durrant, S. Santos de Oliveira, R. Boca, C. Whitmore, C. Giovando, G. Libertà, P. Corti, et al., 2011: Forest fires in europe 2010.

Segal, M., R. Avissar, and M. M. R. Pielke, 1988: Evaluation of vegetation effects on the generation and modification of mesoscale circulations. *J. Atmos. Sci.*, **45**, 2268–2292.

Sellers, P., R. Dickinson, D. Randall, A. Betts, F. Hall, J. Berry, G. Collatz, A. Denning, H. Mooney, C. Nobre, et al., 1997: Modeling the exchanges of energy, water, and carbon between continents and the atmosphere. *Science*, **275**, 502–509.

Sellers, P., Y. Mintz, Y. Sud, and A. Dalcher, 1986: A simple biosphere model (sib) for use within general circulation models. *J. Atmos. Sci.*, **43**, 505–531.

Sellers, P. J., S. O. Los, C. J. Tucker, C. O. Justice, D. A. Dazlich, G. J. Collatz, and D. A. Randall, 1996: A revised land surface parameterization (sib2) for atmospheric gcms. part ii: The generation of global fields of terrestrial biophysical parameters from satellite data. *J. Climate*, **9**, 706–737.

Seneviratne, S. I., T. Corti, E. L. Davin, M. Hirschi, E. B. Jaeger, I. Lehner, B. Orlowsky, and A. J. Teuling, 2010: Investigating soil moisture–climate interactions in a changing climate: A review. *Earth-Science Reviews*, **99**, 125–161.

Shukla, J. and Y. Mintz, 1982: Influence of land-surface evapotranspiration on the earth's climate. *Science*, **215**, 1498–1501.

Shukla, P., J. Skea, E. Calvo Buendia, V. Masson-Delmotte, H. Pörtner, D. Roberts, P. Zhai, R. Slade, S. Connors, R. Van Diemen, et al., 2019: Ipcc, 2019: Climate change and land: an ipcc special report on climate change, desertification, land degradation, sustainable land management, food security, and greenhouse gas fluxes in terrestrial ecosystems.

Stensrud, D. J., 2007: *Parameterization Schemes: Keys to Understanding Numerical Weather Prediction Models*. Cambridge University Press.

Stockli, R. and P. L. Vidale, 2004: European plant phenology and climate as seen in a 20 year avhrr land-surface parameter dataset. *Int. J. Remote Sensing*, **17**, 3303–3330.

Sud, Y. and W. Smith, 1985: The influence of surface roughness of deserts on the july circulation. *Bound. Lay. Meteor.*, **33**, 15–49.

Tarpley, J. P., S. R. Schneider, and R. L. Money, 1984: Global vegetation indices from noaa-7 meteorological satellite. *J. Climate Appl. Meteor.*, **23**, 491–494.

Tucker, C. J., J. E. Pinzon, and M. E. Brown, 2004: Global inventory modeling and mapping studies 2.0. Digital media. [Available online at `http://staff.glcf.umd.edu/sns/htdocs/data/gimms/`.].

Tucker, C. J., J. E. Pinzon, M. E. Brown, D. Slayback, E. W. Pak, R. Mahoney, E. Vermote, and N. E. Saleous, 2005: An extended avhrr 8-km ndvi data set compatible with modis and spot vegetation ndvi data. *Int. J. Remote Sensing*, **26**, 4485–4498.

Tullot, I. F., 2000: *Climatología de España y Portugal*, volume 76. Universidad de Salamanca.

Vahmani, P. and G. Ban-Weiss, 2016: Impact of remotely sensed albedo and vegetation fraction on simulation of urban climate in wrf-urban canopy model: A case study of the urban heat island in los angeles. *J. Geophys. Res.*, **121**, 1511–1531.

Vahmani, P. and T. Hogue, 2014: High-resolution land surface modeling utilizing remote sensing parameters and the noah ucm: a case study in the los angeles basin. *Hydrol. and Earth System Sciences*, **18**, 4791–4806.

Verger, A., F. Baret, and M. Weiss, 2014: Near real-time vegetation monitoring at global scale. *IEEE Journal of Selected Topics in Applied Earth Observations and Remote Sensing*, **7**, 3473–3481.

Vilá Valentí, J., 1983: *La península ibérica*. Ariel Geografía.

Viterbo, P. and A. C. Beljaars, 1995: An improved land surface parameterization scheme in the ecmwf model and its validation. *J. Climate*, **8**, 2716–2748.

Wen, J., X. Lai, X. Shi, and X. Pan, 2013: Numerical simulations of fractional vegetation coverage influences on the convective environment over the source region of the yellow river. *Meteor. Atmos. Phys.*, **120**, 1–10.

Wong, M. M. F., J. C. H. Fung, and P. P. S. Yeung, 2019: High-resolution calculation of the urban vegetation fraction in the pearl river delta from the sentinel-2 ndvi for urban climate model parameterization. *Geoscience Letters*, **6**, 1–10.

Xu, L., R. D. Pyles, K. T. P. U, R.-H. Snyder, E. Monier, M. Falk, and C. S-H, 2017: Impact of canopy representations on regional modeling of evapotranspiration using the wrf-acasa coupled model. *Agric. For. Meteor.*, **247**, 79–92.

Yan, D., T. Liu, W. Dong, X. Liao, S. Luo, K. Wu, X. Zhu, Z. Zheng, and X. Wen, 2020a: Integrating remote sensing data with wrf model for improved 2-m temperature and humidity simulations in china. *Dynamics of Atmospheres and Oceans*, **89**, 101127.

Yan, H. and R. Anthes, 1988: The effects of variations in surface moisture on mesoscale circulations. *Mon. Wea. Rev.*, **116**, 192–208.

Yan, M., J. Liu, Z. Wang, and L. Ning, 2020b: Biogeophysical impacts of land use/land cover change on 20th century anthropogenic climate compared to the impacts of greenhouse gas change. *Int. J. Climatol.*, **40**, 6560–6573.

Yan, Y., J. Tang, and G. L. J. Wu, 2019: Effects of vegetation fraction variation on regional climate simulation over eastern china. *Global Planet. Change*, **175**, 173–189.

Yang, K., T. Koike, B. Ye, and L. Bastidas, 2005: Inverse analysis of the role of soil vertical heterogeneity in controlling surface soil state and energy partition. *J. Geophys. Res. Atmospheres (1984–2012)*, **110**.

Yang, Y., R. J. Donohue, and T. R. McVicar, 2016a: Global effective plant rooting depth. v1.

— 2016b: Global estimation of effective plant rooting depth: Implications for hydrological modeling. *Water Resources Research*, **52**, 8260–8276.

Yang, Z.-L., Y. Dai, R. Dickinson, and W. Shuttleworth, 1999: Sensitivity of ground heat flux to vegetation cover fraction and leaf area index. *J. Geophys. Res. Atmospheres (1984–2012)*, **104**, 19505–19514.

Zeng, X., R. E. Dickinson, A. Walker, and M. Shaikh, 2000: Derivation and evaluation of global 1-km fractional vegetation cover data for land modelling. *J. Appl. Meteor.*, **39**, 826–839.

Zhang, G., G. Zhou, F. Chen, M. Barlage, and L. Xue, 2014: A trial to improve surface heat exchange simulation through sensitivity experiments over a desert steppe site. *J. Hydrometeor.*, **15**, 664–684.

Zhang, M., L. Geping, P. D. Maeyer, P. Cai, and A. Kurban, 2017: Improved atmospheric modelling of the oasis-desert system in central asia using wrf with actual satellite products. *Remote Sensing*, **9**, doi:10.3390/rs9121273.
URL http://www.mdpi.com/2072-4292/9/12/1273

Zheng, D., R. van der Velde, Z. Su, X. Wang, J. Wen, M. Booij, A. Hoekstra, and Y. Chen, 2015: Augmentations to the noah model physics for application to the yellow river source area. part ii: Turbulent heat fluxes and soil heat transport. *J. Hydrometeor.*, **16**, 2677–2694.

Zhou, L., R. K. Kaufmann, Y. Tian, R. B. Mineny, and C. J. Tucker, 2003: Relation between interannual variations in satellite measures of northern forest greenness and climate between 1982 and 1999. *J. Geophys. Res.*, **108**, ACL 3–1–ACL 3–16.

Zhou, L., C. J. Tucker, R. K. Kaufmann, D. Slayback, N. V. Shabanov, and R. B. Myneni, 2001: Variations in northern vegetation activity inferred from satellite data of vegetation index during 1981 to 1999. *J. Geophys. Res. Atmospheres (1984–2012)*, **106**, 20069–20083.

Appendix A: Academic contributions of the author

Publications in which the author has participated

1. P. A. Jiménez, J. P. Montávez, E. García-Bustamante, J. Navarro, **J. M. Gutiérrez**, E. E. Lucio-Eceiza , and J. F. González-Rouco, 2010: Diurnal surface wind variations over complex terrain. *Revista de Geofísica*, **21**, 79-91.

2. S. Jerez, J. P. Montávez, J. J Gómez-Navarro, P. Jiménez-Guerrero, **J. Jiménez**, and J. F. González-Rouco, 2010: Temperature sensitivity to the land-surface model in MM5 climate simulations over the Iberian Peninsula. *Meteorologische Zeitschrift*, 19(4), 363-374.
3. **J. M. Jiménez-Gutiérrez**, F. Valero, S. Jerez, and J. P. Montávez, 2019: Impacts of green vegetation fraction derivation methods on regional climate simulations. *Atmosphere*, 10(5), 281.
4. **J. M. Jiménez-Gutiérrez**, J. P. Montávez, J. Ruiz-Martínez and F. Valero, 2021: Temperature response to changes in Vegetation Fraction Cover in a Regional Climate Model. *Atmosphere*, 12(5), 599.

Participation in Scientific Conferences

1. **J. M. Jiménez-Gutiérrez**, J. P. Montávez, 2006: Respuesta de la dinámica mesoescalar a los cambios en la cubierta del suelo derivados de un incendio. *V Asamblea Hispano Portuguesa de Geodesia y Geofísica*. Sevilla. Spain.
2. S. Jerez, J. P. Montávez, P. Jiménez-Guerrero, J. J. Gómez-Navarro, J. A. García Valero, J. F. González-Rouco, and **J. M. Jiménez-Gutiérrez**, 2009: Implications of land-atmosphere coupling on the present and projected climate over the Iberian Peninsula *EGU General Assembly Conference Abstracts. Geophysical Research Abstracts*. Vol. 11, EGU2009-10861-2.
3. J. P. Montávez, **J. M. Jiménez-Gutiérrez**, S. Jerez, J. J. Gómez-Navarro, R. Lorente, J. A. García Valero, P. Jiménez-Guerrero, 2010: Evolución de la cubierta vegetal y su papel sobre las tendencias térmicas de la Península Ibérica. *Segones jornades de Meteorologia i Climatologia de la Mediterrània occidental*. Valencia.
4. **J. M. Jiménez-Gutiérrez**, J. P. Montávez, S. Jerez and F. Valero, 2015: Sensitivity of Regional Climate Simulations to the vegetation variability. *Simposio Internacional CLIMA-ES 2015*. Tortosa. Spain.
5. **J. M. Jiménez-Gutiérrez**, J. P. Montávez, S. Jerez and F. Valero, 2018: Sensibilidad de la fracción de cubierta vegetal en modelos climáticos regionales . *XI Congreso Internacional de la Asociación Española de Climatología (AEC)*. Cartagena. Spain.

Participation in Workshops and Meetings

1. **J. M. Jiménez-Gutiérrez**, R. Aznar-Lecoq. Aplicación de los Sistemas de Información Geográfica (GIS) al modelo MM5. *III Reunión del proyecto Red Ibérica para la investigación y el desarrollo de aplicaciones en base al modelo atmosférico MM5*, 2005. *Oral communication*. Valencia.
2. **J. M. Jiménez-Gutiérrez**, J. P. Montávez, S. Jerez, J. J. Gómez-Navarro and F. Valero, 2009: Sensibilidad de simulaciones regionales climáticas a la fracción de vegetación. *Clima en España: pasado, presente y futuro. Contribución a un informe de evaluación del cambio climático regional*. *Poster*. Madrid. CSIC.
3. *Land-atmosphere interactions at the regional scale*. CIEMAT. Madrid. 2012